Adaptive Control Techniques for Multirotor Aircrafts

A Dissertation

Presented to

the Faculty of the School of Engineering and Applied Science

University of Virginia

In Partial Fulfillment

of the requirements for the Degree

Doctor of Philosophy

in

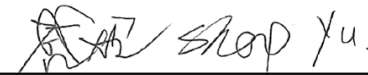Electrical Engineering

---

by

Yu Sheng

May 2019

Approval Sheet

This Dissertation

is submitted in partial fulfillment of the requirements

for the degree

Doctor of Philosophy

in Electrical Engineering

_____
AUTHOR

This Dissertation has been read and approved by the Examining Committee:

_____
Prof. Gang Tao, *Advisor*

_____
Prof. Zongli Lin, *Committee Chairperson*

_____
Prof. Stephan de Wekker, *Committee Member*

_____
Prof. Stephen G. Wilson, *Committee Member*

_____
Prof. Daniel Quinn, *Committee Member*

Accepted for the School of Engineering and Applied Science:

Craig H. Benson, Dean, School of Engineering and Applied Science

May 2019

Dedicated to TJ and UVa Bicentennial.

Abstract

Multirotor unmanned aerial vehicles (UAVs) have shown evident advantages over traditional fixed wing UAVs in remote sensing. They are also believed to hold enormous potential in logistics, infrastructure maintenance and agriculture management. Such emerging applications bring the multirotor drones into new working environments with more uncertainties and higher levels of safety requirements. Study has shown that the desired performance of multirotors, such as fast maneuver and fault resilience, has not been rigorously achieved by current applied control approaches. The control goal of this research is to guarantee closed-loop system stability and enhance tracking performance under abnormal and uncertain system conditions. This research develops advanced adaptive control techniques for multirotors to accommodate parameter uncertainties, compensate actuator failures, and reject uncertain disturbances. The results of the research have formed some desired foundations for advanced unmanned multirotor systems and intelligent aerial systems.

The dissertation research studies both the traditional quadrotor-like under-actuated multirotors and the novel tilted-rotor fully-actuated omni-directional multirotors. Some fundamental system characteristics such as nonlinear and linearized model parameterization, relative degree, high-frequency gain matrix variation, and control allocation scheme are investigated for different multirotor systems at various operating conditions. Such studies are crucial for developing adaptive control designs which enable the multirotors working at non-hover conditions under uncertain system parameters, such

as mass, inertial momentum and drag coefficients. Different rotor arrangements of hexarotor (NPNPNP and NNPPNP) and octorotor (NPNPNPNP and NNPPNNPP) aircrafts are surveyed to specify the compensable actuator failure patterns.

An input compensator is developed for multirotor systems to assure a uniform interactor matrix and a consistent pattern of the gain matrix signs over different typical operating conditions. An adaptive control scheme with input compensator is designed for quadrotors with nonlinear offsets at the non-equilibriums and uncertain parameters. Adaptive failure compensation schemes are designed to deal with unknown loss-of-control actuator failures whose pattern, time and value are all uncertain. A control signal distribution technique is developed to ensure the invariant gain matrix sign pattern under all the compensable actuator failure patterns, which enables the integrated adaptive control scheme for hexarotors subject to uncertain parameters and unknown failures simultaneously. Adaptive disturbance rejection schemes are developed to reject wind uncertainties for a multirotor-based atmospheric measurement platform. Nonlinear adaptive controllers are constructed to achieve more sophisticated maneuvers. Both analytical and simulation results are presented to verify the desired properties of the developed adaptive multirotor control systems.

Contents

List of Figures

List of Tables

Nomenclature

c_f thrust coefficient, N·s^2
c_m ratio between drag and thrust coefficients of a rotor, m·s
c_r rotational drag coefficient, N·m·s
c_t translational drag coefficient, N·m·s
d arm length, m
F_z lift force in the direction of the z_B axis, N
f_i thrust force provided by the ith rotor, N
g gravity acceleration, 9.8 m/s^2
J_x moment of inertia about the x_B axis, kg·m^2
J_y moment of inertia about the y_B axis, kg·m^2
J_z moment of inertia about the z_B axis, kg·m^2
m mass, kg
p angular velocity around the x_B axis, rad/s
q angular velocity around the y_B axis, rad/s
r angular velocity around the z_B axis, rad/s
T_x net torque in the direction of the x_B , N·m
T_y net torque in the direction of the y_B , N·m
T_z net torque in the direction of the z_B , N·m
x_E position in x direction of the earth frame, m
y_E position in y direction of the earth frame, m
z_E position in z direction of the earth frame, m
θ pitch angle, rad
ϕ roll angle, rad
ψ yaw angle, rad
ω_i rotation speed of rotor i, rad/s

Subscript
E in the earth frame
t translational
r rotational
e at equilibrium condition
o at non-equilibrium operating condition

Chapter 1

Introduction

Multirotors are unmanned aerial vehicles (UAVs) with multiple propulsion rotors, like quadrotor, hexarotor and octorotor. Compared to the unmanned helicopters and other fixed wing UAVs, the multirotors have significant advantages in mechanical simplicity, user safety and landing convenience. Current multirotor control techniques are designed for the remote controlled drones to convey photography devices. With the technological improvement in battery capacity, propeller design and planning algorithm, the utilization of the multirotors is expanding to many new aspects, for example infrastructure maintenance, meteorological measurement, and cargo delivery. The emerging applications require the multirotor drones to work autonomously, accurately and safely. In order to realize various tasks from different application scopes, a multirotor should be able to track known trajectories against the disturbance from the environment and uncertain parameters of itself or its loads.

Actuator failure is a critical issue for multirotor systems, which includes but not limited to loss-of-effectiveness, lock-in-place, and loss-of-control. In order to enhance the tracking performance and guarantee the system stability, multirotor systems should be equipped with failure compensation controllers. Most of the existing compensation approaches only deal with loss-of-efficiency failures but can not accommodate the

loss-of-control failures. To tolerant the failure and fault of actuators, a multirotor should have redundancy in actuation. So a quadrotor is regarded as unqualified for failure compensation control designs as the result of its under-actuated nature. Moreover, even a hexarotor, who has two extra actuators than a quadrotor, could not always guarantee its controllability when single actuator failure happens. Therefore it is crucial to verify the design conditions, like compensable actuator failures and control gain matrix signs, before the development of adaptive controllers.

1.1   Research Motivations

Figure 1.1: Different types of multirotor drones. (*copyright: Joseph Flynt [1]*)

Multirotor (or multicopter, like quadcopter, hexacopter and octocopter) UAVs are more and more popular in recent years because of their ability of hovering and vertical-take-off-and-landing (VTOL) compared with the fixed wing UAVs. Multirotor UAVs are more and more considered as flying robots that can not only observe but also actively interact with the environment. However, the stability and performance of multirotor systems are not fully guaranteed for sophisticated tasks in the presence of uncertain parameters, failures, and wind disturbances. The expected performance

of multirotors will be discussed in the following parts; and the insufficient of current control techniques, especially PID control, will also be pointed out.

1.1.1 Broad Applications of Multirotors

The most significant difference between multirotor UAVs and fix wing aircrafts is that the propulsion of a multirotor is generated along the z-axis in its body frame. This aspect of the multirotor does not only provide the capability of vertical take-off and landing (VTOL) but also makes it possible to hover at a given position in the air. Unlike the smooth routes of fixed wing aircrafts, the target trajectories for multirotors may include steady points for hovering, sharp turns in the sky, elevation or descending vertically. They are competent in many fields that fix wing aircrafts can not well handle. Following are some examples of the emerging applications of multirotors.

- **Aerial photography**

  This is one of the most traditional usages of drones. When a fix wing UAV is required to keep monitoring a small area, it has to linger around the spot, which is neither energy efficient nor with good sensing quality. Since the multirotor UAVs are not restricted by the minimum cruising speed, which is a common constraint for the fixed wing aircrafts, they can work at a wider range of velocities.

- **Meteorological measurement**

  Multirotor drones can collect meteorological information more accurately and timely than the current balloon systems. However, a drone is much expensive than a balloon. What is more, the propellers of a multirotor are always subjected to failure in severe environment. So the fault tolerant control technique is very meaningful for the utilization of drones in this field.

- **Infrastructure maintenance**

  With the abilities of hovering, VTOL and sharp turning, multirotors can track

complicated trajectories in complex environment. Such ability enables multirotor drones to monitor infrastructures like wind turbines, pipes, tunnels, mines and buildings. Moreover, the multirotor drones can even fix facilities if they are equipped with manipulators.

Figure 1.2: A drone from Cyberhawk Innovations is inspecting a wind turbine in UK. *(copyright: Ascending Technologies [2])*

- **Disaster relief**

  Unmanned multirotor vehicles can fly through narrow ruins and land on small fields. They are ideal platforms for fast response after emergencies. Different from the infrastructure maintenance and package delivering, the site maps are often not accurate after disasters. There are uncertainties from environment that not only disturb the motion but also cause actuator failures.

- **Package delivering**

  UVAs can improve the efficiency of logistics industry by working together with trucks. The ground vehicles are playing the roles of command centers, mobile warehouses and charging stations for the drones in the team. The drones must track given trajectories precisely to avoid trespassing the neighbor's property of

the target. The drones should also tolerate faults, failures and disturbances to guarantee the public safety.

Figure 1.3: A drone from UPS is delivering blood for a hospital. *(copyright: Ryan Davis/UPS [3])*

These innovative enterprises are calling for different capabilities of multirotor unmanned vehicles. A multirotor is expected to fulfill different tasks accurately and keep the system stable and safety.

1.1.2 Advanced Tasks and Technical Challenges

A bright future has been depicted for multirotor systems , but the utilization of them is still limited by many factors, like battery capacity, blade aerodynamics, and legislative process. For control design and system integration, the main challenges can be summarized in the following aspects.

From Flying Camera to Aerial Robot

The quadrotor drones are very popular consumer electronics and their market keeps booming. They are also adopted as a powerful remote sensing platform in film shooting, construction and agricultural monitoring. Therefore most current efforts from researchers and manufacturers were made for the development of gimbals system,

attitude stabilization controllers, and corresponding guidance systems. In recent years, the multirotor UAVs are more and more considered as flying robots which not only observes but also actively interacts with the environment. However, for the multirotors work for delivering, manipulating and assembling, there emerges many new problems.

Figure 1.4: A manipulator arm developed by Energid. *(copyright: Energid [4])*

From Remotely Controlled to Autonomously Operating

The output tracking problem of drones has not attracted much attention because the multirotors were manipulated by a human operator via remote controllers. The position control problem is shirked to the human; and the controller is only responsible for control allocation and attitude stabilization. As explained, the emerging applications require the multirotor drones to work on their own accurately and safely. Then advanced control algorithms are needed to deal with the uncertainties and enhance the autonomy.

1.1.3   Issues of Current Multirotor Control Techniques

The promising missions of multirotors require fast, agile and accurate maneuvers. Different models and control methods have been proposed for better performance of

multirotors, like quadrotors [5–9], hexarotors [10–14],and octorotors [15–17]. Though the multirotor market is blooming now, their desired performances are still not fully satisfied. For example, the users need to purchase expensive gimbals and cameras to compensate the insufficiency of the tracking control algorithms. It should be articulated that some of the issues are intrinsic drawbacks of the PID control method which is widely used in the design of rotor controllers.

- **No Guarantee of Stability for Fast Maneuver**

  Among the linearization-based designs, PID controllers are most widely used to control quadrotors at the hover condition, for example [18–23]. However, a PID controller can only work with constant reference signals and cannot deal with high-order dynamic systems like multirotors at other fast maneuver conditions (that is, a PID controller is not able to ensure the rotor system to track an arbitrary trajectory signal). Moreover, the closed-loop system stability is not guaranteed by a PID controller applied to multirotor systems (which is only analytically ensured to stabilize low-order systems).

- **Insufficient Capacity to Handle Parameter Uncertainties**

  Many of the system parameters of multirotors are subject to change even within one flight. For example, the friction coefficients are dependent on the density and humidity of the airflow. If the multirotor delivers a cargo or picks up something, the mass and moments of inertia will change. For the multirotors with manipulators, the stretch and shrink of the joints often lead to the moving of the center of mass, which affects the stability and efficiency of control allocation.

- **Inadequate Treatment for Actuator Failures**

  Multirotors are often working in complicated and severe environments and facing the threaten of actuator failures. The unpredicted circumstances may cause physical damage to propellers. Moreover, the dust and moisture in harsh

working conditions may lead to the burn of motors. If a proper control strategy is not equipped to a multirotor, it may fail to complete its task when there is emergency. Actuator failure is a major challenge for multirotor systems. Faults in the actuation components often lead to decreased performance. A loss-of-control rotor may cause severe crash and even threaten public safety.

Insufficient ability of quadrotors in dealing with actuator failures

Quadrotors and other 4-DOF multirotors are under-actuated aerial vehicles, because they can only control four degrees of freedom out of their six degrees of freedom [24–26]. Due to the underactuation nature of such aerial vehicles, their roll angle ϕ and pitch angle θ are often coupled with the horizontal position (x, y). Hence, a trade-off must be made between full attitude control and full position control. For the underactuated multirotors, the position (x, y, z) together with the yaw angle ψ are chosen to be the system outputs for most tracking tasks. When a multirotor without actuation redundancy is subject to actuator failures, it may fail to track the given trajectory. Hence, special control scheme is needed to deal with failures.

1.2   Control Problem Formulation

The fundamental ideas of adaptive control theory are summarized in [27–29]. The advanced control techniques developed in this dissertation for multirotors are based on the multivariable model reference control framework which is suitable for multirotor applications in terms of critical technical aspects of system stabilization and trajectory tracking. This section describes and formulates the general control problem to be solved in this dissertation research.

1.2.1 Nominal System

We start with a multirotor system model without any uncertainty or fault, its dynamics can be characterized by a nonlinear model as

$$\dot{x}_p(t) = f(x_p(t), u_p(t)),$$

where $x_p(t)$ is a signal vector of system states, $u_p(t)$ is a signal vector of system inputs, the subscript $_p$ stands for plant, and f is a known nonlinear function. The components of $x_p(t)$ often include positions, velocities, attitude angles and angular velocities. The components of $u_p(t)$ vary for different levels of the control problem, which may contain thrust force, momentum torque, or motor speed.

The output tracking problems are studied in this research. A subset of the state vector x_p is chosen to be the components of the system output vector as

$$y_p(t) = Cx_p(t),$$

where C is the known output matrix. The desired output or trajectory to be tracked is often represented by $y_m(t)$. The selection of the components in the output vector depends on the nature of given task. Popular choices include but not limited to position tracking, attitude tracking, position-yaw tracking, and attitude-altitude tracking.

1.2.2 System with Uncertainties and Faults

The next step is to introduce parameter uncertainty and disturbance into the system, which leads to the following new system model as

$$\dot{x}_p(t) = f(x_p(t), u_p(t), f_d(t), t),$$

where f_d represents the disturbance to the system. At this stage, the system parameters in f could be uncertain. Since multirotors are man-made vehicles, so their physical structures and benchmark parameters are known. As a result of such facts, the structure of f and the order of the system are known. The time term t is also included in the formula to indicate that some of the parameters might be time-varying. For example, a quadrotor is spraying pesticides upon a farm, the total mass and the weight distribution of the system would keep changing.

Then we consider the actuator failure problem of the system. Recall that in the previous two system models we assume that the system input $u_p(t)$ should be exact what we command. However, such assumption does not stand for an abnormal actuation system. In order to depict the cases with actuator failures, we replace $u_p(t)$ in the former model and get

$$\dot{x}_p(t) = f(x_p(t), v(t), \bar{u}(t), f_d(t), t),$$

where $v(t)$ is the applied control signal (which is identical to $u_p(t)$ for the cases without actuator failure), $\bar{u}(t)$ represents the uncertain effect of failure to the system. Note that the nonlinear function f should contain some more uncertain parameters that associated with the failure pattern.

Remark 1. In this dissertation research , we work on the problems of parameter uncertainty, environment disturbance, and actuator failure. Adaptive control and compensation schemes will be developed to deal with different cases and guarantee tracking performance. The issues of system noise and sensor failure are not considered in this work. They should be resolved by observer designs and estimation algorithms, for example [30–34]. □

1.2.3 Control Design Objective

The goal of control design is to develop an adaptive controller to generate an applied control signal $v(t)$ for the system

$$\dot{x}_p(t) = f(x_p(t), v(t), \bar{u}(t), f_d(t), t) \tag{1.1}$$

$$y_p(t) = C x_p(t) \tag{1.2}$$

which is subject to uncertain system parameters in f, unknown disturbance $f_d(t)$, and unknown actuator failure $\bar{u}(t)$, to guarantee the boundedness of the closed-loop signals and asymptotic tracking of a given reference output signal $y_m(t)$.

1.3 Literature Review

This section reviews the relevant literature published in journals and conference proceedings, which pertain to the research and development of the multirotor control techniques. We will introduce and discuss related research approaches on multirotor design, adaptive control, and fault-tolerant control, which provide solid technical foundation for this research. This survey of the state-of-the-art is also important for better understanding of the contribution of the research work to be presented.

1.3.1 Background

The models of quadrotors have been widely studied during the past years [5, 9, 24, 35]. Different control techniques have been used upon quadrotors, for example optimal control [36], robust control [7, 8, 37], adaptive control [38], sliding mode control [39–41], LQ regulation [42], and neural networks [43–45]. A feedback linearization control approach is given in [6]; an input-output linearization control scheme is introduced in [46]; and a multivariable model reference adaptive control (MRAC) approach is

addressed in [47]. A fault detection and isolation approach is proposed in [48] to construct an active fault-tolerant controller. The adaptive control problem at the non-hover conditions is dealt by various methods, for example [49–51].

Hexarotors are multirotor UAVs with six rotors. They have two more rotors than the quadrotors, which help them achieve better performance than quadrotors and also bring more control challenges. Most of the control approaches for hexarotors are based on hexarotor designs with four degrees of freedom (DOF), like [10, 11, 52–54]. The two redundant rotors of the 4-DOF hexarotor systems are very important in keeping safety when actuator failures happen. For the designs with tilted rotors as in [12–14, 55–57], the actuation redundancy is exchanged for six degrees of freedom and agile maneuver. The key advantage of such design is the ability to reject random disturbances, like the wind gusts , without changing its attitude.

Linearization-based methods are widely used in studying nonlinear systems. As shown by extensive literature, for example [42, 47, 58–61], it is efficient and reliable to linearize the model of quadrotors at typical operating points for investigating the input-output relation and designing control methods. An adaptive controller is developed in [38] as a supplement of a baseline controller for known system dynamics, a feedback linearization control approach was given in [6], an input-output linearization control scheme is introduced in [46]. The PID control technique is still widely used upon multirotor systems for desired performance, for example [18–23, 62, 63]. However, PID controllers are not very capable in working with arbitrary reference signals of multivariable nonlinear systems under parameter uncertainties. To deal with the uncertain parameters, different adaptive controllers are designed for multirotor systems, like [7, 8, 47, 49, 58, 64, 65].

Model reference adaptive control (MRAC) is a well-established control method dealing with the parameter uncertainties and unknown actuator failures. It has been widely used upon different kinds of aircrafts and of course the multirotor systems.

It is shown in [47] and [58] that MRAC is effective for the quadrotors at hover condition. Then the result is extended to different typical operating conditions of 4-DOF multirotors in [50] and [66]. The compensable failure patterns and corresponding adaptive compensation scheme are investigated in [67] for a hexarotor system with unknown failure and known parameters. This work will extend previous effort of adaptive control design for 4-DOF multirotors.

Multirotors are expected to be working in unstructured and uncertain environments which may lead to various actuator failures. To guarantee the fulfillment of missions and the safety, researchers developed many different compensation schemes. A fault tolerant control scheme is designed in [68] for a quadrotor system to work despite the total loss of an actuator. The controllability of hexarotor systems with different rotor arrangement under single loss-of-control actuator failure is studied in [69]. A learning-based failure compensation scheme is proposed in [70] for the output tracking problem of quadrotors under loss-of-efficiency failures. The controllability and hovering problem of a quadrotor under one, tow, or three failed rotors is studied in [9] to fully understand the redundancy of quadrotor systems.

1.3.2 Multirotor Systems

The quadrotor is the most used and studied type of multirotor unmanned aerial vehicles (UAVs) as a result of its simplicity in mechanism and the increasing demands in aerial photography. Different advanced control techniques have been tested on quadrotors for better performance, like nonlinear robust control [37], disturbance-observer-based sliding mode control [71], nonlinear back-stepping control [72], L1 adaptive control [49], and model reference adaptive control (MRAC) [50, 58, 73]. Since a quadrotor only has four actuators, it can track no more than four output signals and cannot control all its six degrees of freedom (DOF). To achieve more agile motion, different designs of omni-directional multirotors are proposed to make the system fully-actuated and

robust to disturbances. Such designs depend on the tilted rotor systems that generate thrust forces not only parallel to the z-axis of the body frame.

The main advantage of 4-DOF hexarotors over quadrotors is the actuation redundancy realized by the two extra rotors. Intuitively, a 4-DOF hexarotor with proper control scheme should be able to bear at most two failed actuators and still fulfill its original tracking task. The fact is that only the hexarotors with a specific rotor arrangement can tolerate the failure of one actuator [69]. The compensable patterns of one actuator failure are also given in [69], but the compensable patterns of two actuators failure are not explored. It is also shown in [74] that the traditional NPNPNP rotor arrangement is not able to guarantee the stability and performance with a loss-of-control rotor. Meanwhile, a novel rotor arrangement (NNPPNP) is investigated in [69] and [75], with which the controllability of a 4-DOF hexarotor could be remained under the loss-of-thrust failure of a single rotor. However, the corresponding adaptive failure compensation design is not provided; and the cases of two failed actuators are not surveyed yet.

To achieve better performance in manipulator operation and disturbance rejection, fully-actuated multirotor systems are proposed in recent years. However, the tilted rotor system of these designs also leads to the energy inefficiency of control allocation. The early prototypes include but not limited to the non-planar multirotor vehicle in [76], the fully-actuated hexarotor in [12], and the omni-directional aerial vehicle from [55]. The maneuverability of fully-actuated hexarotor systems is evaluated in [77] based on different tilted angles and rotor arrangement. A connection between the motion planning and the control problem of fully-actuated multirotors is established in [78] by constructing a computationally efficient method of trajectory generating. An explicit reference governor scheme is introduced in [79] for fully-actuated aerial vehicles under actuator saturation. A double-loop geometric control architecture is proposed and validated in [80] to tackle with environmental disturbance and physical

interaction with human.

Figure 1.5: The Voliro hexacopter's tilting rotors let it hover and fly in any orientation. (*copyright: Voliro [81]*)

1.3.3 Adaptive Control Designs

One of the key challenges for multirotor control is to deal with the parameter uncertainty. For example, multirotors are often carrying additional loads like cameras, manipulators or cargoes, whose center of mass and shape might change during different missions. Moreover, the dynamics of propellers are often not precisely modeled and the force they generate might vary according to the real environment. The PID control technique is still widely used upon multirotor systems for desired performance, for example [18–20, 23, 62]. However, PID controllers are not very capable in working with arbitrary reference signal of multivariable nonlinear systems under parameter uncertainties. To deal with the uncertain parameters, different adaptive controllers are design for multirotor systems, like [7, 8, 47, 49, 58, 64, 65].

The model reference adaptive control (MRAC) technique is a well-established control method dealing with parameter uncertainties, which has rich literature [27, 82, 83]. It is shown in [47] and [58] that the architecture of the MRAC could be used to control a quadrotor with unknown parameters at the hover condition where

all attitude angle are around zero. Further, the linearized models of quadrotors at typical operating conditions were studied in [84] together with the essential design information for MRAC design as the interactor matrices and the signs of the leading principal minors of the high-frequency gain matrices.

The restriction to the hover condition that all attitude angles are around zero is the most common condition in literatures, for example [47, 49, 59]. It should be relaxed because the quadrotors can neither maintain high cruising speed nor reject strong disturbance at hover condition. In practice a quadrotor needs to change the yaw angle at some circumstances, for example, a manipulator may need an extra degree of freedom to work. What is more, as a result of the underactuated nature of the quadrotors, the horizontal propulsions are coupled with the attitude angles [24]. So when there is disturbance in the horizontal plane, a quadrotor should have a non-zero roll or pitch angle for compensation. However, as shown in [84], different typical operating conditions of the quadrotor are with different interactor matrices and different gain matrix signs, which lead to difficult problems for constructing a MRAC scheme working for multiple operating conditions. For the adaptive control methods that can deal with parameter uncertainties at operating points other than the hover condition, there are also some limitations need to be relaxed. For example, the controller developed in [38] is able to work with the parameter uncertainties in the state matrix but not the input matrix. the approach in [8] achieved good results in attitude tracking but needs further efforts in trajectory tracking.

The center of gravity variation (c.g.v.) is another challenge for the control design of multirotor systems. The center of gravity significantly changes both the dynamic model and actuation model of a multirotor system. In the view of adaptive control, though c.g.v. can transfigure the inertial momentum matrix in the dynamics equations, the design conditions remain the same for most cases. Most of the existing control approaches assume known control allocation schemes. Some adaptive control allocations

have been presented in [85–87], which assume that there only exist multiplication parameter uncertainties but no additional parameter uncertainties. Such assumptions may not be appropriate for multirotors equipped with manipulators. The extension and flexing of the mechanical arm may cause shifting of the system mass center, which leads to uncertain control allocation scheme. If the multirotor delivers a cargo or picks up something, the mass and moments of inertia may change. Thus the adaptive control design for uncertain control allocation is another open problem for multirotors.

1.3.4 Fault Compensation Schemes

Actuator failure is another major challenge for multirotor systems. When the actuator failures happen in severe environment or caused by emergencies, they are often accompanied by structure damage and system parameter changing. Such uncertainties may lead a hexarotor to fail its task and even be a huge risk for public safety. The actuator failure of a multirotor often happens in the components of motor, propeller and electronic speed controller (ESC) [88]. The failure modes of motors and ESCs include seizing, degradation, overheating, and burnt [89]. The propellers suffer from failures like fracture, broken and vibration [88]. The hexarotors and octorotors are considered to be better candidates for tolerating actuator failures for they have more actuators than quadrotors.

The failures would occur in unexpected situations in which the failure time, failed actuator and failure value are all unknown. The technique of fault detection and isolation [16, 17, 48, 91, 92] is often used to deal with the case. However, the detection process itself may take some time and delay the reconfiguration of the control allocation. Moreover, failures are usually accompanied by disturbance, structure damage and system parameter shifting. These uncertainties are great challenges for designing reconfiguration schemes in advance and constructing fault tolerant controllers. The adaptive controller for actuator failure compensation does not need the step of fault
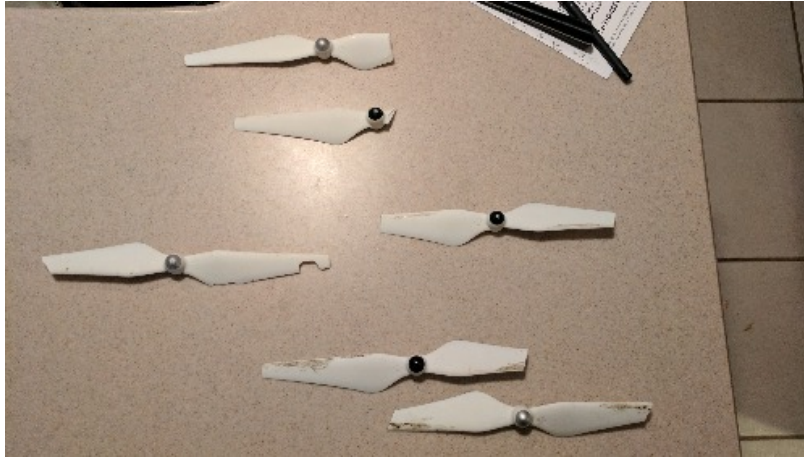
Figure 1.6: Broken propeller blades of drones. (*copyright: Day_Dreamer [90]*)

detection, whose parameters for control allocation are updated by adaptive laws. Many adaptive fault tolerant controllers have been constructed for hexarotors, for example, loss-of-effectiveness compensation [93–95], 3-DOF attitude tracking [96], and 3-DOF position tracking [97]. But for more challenging failure types, like loss-of-control, the adaptive controller design is still an open problem for the output tracking of 4-DOF with guaranteed stability.

Though the quadrotors cannot track four outputs when one actuator is subjected to loss-of-control failure, many fault tolerant controllers are developed for other issues in the literature. For the loss-of-effectiveness failure, fault tolerant controllers are constructed in [38, 70, 98–100] to retain the tracking performance for four outputs. However, one of the four outputs needs to be sacrificed when more severe actuator failures happen, like loss-of-thrust, lock-in-place, or even loss of control. In [6, 48, 101, 102], control techniques are developed for 3-DOF position tracking in case of the complete loss of one rotor. The yaw angles of the quadrotors are not under control in any of the mentioned fault tolerant position tracking controllers. As a result, the quadrotors are spinning in the yaw direction when a failure happens. Such spinning can undermine the ability of a quadrotor in tasks of photographing, manipulating and delivering. The centrifugal force is also a potential threaten, which may cause

disintegration of the system. In order to enhance the flight safety, quadrotors should be replaced by 4-DOF hexarotors equipped with the failure compensation algorithm.

The 4-DOF hexarotors are under-actuated UAVs as quadrotors that can only control four out of six DOF [7, 24, 103]. Moreover, the 4-DOF hexarotors are also over-actuated [104–106], because they have more actuators than outputs. The nature as both over-actuated and under-actuated of them provides us many interesting and yet unsolved control problems. For example, The parameter uncertainty of a hexarotor is well handled in [94], but only the loss-of-effectiveness failures can be compensated by the approach. In [74], a degraded control scheme is developed for hexarotors for total rotor failures, but only the three position outputs can be tracked. A fault tolerant algorithm for four outputs tracking is presented in [87], but the parameters are assumed to be known. So the main problem we consider is the systematic study of the composite controller for the 4-DOF hexarotors under both parameter and failure uncertainty.

The nonlinear adaptive control design for a multirotor system under both parameter and failure uncertainties is still a open problem. The loss-of-control failure problem is investigated on linearized multirotor systems in [107–110]. Though the adaptive controllers in [93–97] cannot guarantee the tracking performance and stability of 4-DOF hexarotors under actuator failures, they have displayed the potential of adaptive control designs in dealing with the problem. The abilities of adaptive control methods in failure compensation have been demonstrated on various systems, especially on spacecrafts [111–113] and aircrafts [114–117]. Adaptive controllers are also widely used in dealing with the system parameter uncertainties of quadrotor systems, for example [7, 8, 47, 49, 58, 64, 65]. However, unsolved adaptive control challenges still exist on the original nonlinear systems.

1.4   Dissertation Organization

The dissertation is organized as follows.

The first part is the foundation of the research, which contains Chapter 1 - 3. This part summarizes knowledge and information related to the research. The purpose is to aid the audience to understand the technical approaches and contributions presented in later parts. In Chapter 1, the research motivation and related literature are discussed; the general research problem is also formulated. In Chapter 2, the basic mathematical and physical knowledge together with system and control theory are provided. In Chapter 3, we listed the multirotor system models related to the research, which include nonlinear and linearized dynamic model, actuation model, wind disturbance model, center of gravity variation model, and actuator failure model.

The second part derives the important system characteristics, which contains Chapter 4 and 5. The verification of such information is crucial for designing adaptive control and compensation schemes, In Chapter 4, system features of the dynamic models for both under-actuated and fully-actuated multirotors are studied at several typical operating conditions, which are the transfer matrix, the interactor matrix, and the high frequency gain matrix. In Chapter 5, the compensable failure patterns are investigated for different rotor arrangements of hexarotor and octorotor systems.

The third part develops a series of MRAC schemes to deal with different uncertainties and faults, which contains Chapter 6 - 9. These linearization-based adaptive control and compensation designs are demonstrated to be effective on the typical operating conditions. In Chapter 6, an adaptive control scheme with state-dependent interactor matrices is constructed for working at different equilibrium and non-equilibrium conditions. In Chapter 7, an input compensator is designed to achieve a uniform interactor matrix for all the typical operating conditions to enhance the system performance. In Chapter 8, we develop an adaptive compensation scheme for multirotor systems under loss-of-control actuator failures with unknown failure time, value and pattern. In

Chapter 9, a control signal distribution scheme is constructed to reduce the dimension of parameters to be estimated for an adaptive controller against both parameter uncertainty and actuator failure.

The last part, as Chapter 10, is a conclusion of the research. The possible future work is also discussed.

Chapter 2

Preliminaries

2.1 Coordination Transformation

Since the position and attitude of the quadrotor are described in an initial coordinate system, while the mechanical analysis are made in the body coordinate frame of the quadrotor. It is necessary to take some coordinate transformation for the system.

The origin of the body frame is set at the geometry center of the quadrotor and it is assumed that the mass center of the quadrotor coincides its geometry center. And the x and y axis are set on the arms of rotor 1 and 2, the z axis could be determined via right hand rule. Here we use Tait-Bryan angles [118] to present the orientation of the quadrotor to the earth frame, where ϕ, θ, ψ represent the roll, pitch and yaw angles. The definition of the attitude angles is shown as in Fig. 2.1.

Then we could use a rotation matrix R to represent the relationship between the position of a point in the body frame and earth frame as

$$\begin{bmatrix} x_E \\ y_E \\ z_E \end{bmatrix} = R \begin{bmatrix} x_B \\ y_B \\ z_B \end{bmatrix} \tag{2.1}$$
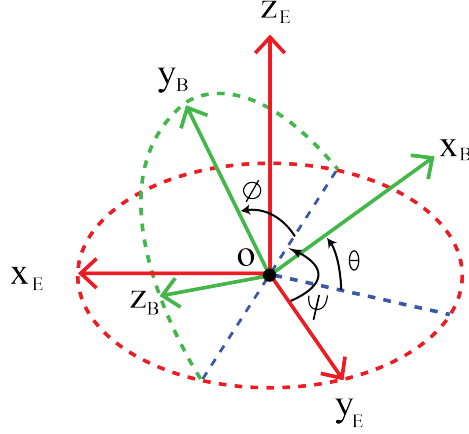
Figure 2.1: Tait-Bryan angles in Z-Y-X sequence.

where (x_E, y_E, z_E) is the position in earth frame, (x_B, y_B, z_B) is the position in body frame, and the rotation matrix

$$
R = \begin{bmatrix}
C_\theta C_\psi & -C_\phi S_\psi + S_\phi S_\theta C_\psi & S_\phi S_\psi + C_\phi S_\theta C_\psi \\
C_\theta S_\psi & C_\phi C_\psi + S_\phi S_\theta S_\psi & -S_\phi C_\psi + C_\phi S_\theta S_\psi \\
-S_\theta & S_\phi C_\theta & C_\phi C_\theta
\end{bmatrix}.
\tag{2.2}
$$

The quaternions could be used here to avoid the gimbal lock problem [119–123]. Since the quadrotor will lose control against the gravity, a 90 degree pitch angle should not be allowed, so the rotation matrix should suit our problem.

2.2 Rigid Body Dynamics

The dynamics of a rigid body under external forces and moments expressed in in inertial frame are governed by

$$
m\dot{v} + \omega \times mv = \Sigma F
\tag{2.3}
$$

$$
J\dot{\omega} + \omega \times J\omega = \Sigma T
\tag{2.4}
$$

where $\Sigma F \in \mathbb{R}^3$ and $\Sigma T \in \mathbb{R}^3$ represents the external forces and torques acting on the vehicle, v is the velocity in the body frame, ω is the angular rate of the vehicle, m is the quadrotor mass, and J the moment of inertial matrix.

The dynamic model used in this work is similar to the ones in [6] and [124], which includes kinematics, centripetal forces, gyroscopic moment as well as the drag effect. The effect of the angular velocity changing of rotors is omitted because it is relatively small [124].

2.2.1 Kinematics

The Newton equation for acceleration is

$$\ddot{\boldsymbol{\xi}}_E = \boldsymbol{F}_E/m, \tag{2.5}$$

where $\boldsymbol{\xi}_E = [x_E, y_E, z_E]^T$, the net external force $\boldsymbol{F}_E$ applied on the quadrotor in the earth frame is

$$\boldsymbol{F}_E = R_{EB}\boldsymbol{F}_B - \boldsymbol{G} - \boldsymbol{f}_t, \tag{2.6}$$

where the translational drag effect $\boldsymbol{f}_t$ is related to $\dot{\boldsymbol{\xi}}_E$, the rotation matrix from the body frame to the earth frame

$$R_{EB} = \begin{bmatrix} C_\theta C_\psi & S_\phi S_\theta C_\psi - C_\phi S_\psi & S_\phi S_\psi + C_\phi S_\theta C_\psi \\ C_\theta S_\psi & C_\phi C_\psi + S_\phi S_\theta S_\psi & C_\phi S_\theta S_\psi - S_\phi C_\psi \\ -S_\theta & S_\phi C_\theta & C_\phi C_\theta \end{bmatrix}, \tag{2.7}$$

where C_* and S_* represent the cosine and sine function for certain attitude angle respectively. We use Tait-Bryan angles [118] with Z-Y-X rotation sequence in this work to present the orientation of the body frame according to the earth frame, where ϕ is the roll angle, θ is the pitch angle, and ψ is the yaw angle. For a quadrotor, the forces generated by the rotors are all parallel to z_B axis. So the components of $\boldsymbol{F}_B$ on

x_B and y_B are zero. Then (2.5) can be written as

$$\ddot{\boldsymbol{\xi}}_E = R_{EB}[0, 0, F_z]^T/m - [0, 0, g]^T - \boldsymbol{f}_t/m. \tag{2.8}$$

The entries of matrix R_{EB} is dependent on the current attitude of the quadrotor. The attitude angles are dominated by the torques generated from the rotors as explained in following section .

2.2.2 Rolling Moments

The Euler-Lagrangian equation for centripetal forces and gyroscopic moment is

$$\boldsymbol{J}\dot{\boldsymbol{\nu}} + \boldsymbol{\nu} \times \boldsymbol{J}\boldsymbol{\nu} = \boldsymbol{T}_B - \boldsymbol{f}_r, \tag{2.9}$$

where $\boldsymbol{J} = \text{diag}\{J_x, J_y, J_z\}$, $\boldsymbol{T}_B = [T_x, T_y, T_z]^T$, $\boldsymbol{\nu} = [p, q, r]^T$, the rotational drag effect $\boldsymbol{f}_r$ is related to $\boldsymbol{\nu}$.

The values of the attitude angle are important for solving (2.8), but the angular velocities are not the first order derivatives of the attitude angles. It is known that there exists a transformation relationship for angular velocities from the earth frame to the body frame as

$$\boldsymbol{\nu} = W_\eta \dot{\boldsymbol{\eta}}, \tag{2.10}$$

where $\boldsymbol{\eta} = [\phi, \theta, \psi]^T$, W_η is the transformation matrix

$$W_\eta = \begin{bmatrix} 1 & 0 & -S_\theta \\ 0 & C_\phi & S_\phi C_\theta \\ 0 & -S_\phi & C_\phi C_\theta \end{bmatrix}. \tag{2.11}$$

W_η is only invertible when $\theta \neq \pm\frac{\pi}{2}$, so the pitch angle θ is not allowed to be $\pm\frac{\pi}{2}$. By applying W_η^{-1} to both sides of (2.10), we have the transformation relationship for

angular velocities from the body frame to the earth frame as

$$\dot{\boldsymbol{\eta}} = W_\eta^{-1}\boldsymbol{\nu}, \tag{2.12}$$

where

$$W_\eta^{-1} = \begin{bmatrix} 1 & S_\phi T_\theta & C_\phi T_\theta \\ 0 & C_\phi & -S_\phi \\ 0 & S_\phi/C_\theta & C_\phi/C_\theta \end{bmatrix}. \tag{2.13}$$

Then the attitude angles can be found by the angular speed; and the there is no missing information for equation (2.8).

2.3 Model Reference Adaptive Control

Model reference adaptive control is a well established advanced control method for systems with uncertainties. The fundamental idea of the method is expressed in [27,82]. The design for multirotors will follow the approach of the multivariable MRAC with state feedback for output tracking in [125], the technique of single input single output (SISO) MRAC with state feedback for output tracking in [27] and the high-frequency gain matrix decompositions technique in [126].

The interactor matrix $\xi_m(s)$ and high-frequency gain matrix K_p are crucial for selecting the reference model and updating the parameters of the adaptive controller. For example, the controller structure of state feedback output tracking is given as

$$\Delta u_p(t) = K_x \Delta x_p(t) + K_r r(t) + k_f, \tag{2.14}$$

the adaptive parameter matrices K_x, K_r and k_f will be updated from adaptive laws as in [125] using the knowledge of $\xi_m(s)$ and the signs of leading principal minors of K_p.

Limited by the ability of measurement, the output information is not always available. Then an adaptive controller with output feedback for output tracking can be designed as

$$\Delta u_p(t) = \Theta_1^T w_1(t) + \Theta_2^T w_2(t) + \Theta_{20}\Delta y_p(t) + \Theta_3 r(t) + \Theta_f, \qquad (2.15)$$

for some filter signal $w_1(t)$ on $\Delta u_p(t)$ and filter signal $w_2(t)$ on $\Delta y_p(t)$, the adaptive parameters $\Theta_1, \Theta_2, \Theta_{20}, \Theta_3$ and Θ_f are updated according to the information of the interactor matrix $\xi_m(s)$ and the signs of the leading principal minors of K_p.

A controller structure of state feedback for state tracking is also given in [27], which will not be discussed in this paper. The state tracking requires complete information of the matrix B_p in (3.14), which is impossible for a quadrotor with parameter uncertainties. However, as shown in [47] and [58], the prior information for the output tracking remains fixed when the system parameters are changing for a quadrotor at hover condition.

The important preliminaries for MRAC design are given as follows.

Interactor matrix and high frequency gain matrix

The transfer function of the linearized system at (x_o, u_o) is defined as $G(s) = C(sI - A)^{-1}B$. Then the crucial priori information for the design of the MRAC scheme, can be specified form the following lemma.

Lemma 1 [27]. *For any $M \times M$ strictly proper and full rank rational matrix $G(s)$, there exists a lower triangular polynomial matrix $\xi_m(s)$, defined as the left modified*

interactor matrix (LMI) of $G(s)$, of the form

$$\xi_m(s)=\begin{bmatrix} d_1(s) & 0 & \cdots & & 0 \\ h_{21}^m(s) & d_2(s) & & \ddots & \vdots \\ & & \ddots & & \\ \vdots & \ddots & & d_{m-1}(s) & 0 \\ h_{m1}^m(s) & \cdots & & h_{m\ m-1}^m(s) & d_m(s) \end{bmatrix}, \qquad (2.16)$$

where $h_{ij}^m(s)$ are polynomials, and $d_k(s)$ are monic stable polynomials, such that the high-frequency gain matrix

$$K_p = \lim_{s\to\infty} \xi_m(s)G(s), \qquad (2.17)$$

is finite and nonsingular.

Plant assumptions

The following conditions are required for the design of a multivariable MRAC scheme of state feedback output tracking [27]:

(A1) all zeros of $G(s)$ have negative real parts;

(A2) (A, B) is stabilizable and (A, C) is detectable;

(A3) $G(s)$ has full rank and its modified left interactor matrix $\xi_m(s)$ of $G(s)$ is known; and

(A4) all leading principal minors Δ_k of the high-frequency gain matrix K_p are nonzero and their signs are known.

The condition (A1) is needed for stable plant-model output matching. Condition (A2) is needed for internal stability under stable output matching. Condition (A3) is needed to select a reference model system for plant-model output matching, and (A4) is needed for designing adaptive laws which converge in the correct direction.

Chapter 3

Models of Multirotors

This chapter investigates the models of multirotor systems at different levels. There are two major ways to category multirotor systems. Form the view of dynamics, they are either under-actuated or fully-actuated. In respect to actuation, they are systems of different numbers of actuators or/and with different arrangements of these actuators. The mathematical model of actuator failures is also explained.

3.1 Structures of Multirotor Systems

In this section, we display the physical structure of quadrotors, which have four rotors, and hexarotors, which have six rotors. The octorotors with eight rotors and other multirotors with ten or more rotors are similar in structure.

3.1.1 Quadrotor System

A quadrotor, as shown in Figure 3.1, has four arms with same length and weight. The extended lines of the arms should intersect at the center of the quadrotor. There is a rotor at each arm and the rotors are assumed to be the same. We define two coordinate systems in Figure 3.1, which are the body frame (o_B, x_B, y_B, z_B) and the
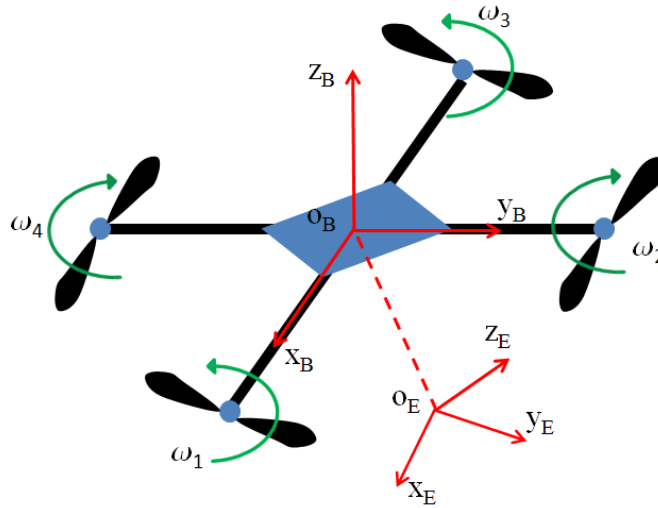
Figure 3.1: The structure and coordinate frames of a quadrotor.

earth frame (o_E, x_E, y_E, z_E). The origin of the body frame o_B is set at the geometry center of the quadrotor; and it is assumed that the mass center of the quadrotor also coincides with o_B. The x_B and y_B axes are set on the arms of rotor 1 and 2, the z_B axis is determined via right hand rule. For the convenience of analyzing the system in a precise and clear way, the variables are often not studied in one single coordinate frame. For example, the position and attitude of the quadrotor are described in the earth coordinate system, while the forces, torques and angular velocities are in the body frame of the quadrotor.

Note that the rotation direction for rotor 1 and 3 are set as counter clockwise and for rotor 2 and 4 clockwise. The directions of the rotors are preset and should not rotate in reverse at most occasions. Though most quadrotors are equipped with DC motors and able to rotate reversely with a reverse current, we could achieve same dynamic effect through control the symmetrical rotors strategically.

3.1.2   Hexarotor Systems

Unlike a quadrotor, a hexarotor has many different designs in structure and rotor arrangement. In this work, we study the hexarotor with its six rotors placed at the six

vertices of a regular hexagon, whose structure is shown in Figure 3.2. The mass center
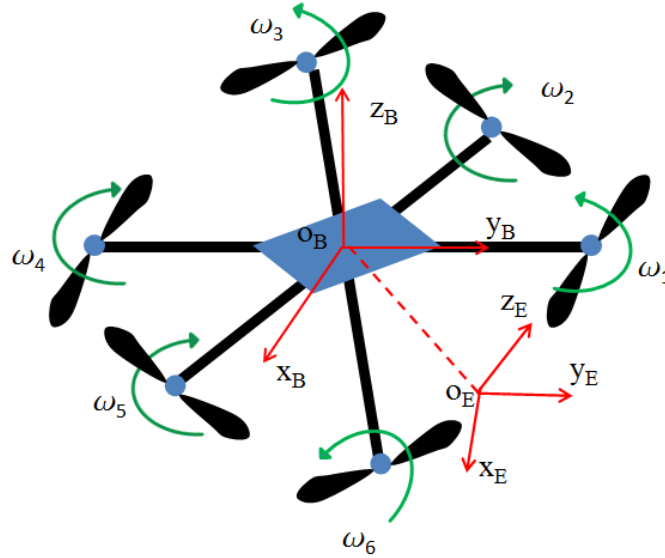
Figure 3.2: The structure of a hexarotor with NNPPNP rotor arrangement.

of the whole system is assumed to be at the geometry center of the hexagon. Such symmetric design can enhance the stability of the system and decrease the difficulty of control allocation design. This research studies the compensation scheme dealing with the uncertainties of the rotor failures but not the system parameter uncertainties caused by mass center shifting.

As shown in Figure 3.2, the rotor 1, 3 and 6 rotate counterclockwise; and the rotor 2, 4 and 5 rotate clockwise. This rotor arrangement is called as NNPPNP [75] compared to the NPNPNP rotor arrangement used in most of the past literature and shown in Figure 3.3. For the hexarotor in Figure 3.3, the rotor 1, 3 and 5 rotate counterclockwise; and the rotor 2, 4 and 6 rotate clockwise. The NNPPNP rotor arrangement leads to more difficulty in control allocation than NPNPNP, but as demonstrated in [74] and [69] that a hexarotor with NNPPNP rotor arrangement has better performance in fault tolerance than the one with NPNPNP. So in this paper the hexarotor with NNPPNP rotor arrangement is studied for the adaptive compensation of actuator failures.
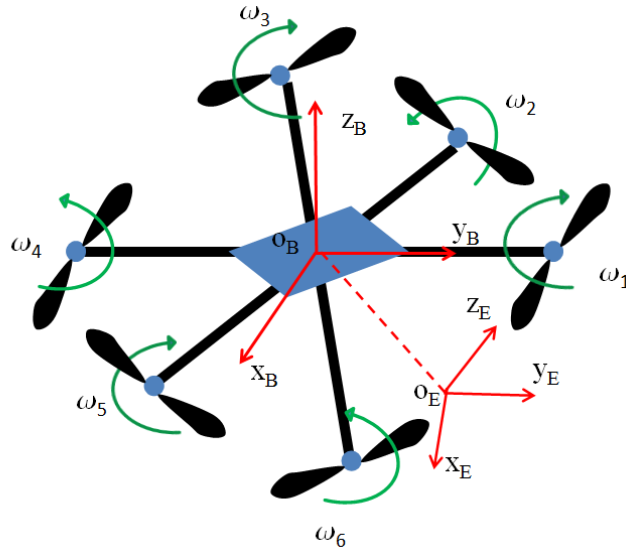
Figure 3.3: The structure of a hexarotor with NPNPNP rotor arrangement.

Remark 2. Note that the rotor arrangement in Figure 3.2 is actually PNPNNP. In the view of actuation, PNPNNP has no difference as NNPPNP. Similarly, PNPNPN should be the same compensability as NPNPNP.   □

3.2   Dynamics Model for Motion Control

3.2.1   Under-Actuated Multirotor Systems

Nonlinear model

By integrating the kinematics equation as (2.8), the rolling moments equation as (2.9), and the rotational relationship as (2.12), the nonlinear model of the quadrotor model

can be built into state-space form as

$$\ddot{x}_E = (S_\phi S_\psi + C_\phi S_\theta C_\psi)\frac{F_z}{m} - \frac{c_t}{m}\dot{x}_E \tag{3.1}$$

$$\ddot{y}_E = (C_\phi S_\theta S_\psi - S_\phi C_\psi)\frac{F_z}{m} - \frac{c_t}{m}\dot{y}_E \tag{3.2}$$

$$\ddot{z}_E = C_\phi C_\theta \frac{F_z}{m} - g - \frac{c_t}{m}\dot{z}_E \tag{3.3}$$

$$\dot{p} = qr(\frac{J_y - J_z}{J_x}) - \frac{1}{J_x}c_r p + \frac{T_x}{J_x} \tag{3.4}$$

$$\dot{q} = pr(\frac{J_z - J_x}{J_y}) - \frac{1}{J_y}c_r q + \frac{T_y}{J_y} \tag{3.5}$$

$$\dot{r} = pq(\frac{J_x - J_y}{J_z}) - \frac{1}{J_z}c_r r + \frac{T_z}{J_z} \tag{3.6}$$

$$\dot{\phi} = p + qS_\phi T_\theta + rC_\phi T_\theta \tag{3.7}$$

$$\dot{\theta} = qC_\phi - rS_\phi \tag{3.8}$$

$$\dot{\psi} = \frac{1}{C_\theta}(qS_\phi + rC_\phi). \tag{3.9}$$

The state vector of the system is chosen as

$$x_p = [x_E, y_E, z_E, \dot{x}_E, \dot{y}_E, \dot{z}_E, \phi, \theta, \psi, p, q, r]^T. \tag{3.10}$$

The most significant difference between our dynamic model in this paper and the one used in [47] and [58] is that the angular velocities of the quadrotor are not considered as the first-order derivatives of the attitude angles. The relation between the attitude angles and the angular velocities in the body frame are depicted in (2.12). Then the quadrotor is relaxed to work at non-equilibrium operating points other than the special hover condition. The other significant difference is that the drag effect is taken into consideration.

Output selection

Though a quadrotor with the structure in Figure 3.1 has six degrees of freedom (DOF), a quadrotor is an under-actuated system with four actuators since only four degrees of freedom can be controlled [24]. We choose the output vector of the system in this work as

$$y_p = [z_E, y_E, x_E, \psi]^T. \tag{3.11}$$

Linearized model

Let us rewrite the dynamics model in (3.1) - (3.9) into the more concise form as

$$\dot{x}_p(t) = f(x_p(t), u_p(t)). \tag{3.12}$$

Denoting an operating point as (x_o, u_o), the Taylor series expansion yields

$$\dot{x}_p(t) \cong f(x_o, u_o) + \frac{\partial f}{\partial x_p}\Big|_{(x_o, u_o)} (x_p(t) - x_o) + \frac{\partial f}{\partial u}\Big|_{(x_o, u_o)} (u_p(t) - u_o) + \text{H.O.T.} \tag{3.13}$$

Omitting the higher order terms (H.O.T.), we have

$$\Delta \dot{x}_p(t) = A_p \Delta x_p(t) + B_p \Delta u_p(t) + f(x_o, u_o), \tag{3.14}$$

where $\Delta x_p(t) = x_p(t) - x_o$, $\Delta u_p(t) = u_p(t) - u_o$, the parameter matrices

$$A_p = \begin{bmatrix} 0_{3\times3} & I_{3\times3} & 0_{3\times3} & 0_{3\times3} \\ 0_{3\times3} & -c_t I_{3\times3} & A_t & 0_{3\times3} \\ 0_{3\times3} & 0_{3\times3} & A_s & A_w \\ 0_{3\times3} & 0_{3\times3} & 0_{3\times3} & A_r \end{bmatrix}$$

$$
B_p =
\begin{bmatrix}
0_{3\times1} & 0_{3\times3} \\
B_t & 0_{3\times3} \\
0_{3\times1} & 0_{3\times3} \\
0_{3\times1} & B_r
\end{bmatrix},
$$

with the submatrices

$$
A_t =
\begin{bmatrix}
C_\phi S_\psi - S_\phi S_\theta C_\psi & C_\phi C_\theta C_\psi & S_\phi C_\psi - C_\phi S_\theta S_\psi \\
-C_\theta C_\psi - S_\phi S_\theta S_\psi & C_\phi C_\theta S_\psi & S_\phi S_\psi + C_\phi S_\theta C_\psi \\
-S_\phi C_\theta & -C_\phi S_\theta & 0
\end{bmatrix}
\frac{F_z}{m}
$$

$$
A_r =
\begin{bmatrix}
-\dfrac{c_r}{J_x} & r\left(\dfrac{J_y - J_z}{J_x}\right) & q\left(\dfrac{J_y - J_z}{J_x}\right) \\
r\left(\dfrac{J_z - J_x}{J_y}\right) & -\dfrac{c_r}{J_y} & p\left(\dfrac{J_z - J_x}{J_y}\right) \\
q\left(\dfrac{J_x - J_y}{J_z}\right) & p\left(\dfrac{J_x - J_y}{J_z}\right) & -\dfrac{c_r}{J_z}
\end{bmatrix}
$$

$$
A_s =
\begin{bmatrix}
qC_\phi T_\theta - rS_\phi T_\theta & \dfrac{qS_\phi + rC_\phi}{C_\theta^2} & 0 \\
-qS_\phi - rC_\phi & 0 & 0 \\
\dfrac{qC_\phi - rS_\phi}{C_\theta} & \dfrac{S_\theta}{C_\theta^2}(qS_\phi + rC_\phi) & 0
\end{bmatrix}
$$

$$
A_w =
\begin{bmatrix}
1 & S_\phi T_\theta & C_\phi T_\theta \\
0 & C_\phi & -S_\phi \\
0 & \dfrac{S_\phi}{C_\theta} & \dfrac{C_\phi}{C_\theta}
\end{bmatrix}
$$

$$
B_t =
\begin{bmatrix}
S_\phi S_\psi + C_\phi S_\theta C_\psi \\
-S_\phi C_\psi + C_\phi S_\theta S_\psi \\
C_\phi C_\theta
\end{bmatrix}
\frac{1}{m}
$$

$$
B_r = \mathrm{diag}\left\{ \dfrac{1}{J_x} \quad \dfrac{1}{J_y} \quad \dfrac{1}{J_z} \right\}.
$$

Recall that the output is chosen as (3.11), then the output of the linearized model is

$$\Delta y_p = C_p \Delta x_p, \tag{3.15}$$

with

$$C_p = \begin{bmatrix} C_t & 0_{3\times3} & 0_{3\times3} & 0_{3\times3} \\ 0_{1\times3} & 0_{1\times3} & C_r & 0_{1\times3} \end{bmatrix}$$

where the submatrices

$$C_t = \begin{bmatrix} 0 & 0 & 1 \\ 0 & 1 & 0 \\ 1 & 0 & 0 \end{bmatrix}, \quad C_r = \begin{bmatrix} 0 & 0 & 1 \end{bmatrix}.$$

Then with the information of certain operating points, we can deduct the transfer matrices at some typical operating points, which have the form

$$G_0(s) = C_p(sI - A_p)^{-1}B_p. \tag{3.16}$$

The transfer matrix is a useful system characteristic of the linearized model, which represents the input-output relationship. It is also important for investigating the prior system information for the design of adaptive controllers.

3.2.2   Fully-Actuated Multirotor Systems

The fully-actuated multirotors have a different propeller system from the underactuated multirotors. The thrust force generated by a rotor does not parallel to the z_B axis in the body frame. As shown in Figure 3.4, z_p is not parallel to z_B. In this paper we choose the rotation angles from the body frame to the propeller frame as $(-\pi/6, \pi/6, \pi/6)$.
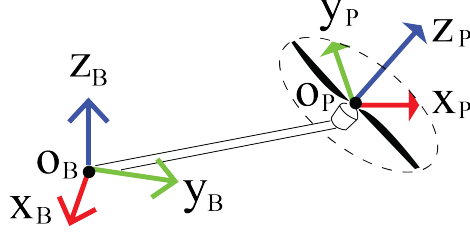
Figure 3.4: A propeller system with tilted rotor.

Nonlinear dynamic model

The nonlinear dynamic model of fully-actuated omni-directional multirotor systems

for motion control is

$$\ddot{x}_E = C_\theta C_\psi \frac{F_x}{m} + (S_\phi S_\theta C_\psi - C_\phi S_\psi)\frac{F_y}{m} + (S_\phi S_\psi + C_\phi S_\theta C_\psi)\frac{F_z}{m} - \frac{c_t}{m}\dot{x}_E \qquad (3.17)$$

$$\ddot{y}_E = C_\theta S_\psi \frac{F_x}{m} + (C_\phi C_\psi + S_\phi S_\theta S_\psi)\frac{F_y}{m} + (C_\phi S_\theta S_\psi - S_\phi C_\psi)\frac{F_z}{m} - \frac{c_t}{m}\dot{y}_E \qquad (3.18)$$

$$\ddot{z}_E = -S_\theta \frac{F_x}{m} + S_\phi C_\theta \frac{F_y}{m} + C_\phi C_\theta \frac{F_z}{m} - g - \frac{c_t}{m}\dot{z}_E \qquad (3.19)$$

$$\dot{p} = qr\left(\frac{J_y - J_z}{J_x}\right) - \frac{1}{J_x}c_r p + \frac{T_x}{J_x} \qquad (3.20)$$

$$\dot{q} = pr\left(\frac{J_z - J_x}{J_y}\right) - \frac{1}{J_y}c_r q + \frac{T_y}{J_y} \qquad (3.21)$$

$$\dot{r} = pq\left(\frac{J_x - J_y}{J_z}\right) - \frac{1}{J_z}c_r r + \frac{T_z}{J_z} \qquad (3.22)$$

$$\dot{\phi} = p + qS_\phi T_\theta + rC_\phi T_\theta \qquad (3.23)$$

$$\dot{\theta} = qC_\phi - rS_\phi \qquad (3.24)$$

$$\dot{\psi} = \frac{1}{C_\theta}(qS_\phi + rC_\phi). \qquad (3.25)$$

Different from the widely studies under-actuated multirotors (like a quadrotor), the

multirotor systems in this paper can generate thrust forces in the y_B and x_B direction

of its body frame.

  The state vector is

$$x_p = [x_E, y_E, z_E, \dot{x}_E, \dot{y}_E, \dot{z}_E, \phi, \theta, \psi, p, q, r]^T, \qquad (3.26)$$

The input vector is chosen as

$$u_p(t) = [F_x, F_y, F_z, T_x, T_y, T_z]^T. \tag{3.27}$$

The output vector is chosen as

$$y_p = [x_E, y_E, z_E, \phi, \theta, \psi]^T. \tag{3.28}$$

Linearized model

The Taylor series expansion of the nonlinear system around an operating condition (x_o, u_o) yields

$$\dot{x}_p(t) \cong f(x_o, u_o) + \frac{\partial f}{\partial x_p}\bigg|_{(x_o,u_o)} (x_p(t) - x_o) + \frac{\partial f}{\partial u}\bigg|_{(x_o,u_o)} (u_p(t) - u_o) + \text{H.O.T.} \tag{3.29}$$

Omitting the higher order terms (H.O.T.), we have

$$\Delta \dot{x}_p(t) = A_p \Delta x_p(t) + B_p \Delta u_p(t) + f(x_o, u_o), \tag{3.30}$$

where $\Delta x_p(t) = x_p(t) - x_o$, $\Delta u_p(t) = u_p(t) - u_o$, the parameter matrices

$$A_p = \begin{bmatrix} 0_{3\times3} & I_{3\times3} & 0_{3\times3} & 0_{3\times3} \\ 0_{3\times3} & -c_t I_{3\times3} & A_t & 0_{3\times3} \\ 0_{3\times3} & 0_{3\times3} & A_s & A_w \\ 0_{3\times3} & 0_{3\times3} & 0_{3\times3} & A_r \end{bmatrix}$$

$$B_p = \begin{bmatrix} 0_{3\times3} & 0_{3\times3} \\ B_t & 0_{3\times3} \\ 0_{3\times3} & 0_{3\times3} \\ 0_{3\times3} & B_r \end{bmatrix},$$

with the submatrices

$$A_t = \begin{bmatrix} C_\phi S_\psi - S_\phi S_\theta C_\psi & C_\phi C_\theta C_\psi & S_\phi C_\psi - C_\phi S_\theta S_\psi \\ -C_\theta C_\psi - S_\phi S_\theta S_\psi & C_\phi C_\theta S_\psi & S_\phi S_\psi + C_\phi S_\theta C_\psi \\ -S_\phi C_\theta & -C_\phi S_\theta & 0 \end{bmatrix} \frac{g}{C_{\theta_o} C_{\phi_o}}$$

$$A_r = \begin{bmatrix} -\dfrac{c_r}{J_x} & r\left(\dfrac{J_y - J_z}{J_x}\right) & q\left(\dfrac{J_y - J_z}{J_x}\right) \\ r\left(\dfrac{J_z - J_x}{J_y}\right) & -\dfrac{c_r}{J_y} & p\left(\dfrac{J_z - J_x}{J_y}\right) \\ q\left(\dfrac{J_x - J_y}{J_z}\right) & p\left(\dfrac{J_x - J_y}{J_z}\right) & -\dfrac{c_r}{J_z} \end{bmatrix}$$

$$A_s = \begin{bmatrix} qC_\phi T_\theta - rS_\phi T_\theta & \dfrac{qS_\phi + rC_\phi}{C_\theta^2} & 0 \\ -qS_\phi - rC_\phi & 0 & 0 \\ \dfrac{qC_\phi - rS_\phi}{C_\theta} & \dfrac{S_\theta}{C_\theta^2}(qS_\phi + rC_\phi) & 0 \end{bmatrix}$$

$$A_w = \begin{bmatrix} 1 & S_\phi T_\theta & C_\phi T_\theta \\ 0 & C_\phi & -S_\phi \\ 0 & \dfrac{S_\phi}{C_\theta} & \dfrac{C_\phi}{C_\theta} \end{bmatrix}$$

$$B_t = \begin{bmatrix} C_\theta C_\psi & S_\phi S_\theta C_\psi - C_\phi S_\psi & S_\phi S_\psi + C_\phi S_\theta C_\psi \\ C_\theta S_\psi & C_\phi C_\psi + S_\phi S_\theta S_\psi & C_\phi S_\theta S_\psi - S_\phi C_\psi \\ -S_\theta & S_\phi C_\theta & C_\phi C_\theta \end{bmatrix} \frac{1}{m}$$

$$B_r = \text{diag}\left\{ \frac{1}{J_x} \quad \frac{1}{J_y} \quad \frac{1}{J_z} \right\}.$$

3.3   Effector Model and Control Allocation

3.3.1   Quadrotor

The four rotors on the quadrotor in Figure 3.1 are the direct actuators of the system. The force generated by rotor i is

$$f_i = c_f \omega_i^2, \quad i = 1, 2, 3, 4. \tag{3.31}$$

However, the forces are not directly expressed in the dynamic equations (2.8) and (2.9). Let us denote a intermediate input vector as

$$u_p(t) = [F_z, T_x, T_y, T_z]^T. \tag{3.32}$$

From the structure of the quadrotor, the relationship between the forces generated by each rotor and u_p can be deducted by Newton's laws as

$$[F_z, T_x, T_y, T_z]^T = C_a[f_1, f_2, f_3, f_4]^T, \tag{3.33}$$

where C_a is the actuation mapping matrix

$$C_a = \begin{bmatrix} 1 & 1 & 1 & 1 \\ 0 & d & 0 & -d \\ -d & 0 & d & 0 \\ -c_m & c_m & -c_m & c_m \end{bmatrix}. \tag{3.34}$$

Since the determinant of the actuation mapping matrix C_a as in (3.34) is $-8c_m d^2 \neq 0$, the matrix is always nonsingular and the value of ω_i can always be solved from the

input vector by

$$[f_1, f_2, f_3, f_4]^T = C_a^{-1}[F_z, T_x, T_y, T_z]^T. \tag{3.35}$$

Then u_p in (3.32) is valid to be the input vector and the force generated by each rotor can be calculated from u_p. Since the goal of this paper is to generate proper control input u_p for the motion control of the quadrotor, we only explain the feasibility of the choice in (3.32) but not discuss the control allocation in detail.

3.3.2   Hexarotors

There are six rotors on a hexarotor UAV, each of which generates a thrust force. We denote the control input vector of the plant as

$$u_p = [f_1, f_2, f_3, f_4, f_5, f_6]^T, \tag{3.36}$$

where f_i is the thrust generated by the ith rotor that

$$f_i = c_f \omega_i^2, \quad i = 1, 2, 3, 4, 5, 6, \tag{3.37}$$

where c_f is the thrust coefficient, ω_i is the rotating velocity of the ith rotor.

When the thrusts from the rotors and the structure of the hexarotor are known, the total forces and torques can be obtained through the linear effector model [127] as

$$w_p(t) = C_a u_p(t), \tag{3.38}$$

where the control effectiveness matrix C_a, which is called actuation mapping matrix in [84], is denoted as

$$
C_a = \begin{bmatrix}
1 & 1 & 1 & 1 & 1 & 1 \\
d & \frac{\sqrt{3}}{2}d & -\frac{\sqrt{3}}{2}d & -d & -\frac{\sqrt{3}}{2}d & \frac{\sqrt{3}}{2}d \\
0 & \frac{1}{2}d & \frac{1}{2}d & 0 & -\frac{1}{2}d & -\frac{1}{2}d \\
-c_m & c_m & -c_m & c_m & c_m & -c_m
\end{bmatrix}. \tag{3.39}
$$

Control allocation

The effector model depicts the mechanical relations of the hexarotor. Control allocation is an inverse problem in control design, which generates a control signal $u_p(t)$ based on the intermediate input $w_p(t)$ obtained by a desired motion control algorithm. The control allocation problem for the hexarotor can be denoted by specifying a matrix Λ for the linear relation

$$
u_p(t) = \Lambda w_p(t), \tag{3.40}
$$

where Λ is the control allocation matrix to be designed.

For a quadrotor, which has four inputs and four outputs, the control allocation matrix is the inverse of the control effectiveness matrix: $\Lambda = C_a^{-1}$. For the hexarotors, the form of Λ is not unique, for example, the matrices

$$
\Lambda_0 = \begin{bmatrix}
\frac{1}{6} & \frac{2}{13d} & 0 & -\frac{3}{26c_m} \\
\frac{1}{6} & \frac{3\sqrt{3}}{26d} + \frac{1}{13d} & \frac{1}{2d} & \frac{\sqrt{3}}{26c_m} + \frac{5}{26c_m} \\
\frac{1}{6} & -\frac{3\sqrt{3}}{26d} - \frac{1}{13d} & \frac{1}{2d} & -\frac{\sqrt{3}}{26c_m} - \frac{5}{26c_m} \\
\frac{1}{6} & -\frac{2}{13d} & 0 & \frac{3}{26c_m} \\
\frac{1}{6} & -\frac{3\sqrt{3}}{26d} + \frac{1}{13d} & -\frac{1}{2d} & -\frac{\sqrt{3}}{26c_m} + \frac{5}{26c_m} \\
\frac{1}{6} & \frac{3\sqrt{3}}{26d} - \frac{1}{13d} & -\frac{1}{2d} & \frac{\sqrt{3}}{26c_m} - \frac{5}{26c_m}
\end{bmatrix} \tag{3.41}
$$

and

$$\Lambda_1 = \begin{bmatrix} 0 & 0 & 0 & 0 \\ \frac{8+\sqrt{3}}{44} & \frac{2+3\sqrt{3}}{22d} & \frac{1}{2d} & \frac{8+\sqrt{3}}{44c_m} \\ \frac{11-\sqrt{3}}{44} & \frac{-3\sqrt{3}}{22d} & \frac{1}{2d} & \frac{-11-\sqrt{3}}{44c_m} \\ \frac{3}{22} & -\frac{2}{11d} & 0 & \frac{3}{22c_m} \\ \frac{8-\sqrt{3}}{44} & \frac{2-3\sqrt{3}}{22d} & -\frac{1}{2d} & \frac{8-\sqrt{3}}{44c_m} \\ \frac{11+\sqrt{3}}{44} & \frac{3\sqrt{3}}{22d} & -\frac{1}{2d} & \frac{-11+\sqrt{3}}{44c_m} \end{bmatrix} \tag{3.42}$$

are both valid candidates for Λ.

3.4   Actuator Failure Model

In the presence of actuator failures, the input of the a system can be expressed as

$$u(t) = v(t) + \sigma(t)(\bar{u}(t) - v(t)) = (I - \sigma(t))v(t) + \sigma(t)\bar{u}(t), \tag{3.43}$$

where

$$v(t) = [v_1(t), v_2(t), ..., v_M(t)]^T \tag{3.44}$$

is the applied control input to be designed,

$$\sigma(t) = \text{diag}\{\sigma_1(t), \sigma_2(t), ..., \sigma_M(t)\} \tag{3.45}$$

is the actuator failure pattern matrix with

$$\sigma_j(t) = \begin{cases} 1 & \text{if the } j\text{th actuator failed} \\ 0 & \text{otherwise} \end{cases}, \tag{3.46}$$

and $\bar{u}(t)$ is the corresponding failure value vector:

$$\bar{u}(t) = [\bar{u}_1(t), \bar{u}_2(t), ..., \bar{u}_M(t)]^T. \tag{3.47}$$

In this work, we consider the loss-of-control failure that the failure value $\bar{u}_j(t)$, the failure time instant t_j and the failure pattern σ are all unknown. The jth element of the failure value vector can be modeled as

$$\bar{u}_j(t) = \sum_{k=1}^{l} \tau_{jk}\theta_k(t), \tag{3.48}$$

where τ_{jk} is the element at the jth row and kth column of a unknown scalar matrix τ, $\theta_k(t)$ is the kth element of a known bounded signal vector $\theta(t)$, l is the number of the candidate signals. Possible choice of $\theta_k(t)$ can be 0, 1, $\sin(t)$, $\cos(2t)$, and so on.

Based on the given actuator failure model, the most common failure types can be model as following:

- loss-of-effectiveness:

$$\bar{u}_j(t) = k_j v_j(t), \tag{3.49}$$

where $j \in \{1, 2, \ldots, M\}$, $k_j \in (0, 1)$ and $v_j(t)$ is the jth element of $v_f(t)$;

- lock-in-place:

$$\bar{u}_j(t) = \bar{u}_{j0}, \tag{3.50}$$

where $\bar{u}_{j0}$ is a constant;

- loss-of-control:

$$\bar{u}_j(t) = \bar{u}_{j0} + \sum_{k=1}^{l} \bar{u}_k \beta_k(t) + \beta_0(t), \tag{3.51}$$

where $\bar{u}_k$ is a scalar, $\beta_k(t)$ is a known signal, l is the number of the candidate signals of the failure value vector, $\beta_0(t)$ is a bounded signal.

Note that the cases of loss-of-effectiveness and lock-in-place can also be modeled by (3.51) So in this work, we use the model of loss-of-control failures where the failure time instant t_j, the failure pattern σ, the bounded signal $\beta_0(t)$, the failure values $\bar{u}_{jo}$ and $\bar{u}_k$ are all unknown.

Remark 3. Possible choices of $\beta_k(t)$ can be 0, 1, $\sin(t)$, $\cos(2t)$, and so on. Complex failure signals can then be approximated by introducing more frequencies in the sine and cosine functions. $\square$

Chapter 4

Dynamic Mutation under Different Operating Conditions

The task of this chapter is to build some technical foundations needed for model reference adaptive control of multirotors by providing the key prior information over the typical operating conditions. The following problems will be solved in this chapter.

- Figure out the typical operating conditions of the nonlinear multirotor systems, at which efficient and enlightening linearization models can be conducted.

- Clarify the mutation and invariance of the system characteristics, especially the interactor and high-frequency gain matrices, at the typical operating conditions.

4.1 Under-Actuated Multirotor Systems

This section presents a systematic study on the important system characteristics of linearized under-actuated system models. Different operating conditions of the nonlinear dynamics model are surveyed by deriving corresponding linearized models and transfer functions. We conduct a thorough study on the dynamics mutation of the systems at different typical operating conditions. We show that the interactor

matrices and the high-frequency gain matrices are parameter dependent. The operating conditions can be divided into two groups as:

1. operating conditions with diagonal interactor matrices that already satisfies the design condition;

2. operating conditions with non-diagonal interactor matrices and needs further treatments.

The first group of operating points could be controlled by one controller directly. While the interactor matrices of the second group are depended on the operating points, then a different control law is needed for every case in a group of typical operating points. It is also shown that with realistic conditions on the attitude of the quadrotor, the pattern of the signs of the leading principal minors of the high-frequency gain matrices in both groups is fixed, known and non-zero.

4.1.1 Flight Conditions with Diagonal Interactor Matrix

In this part, we discuss some fundamental operating conditions of the multirotor which have diagonal interactor matrices. The flight conditions includes general hover condition and vertical motion along the z_E axis. The interactor matrices of these conditions are diagonal, so we can directly use the controller in [47] for tracking task.

General hover condition

The hover condition is the condition that the quadrotor is hovering around some arbitrary position with arbitrary yaw angle and all the angular velocities are zero. In [47] and many other literatures, the behavior of quadrotors is only studied around a special hover condition that even the yaw angle ψ is zero. Here we work on the general hover condition that the yaw angle might not be zero. The key property of this condition is the external forces and torques are all zero and all the elements in

the rotation matrix are constant, therefore The system is at an equilibrium point (x_{hov}, u_{hov}) as

$$x_{\text{hov}} = [x_E, y_E, z_E, 0, 0, 0, 0, 0, \psi_e, 0, 0, 0]^T, \psi_e \in (-\frac{\pi}{2}, \frac{\pi}{2}) \tag{4.1}$$

$$u_{\text{hov}} = [mg, 0, 0, 0]^T, \tag{4.2}$$

where x_E, y_E, z_E are arbitrary and ψ_e is a constant. By substituting (4.1) and (4.2) into the linearized mode, the parameters matrices can be derived as

$$A_t = \begin{bmatrix} gS_{\psi_e} & gC_{\psi_e} & 0 \\ -gC_{\psi_e} & gS_{\psi_e} & 0 \\ 0 & 0 & 0 \end{bmatrix} \tag{4.3}$$

$$A_s = 0_{3\times3} \tag{4.4}$$

$$A_r = -c_r \text{ diag} \left\{ \frac{1}{J_x} \quad \frac{1}{J_y} \quad \frac{1}{J_z} \right\} \tag{4.5}$$

$$A_w = I_{3\times3} \tag{4.6}$$

$$B_t = \begin{bmatrix} 0 & 0 & \frac{1}{m} \end{bmatrix}^T \tag{4.7}$$

$$B_r = \text{diag} \left\{ \frac{1}{J_x} \quad \frac{1}{J_y} \quad \frac{1}{J_z} \right\}. \tag{4.8}$$

The transfer matrix is

$$G_{hov}(s) = \begin{bmatrix} \dfrac{1}{ms(s+c_t)} & 0 & 0 & 0 \\ 0 & -\dfrac{gC_{\psi_e}}{(c_t+s)(c_r+J_x s)s^2} & \dfrac{gS_{\psi_e},}{(c_t+s)(c_r+J_y s)s^2} & 0 \\ 0 & \dfrac{gS_{\psi_e}}{(c_t+s)(c_r+J_x s)s^2} & \dfrac{gC_{\psi_e}}{(c_t+s)(c_r+J_y s)s^2} & 0 \\ 0 & 0 & 0 & \dfrac{1}{s(c_r+J_z s)} \end{bmatrix}. \tag{4.9}$$

Different from the special hover condition studied in [47], the transfer matrix at generalized hover condition is not diagonal. We can tell from (4.9) that the input-

output pairs (F_z, z) and (T_z, ψ) are still independent, while (T_x, y) and (T_y, x) are coupled. The reason for this is when the yaw angle is zero, the axes x_B, y_B coincide with x_E, y_E, so there is no composition. But when the yaw angle is nonzero, because the input torque T_i and the output position are defined in different coordinate frames, the coordinate transformation will lead to decomposition as shown in G_{hov}.

The modified left interactor (MLI) matrix is obtained as

$$\xi_{m,hov}(s) = \begin{bmatrix} (s+1)^2 & 0 & 0 & 0 \\ 0 & (s+1)^4 & 0 & 0 \\ 0 & 0 & (s+1)^4 & 0 \\ 0 & 0 & 0 & (s+1)^2 \end{bmatrix}, \tag{4.10}$$

and the high frequency gain matrix is

$$K_{p,hov} = \begin{bmatrix} 1/m & 0 & 0 & 0 \\ 0 & -gC_{\psi_e}/J_x & gS_{\psi_e}/J_y & 0 \\ 0 & gS_{\psi_e}/J_x & gC_{\psi_e}/J_y & 0 \\ 0 & 0 & 0 & 1/J_z \end{bmatrix}. \tag{4.11}$$

If ψ_e is in $(-\pi/2, \pi/2)$ as (4.1), then the leading principal minors of K_p are known and nonzero as

$$\Delta_1 > 0, \Delta_2 < 0, \Delta_3 < 0, \Delta_4 < 0, \tag{4.12}$$

where Δ_k is the kth order leading principal minors of K_p. With the constraint, $\xi_m(s)$ and the signs of leading principal minors of K_p under this generalized hover condition are consistent with the special hover condition as in [47].

The constraint in (4.1) means the x_B axis of body frame should not point backwards in the view of earth frame. It is a realistic condition if we allow the pitch angle to be

negative and the quadrotor flies backwards.

Vertical motion condition along z_E axis

The operating point is given by (x_{ver}, u_{ver}) as

$$x_{ver} = [x_E, y_E, z_E, 0, 0, \dot{z}_o, 0, 0, 0, 0, 0, 0]^T \tag{4.13}$$

$$u_{ver} = [mg, 0, 0, 0]^T, \tag{4.14}$$

where x, y, z are arbitrary, $\dot{z}_o$ is a constant. The parameter matrices are derived as

$$A_t = \begin{bmatrix} 0 & g & 0 \\ -g & 0 & 0 \\ 0 & 0 & 0 \end{bmatrix} \tag{4.15}$$

$$A_s = 0_{3\times3} \tag{4.16}$$

$$A_r = -c_r \, \text{diag} \left\{ \frac{1}{J_x} \quad \frac{1}{J_y} \quad \frac{1}{J_z} \right\} \tag{4.17}$$

$$A_w = I_{3\times3} \tag{4.18}$$

$$B_t = \begin{bmatrix} 0 & 0 & \frac{1}{m} \end{bmatrix}^T \tag{4.19}$$

$$B_r = \text{diag} \left\{ \frac{1}{J_x} \quad \frac{1}{J_y} \quad \frac{1}{J_z} \right\}. \tag{4.20}$$

The transfer matrix is

$$G_{ver}(s) = \begin{bmatrix} \dfrac{1}{ms(s + c_t)} & 0 & 0 & 0 \\ 0 & -\dfrac{g}{(c_t + s)(c_r + J_x s)s^2} & 0 & 0 \\ 0 & 0 & \dfrac{g}{(c_t + s)(c_r + J_y s)s^2} & 0 \\ 0 & 0 & 0 & \dfrac{1}{s(c_r + J_z s)} \end{bmatrix}. \tag{4.21}$$

The modified left interactor (MLI) matrix is obtained as

$$
\xi_{m,ver}(s) =
\begin{bmatrix}
(s+1)^2 & 0 & 0 & 0 \\
0 & (s+1)^4 & 0 & 0 \\
0 & 0 & (s+1)^4 & 0 \\
0 & 0 & 0 & (s+1)^2
\end{bmatrix},
\tag{4.22}
$$

which is consistent with the general hover condition as (4.10) and the high-frequency gain matrix is

$$
K_{p,ver} =
\begin{bmatrix}
1/m & 0 & 0 & 0 \\
0 & -g/J_x & 0 & 0 \\
0 & 0 & g/J_y & 0 \\
0 & 0 & 0 & 1/J_z
\end{bmatrix}.
\tag{4.23}
$$

The signs of the leading principals of K_p is known and nonzero as

$$
\Delta_1 > 0, \Delta_2 < 0, \Delta_3 < 0, \Delta_4 < 0,
\tag{4.24}
$$

which is consistent with (4.12).

We can summarize the results at these operating points by following proposition:

Proposition 1. *For a quadrotor system given by (3.1)-(3.9) at an operating point satisfying (4.1)-(4.2) or (4.13)-(4.14), there exists an diagonal interactor matrix $\xi_m(s)$ as given in (4.10) and the signs of the leading principal minors of the high frequency gain matrix K_p are known and nonzero as (4.12).*

4.1.2   Flight Conditions with Non-Diagonal Interactor Matrices

We relax ϕ_o and θ_o to be nonzero in this part, so there will be a component of F_z in the direction of x_E, which leads to higher acceleration and velocity than the hover condition. The non-diagonal interactor matrices are accompanied by more complicated transfer matrices than the ones in Section 4.1.1.

Uniform motion condition along the x_E axis

The operating condition is given by (x_{pit}, u_{pit}) as

$$x_{pit} = [x_E, y_E, z_E, \dot{x}_o, 0, 0, 0, \theta_o, 0, 0, 0, 0]^T, \theta_o \in (-\frac{\pi}{2}, \frac{\pi}{2}) \tag{4.25}$$

$$u_{pit} = \left[\frac{mg}{C_{\theta_o}}, 0, 0, 0\right]^T, \tag{4.26}$$

where x_E, y_E, and z_E are arbitrary, θ_o and $\dot{x}_o$ are constants. We are able to derive the relation between $\dot{x}$ and θ_o as

$$\ddot{x} = gT_{\theta_o} - \frac{c_t}{m}\dot{x}_o = 0 \quad \Rightarrow \quad \theta_o = \tan^{-1}\frac{c_t\dot{x}_o}{mg} \text{ or } \dot{x}_o = \frac{mg}{c_t}\tan\theta_o. \tag{4.27}$$

By substituting (4.25) and (4.26) into the linearized model in (3.14), the parameters can be derived as

$$A_t = \begin{bmatrix} 0 & g & 0 \\ -g & 0 & gT_{\theta_o} \\ 0 & -gT_{\theta_o} & 0 \end{bmatrix} \tag{4.28}$$

$$A_r = -c_r \text{ diag}\left\{\frac{1}{J_x} \quad \frac{1}{J_y} \quad \frac{1}{J_z}\right\} \tag{4.29}$$

$$A_s = 0_{3\times3} \tag{4.30}$$

$$A_w = \begin{bmatrix} 1 & 0 & T_{\theta_o} \\ 0 & 1 & 0 \\ 0 & 0 & 1/C_{\theta_o} \end{bmatrix} \tag{4.31}$$

$$B_t = \begin{bmatrix} \dfrac{S_{\theta_o}}{m} & 0 & \dfrac{C_{\theta_o}}{m} \end{bmatrix}^T \tag{4.32}$$

$$B_r = \text{diag} \left\{ \dfrac{1}{J_x} \quad \dfrac{1}{J_y} \quad \dfrac{1}{J_z} \right\} \tag{4.33}$$

and the transfer function is

$$G_{pit}(s) = \begin{bmatrix} \dfrac{C_{\theta_o}}{ms(s+c_t)} & 0 & -\dfrac{gT_{\theta_o}}{(c_t+s)(c_r+J_y s)s^2} & 0 \\ 0 & G_{pit,22} & 0 & G_{pit,24} \\ \dfrac{S_{\theta_o}}{ms(s+c_t)} & 0 & \dfrac{g}{(c_t+s)(c_r+J_y s)s^2} & 0 \\ 0 & 0 & 0 & G_{pit,44} \end{bmatrix}, \tag{4.34}$$

where

$$G_{pit,22} = -\dfrac{g}{(c_t+s)(c_r+J_x s)s^2} \tag{4.35}$$

$$G_{pit,24} = \dfrac{g(T_{\theta_o} - S_{\theta_o})}{C_{\theta_o}(c_t+s)(c_r+J_z s)s^2} \tag{4.36}$$

$$G_{pit,44} = \dfrac{1}{C_{\theta_o}s(c_r+J_z s)}. \tag{4.37}$$

The interactor matrix can be obtained as

$$\xi_{pit}(s) = \begin{bmatrix} (s+1)^2 & 0 & 0 & 0 \\ 0 & (s+1)^4 & 0 & 0 \\ -T_{\theta_o}(s+1)^4 & 0 & (s+1)^4 & 0 \\ 0 & 0 & 0 & (s+1)^2 \end{bmatrix} \tag{4.38}$$

such that the high frequency gain matrix is

$$
K_{p,pit} =
\begin{bmatrix}
C_{\theta_o}/m & 0 & 0 & 0 \\
0 & -\dfrac{g}{J_x} & 0 & \dfrac{g(T_{\theta_o} - S_{\theta_o})}{C_{\theta_o} J_z} \\
0 & 0 & \dfrac{gT_{\theta_o}^2 + C_{\theta_o}}{J_y C_{\theta_o}} & 0 \\
0 & 0 & 0 & 1/C_{\theta_o} J_z
\end{bmatrix}.
\tag{4.39}
$$

If θ_o is in $(-\pi/2, \pi/2)$ as (4.25), then the signs of the leading principal minors of K_p are the same as the general hover condition as (4.12), which are known and nonzero. This is a rational constraint that the quadrotor is able to fly either forward or backward with a large enough acceleration.

Uniform motion condition along the y_E axis

The operating point is given by (x_{rol}, u_{rol}) as

$$
x_{rol} = [x, y, z, 0, \dot{y}_o, 0, \phi_o, 0, 0, 0, 0, 0]^T, \phi_o \in (-\frac{\pi}{2}, \frac{\pi}{2})
\tag{4.40}
$$

$$
u_{rol} = [mg/C_{\phi_o}, 0, 0, 0]^T,
\tag{4.41}
$$

where x, y, z are arbitrary, $\dot{y}_o, \phi_o$ are constants. By substituting (4.40) and (4.41) into the linearized model in (3.14), the parameters can be derived as

$$
A_t =
\begin{bmatrix}
0 & g & gT_{\phi_o} \\
-\dfrac{g}{C_{\phi_o}} & 0 & 0 \\
-gT_{\phi_o} & 0 & 0
\end{bmatrix}
\tag{4.42}
$$

$$
A_r = -c_r \, \text{diag}\left\{ \frac{1}{J_x} \quad \frac{1}{J_y} \quad \frac{1}{J_z} \right\}
\tag{4.43}
$$

$$
A_s = 0_{3\times3}
\tag{4.44}
$$

$$A_w = \begin{bmatrix} 1 & 0 & 0 \\ 0 & C_{\phi_o} & -S_{\phi_o} \\ 0 & S_{\phi_o} & C_{\phi_o} \end{bmatrix} \tag{4.45}$$

$$B_t = \begin{bmatrix} 0 & -\dfrac{S_{\phi_o}}{m} & \dfrac{C_{\phi_o}}{m} \end{bmatrix}^T \tag{4.46}$$

$$B_r = \operatorname{diag}\left\{ \dfrac{1}{J_x} \quad \dfrac{1}{J_y} \quad \dfrac{1}{J_z} \right\}. \tag{4.47}$$

The transfer matrix can be found as

$$G_{rol}(s) = \begin{bmatrix} \dfrac{C_{\phi_o}}{ms(s+c_t)} & -\dfrac{gT_{\phi_o}}{(c_t+s)(c_r+J_x s)s^2} & 0 & 0 \\ -\dfrac{S_{\phi_o}}{ms(s+c_t)} & -\dfrac{g}{C_{\phi_o}(c_t+s)(c_r+J_x s)s^2} & 0 & 0 \\ 0 & 0 & G_{rol,33} & 0 \\ 0 & 0 & G_{rol,43} & G_{rol,44} \end{bmatrix}, \tag{4.48}$$

where

$$G_{rol,33} = \dfrac{g}{C_{\phi_o}(c_t+s)(c_r+J_y s)s^2} \tag{4.49}$$

$$G_{rol,43} = \dfrac{S_{\phi_o}}{s(c_r+J_y s)} \tag{4.50}$$

$$G_{rol,44} = \dfrac{C_{\phi_o}}{s(c_r+J_z s)}. \tag{4.51}$$

The interactor matrix is as

$$\xi_{rol}(s) = \begin{bmatrix} (s+1)^2 & 0 & 0 & 0 \\ T_{\phi_o}(s+1)^4 & (s+1)^4 & 0 & 0 \\ 0 & 0 & (s+1)^4 & 0 \\ 0 & 0 & 0 & (s+1)^2 \end{bmatrix} \tag{4.52}$$

such that the high frequency gain matrix is

$$
K_{p.rol} =
\begin{bmatrix}
C_{\phi_o}/m & 0 & 0 & 0 \\
0 & -\dfrac{g(1+S_{\phi_o}T_{\phi_o})}{C_{\phi_o}J_x} & 0 & 0 \\
0 & 0 & g/J_y & 0 \\
0 & 0 & S_{\phi_o}/J_y & C_{\phi_o}/J_z
\end{bmatrix}.
\tag{4.53}
$$

If ϕ_o is in $(-\pi/2, \pi/2)$ as (4.40), then the signs of the leading principal minors of K_p are the same as the general hover condition as (4.12), which are known and nonzero. This is a realistic constraint that the quadrotor is able to fly either leftward or rightward with a maximum acceleration which is large enough.

We can summarize the results of these flight conditions by following proposition:

Proposition 2. *For a quadrotor system given by (3.1)-(3.9) at an operating point satisfying (4.25)-(4.26) or (4.40)-(4.41), there exists an non-diagonal interactor matrix $\xi_m(s)$ and the signs of the leading principal minors of the high-frequency gain matrix K_p are known and nonzero as (4.12).*

This proposition indicates the existence of an interactor matrix at each condition, which is non-diagonal, changing and parameter-dependent, unlike the cases of Proposition 1 (in which the interactor matrices are diagonal and parameter-independent). For the circumstances with full knowledge of state information, an individual state feedback output tracking control scheme is available for an individual operating condition studied. Then with a proper adaptive law for the control parameter k_f, the result in [47] can be applied to a quadrotor operating at a fixed condition.

4.1.3 General Model of Fixed Attitude

The state vector is given by

$$x_{o,att}(t) = [x_E, y_E, z_E, \dot{x}_E, \dot{y}_E, \dot{z}_E, \phi_o, \theta_o, \psi_o, 0, 0, 0]^T. \tag{4.54}$$

where x_E, y_E, z_E are arbitrary, $\dot{x}_E, \dot{y}_E, \dot{z}_E, \phi_o, \theta_o, \psi_o$ are constants, and the input vector is given by

$$u = [\frac{mg}{C_{\theta_o} C_{\phi_o}}, 0, 0, 0]^T. \tag{4.55}$$

By substituting (4.54) and (4.55) into our linearized model in (3.14), the parameters yields

$$A_t = \begin{bmatrix} C_{\phi_o} S_{\psi_o} - S_{\phi_o} S_{\theta_o} C_{\psi_o} & C_{\phi_o} C_{\theta_o} C_{\psi_o} & S_{\phi_o} C_{\psi_o} - C_{\phi_o} S_{\theta_o} S_{\psi_o} \\ -C_{\theta_o} C_{\psi_o} - S_{\phi_o} S_{\theta_o} S_{\psi_o} & C_{\phi_o} C_{\theta_o} S_{\psi_o} & S_{\phi_o} S_{\psi_o} + C_{\phi_o} S_{\theta_o} C_{\psi_o} \\ -S_{\phi_o} C_{\theta_o} & -C_{\phi_o} S_{\theta_o} & 0 \end{bmatrix} \frac{g}{C_{\theta_o} C_{\phi_o}}$$

$$A_r = -c_r \ \mathrm{diag} \left\{ \frac{1}{J_x} \quad \frac{1}{J_y} \quad \frac{1}{J_z} \right\}$$

$$A_s = 0_{3\times 3}$$

$$A_w = \begin{bmatrix} 1 & S_{\phi_o} T_{\theta_o} & C_{\phi_o} T_{\theta_o} \\ 0 & C_{\phi_o} & -S_{\phi_o} \\ 0 & \dfrac{S_{\phi_o}}{C_{\theta_o}} & \dfrac{C_{\phi_o}}{C_{\theta_o}} \end{bmatrix}$$

$$B_t = \begin{bmatrix} S_{\phi_o} S_{\psi_o} + C_{\phi_o} S_{\theta_o} C_{\psi_o} \\ -S_{\phi_o} C_{\psi_o} + C_{\phi_o} S_{\theta_o} S_{\psi_o} \\ C_{\phi_o} C_{\theta_o} \end{bmatrix} \frac{1}{m}$$

$$B_r = \mathrm{diag} \left\{ \frac{1}{J_x} \quad \frac{1}{J_y} \quad \frac{1}{J_z} \right\}.$$

Then we could derive the transfer function as

$$
G_{att}(s) = \begin{bmatrix}
\dfrac{C_{\phi_o}C_{\theta_o}}{ms(s+c_t)} & G_{att,12} & G_{att,13} & 0 \\[2ex]
-\dfrac{S_{\phi_o}C_{\psi_o} - C_{\phi_o}S_{\psi_o}S_{\theta_o}}{ms(s+c_t)} & G_{att,22} & G_{att,23} & G_{att,24} \\[2ex]
\dfrac{S_{\phi_o}S_{\psi_o} + C_{\phi_o}C_{\psi_o}S_{\theta_o}}{ms(s+c_t)} & G_{att,32} & G_{att,33} & 0 \\[2ex]
0 & 0 & G_{att,43} & G_{att,44}
\end{bmatrix},
\tag{4.56}
$$

where

$$
G_{att,12} = -\frac{gT_{\phi_o}}{(c_t + s)(c_r + J_x s)s^2}
\tag{4.57}
$$

$$
G_{att,13} = -\frac{gT_{\theta_o}}{C_{\phi_o}(c_t + s)(c_r + J_y s)s^2}
\tag{4.58}
$$

$$
G_{att,22} = -\frac{g(C_{\psi_o} + S_{\phi_o}T_{\theta_o}S_{\psi_o})}{C_{\phi_o}(c_t + s)(c_r + J_x s)s^2}
\tag{4.59}
$$

$$
G_{att,23} = \frac{g(S_{\phi_o}T_{\theta_o}C_{\psi_o}(C_{\phi_o} - C_{\theta_o}) + C_{\theta_o}S_{\psi_o})}{C_{\phi_o}C_{\theta_o}(c_t + s)(c_r + J_x s)s^2}
\tag{4.60}
$$

$$
G_{att,24} = \frac{g(C_{\phi_o}T_{\theta_o} - S_{\theta_o})C_{\psi_o}}{C_{\theta_o}(c_t + s)(c_r + J_z s)s^2}
\tag{4.61}
$$

$$
G_{att,32} = \frac{g(S_{\psi_o} - T_{\phi_o}S_{\theta_o}C_{\psi_o})}{C_{\theta_o}(c_t + s)(c_r + J_x s)s^2}
\tag{4.62}
$$

$$
G_{att,33} = \frac{gC_{\psi_o}}{C_{\phi_o}(c_t + s)(c_r + J_y s)s^2}
\tag{4.63}
$$

$$
G_{att,43} = \frac{S_{\phi_o}}{C_{\theta_o}s(c_r + J_y s)}
\tag{4.64}
$$

$$
G_{att,44} = \frac{C_{\phi_o}}{C_{\theta_o}s(c_r + J_z s)}.
\tag{4.65}
$$

The modified left interactor (MLI) matrix is obtained as

$$
\xi_{att}(s) = \begin{bmatrix}
(s+1)^2 & 0 & 0 & 0 \\[2ex]
\dfrac{T_{\phi_o}C_{\psi_o} - S_{\theta_o}S_{\psi_o}}{C_{\theta_o}}(s+1)^4 & (s+1)^4 & 0 & 0 \\[2ex]
-\dfrac{T_{\phi_o}S_{\psi_o} + S_{\theta_o}C_{\psi_o}}{C_{\theta_o}}(s+1)^4 & 0 & (s+1)^4 & 0 \\[2ex]
0 & 0 & 0 & (s+1)^2
\end{bmatrix}
\tag{4.66}
$$

and the high frequency gain matrix is

$$
K_{p,att} =
\begin{bmatrix}
\dfrac{C_{\phi_o}C_{\theta_o}}{m} & 0 & 0 & 0 \\[2ex]
0 & -\dfrac{g(S_{\phi_o}T_{\phi_o} + C_{\theta_o})C_{\psi_o}}{J_x C_{\phi_o} C_{\theta_o}} & K_{att,23} & K_{att,24} \\[2ex]
0 & \dfrac{gS_{\psi_o}}{J_x C_{\phi_o}^2 C_{\theta_o}} & K_{att,33} & 0 \\[2ex]
0 & 0 & \dfrac{S_{\phi_o}}{C_{\theta_o}J_y} & \dfrac{C_{\phi_o}}{C_{\theta_o}J_z}
\end{bmatrix},
\tag{4.67}
$$

where

$$
K_{att,23} = \frac{g(-S_{\phi_o}(S_{\phi_o}T_{\phi_o} + C_{\theta_o})T_{\theta_o}C_{\psi_o} + (S_{\theta_o}T_{\theta_o} + C_{\phi_o})S_{\psi_o})}{J_y C_{\phi_o}C_{\theta_o}}
\tag{4.68}
$$

$$
K_{att,24} = \frac{g(C_{\phi_o}T_{\theta_o} - S_{\theta_o})C_{\psi_o}}{C_{\theta_o}J_z}
\tag{4.69}
$$

$$
K_{att,33} = \frac{g((S_{\theta_o}T_{\theta_o} + 1)C_{\psi_o} + T_{\phi_o}T_{\theta_o}S_{\psi_o})}{J_y C_{\phi_o}C_{\theta_o}}.
\tag{4.70}
$$

If ϕ_o, θ_o and ψ_o are all in $(-\pi/2, \pi/2)$, then the signs of the leading principal minors of K_p are known and nonzero as $\Delta_1 > 0, \Delta_2 < 0, \Delta_3 < 0, \Delta_4 < 0$.

4.2 Fully-Actuated Multirotor Systems

The section derives linearized models and transfer matrices at typical operating conditions of the nonlinear dynamic model of omni-directional multirotor systems which has full actuation on all six degrees of freedom. It is discovered that these models have the same diagonal interactor that is not dependent on system parameters or operating conditions. It is also shown that with realistic conditions on the attitude of a multirotor system, the leading principal minors of the high-frequency gain matrices are all non-zero and their sign patterns are fixed and known.

4.2.1 Special Hover Condition

The parameter matrices for the condition are given as

$$
A_t = g \begin{bmatrix} 0 & 1 & 0 \\ -1 & 0 & 0 \\ 0 & 0 & 0 \end{bmatrix} \tag{4.71}
$$

$$
A_s = 0_{3\times3} \tag{4.72}
$$

$$
A_r = -c_r \ \mathrm{diag} \left\{ \frac{1}{J_x} \quad \frac{1}{J_y} \quad \frac{1}{J_z} \right\} \tag{4.73}
$$

$$
A_w = I_{3\times3} \tag{4.74}
$$

$$
B_t = \frac{1}{m} I_{3\times3} \tag{4.75}
$$

$$
B_r = \mathrm{diag} \left\{ \frac{1}{J_x} \quad \frac{1}{J_y} \quad \frac{1}{J_z} \right\}. \tag{4.76}
$$

The transfer function is

$$
G_{hov}(s) = \begin{bmatrix}
G_{hov,11} & 0 & 0 & 0 & G_{hov,15} & 0 \\
0 & G_{hov,22} & 0 & G_{hov,24} & 0 & 0 \\
0 & 0 & G_{hov,33} & 0 & 0 & 0 \\
0 & 0 & 0 & \dfrac{1}{s(c_r + J_x s)} & 0 & 0 \\
0 & 0 & 0 & 0 & \dfrac{1}{s(c_r + J_y s)} & 0 \\
0 & 0 & 0 & 0 & 0 & \dfrac{1}{s(c_r + J_z s)}
\end{bmatrix}, \tag{4.77}
$$

where

$$
G_{hov,11} = \frac{1}{ms(s + c_t)} \tag{4.78}
$$

$$
G_{hov,15} = \frac{g}{(c_t + s)(c_r + J_y s)s^2} \tag{4.79}
$$

$$
G_{hov,22} = \frac{1}{ms(s + c_t)} \tag{4.80}
$$

$$G_{hov,24} = -\frac{g}{(c_t + s)(c_r + J_x s)s^2} \tag{4.81}$$

$$G_{hov,33} = \frac{1}{ms(s + c_t)}. \tag{4.82}$$

The modified left interactor (MLI) matrix is obtained as

$$\xi_{m,hov}(s) = \begin{bmatrix} (s+1)^2 & 0 & 0 & 0 & 0 & 0 \\ 0 & (s+1)^2 & 0 & 0 & 0 & 0 \\ 0 & 0 & (s+1)^2 & 0 & 0 & 0 \\ 0 & 0 & 0 & (s+1)^2 & 0 & 0 \\ 0 & 0 & 0 & 0 & (s+1)^2 & 0 \\ 0 & 0 & 0 & 0 & 0 & (s+1)^2 \end{bmatrix}, \tag{4.83}$$

and the high frequency gain matrix is

$$K_{p,hov} = \begin{bmatrix} 1/m & 0 & 0 & 0 & 0 & 0 \\ 0 & 1/m & 0 & 0 & 0 & 0 \\ 0 & 0 & 1/m & 0 & 0 & 0 \\ 0 & 0 & 0 & 1/J_x & 0 & 0 \\ 0 & 0 & 0 & 0 & 1/J_y & 0 \\ 0 & 0 & 0 & 0 & 0 & 1/J_z \end{bmatrix}. \tag{4.84}$$

4.2.2   Conditions with Non-Zero Yaw Angle

The parameter matrices for the condition are given as

$$A_t = g \begin{bmatrix} S_{\psi_e} & C_{\psi_e} & 0 \\ -C_{\psi_e} & S_{\psi_e} & 0 \\ 0 & 0 & 0 \end{bmatrix} \tag{4.85}$$

$$A_s = 0_{3\times 3} \tag{4.86}$$

$$A_r = -c_r \, \text{diag} \left\{ \frac{1}{J_x} \quad \frac{1}{J_y} \quad \frac{1}{J_z} \right\} \tag{4.87}$$

$$A_w = I_{3\times 3} \tag{4.88}$$

$$B_t = \frac{1}{m} \begin{bmatrix} C_{\psi_e} & -S_{\psi_e} & 0 \\ S_{\psi_e} & C_{\psi_e} & 0 \\ 0 & 0 & 1 \end{bmatrix} \tag{4.89}$$

$$B_r = \text{diag} \left\{ \frac{1}{J_x} \quad \frac{1}{J_y} \quad \frac{1}{J_z} \right\}. \tag{4.90}$$

The transfer matrix is

$$G_{yaw}(s) = \begin{bmatrix} G_{yaw,11} & G_{yaw,12} & 0 & G_{yaw,14} & G_{yaw,15} & 0 \\ G_{yaw,21} & G_{yaw,22} & 0 & G_{yaw,24} & G_{yaw,25} & 0 \\ 0 & 0 & G_{yaw,33} & 0 & 0 & 0 \\ 0 & 0 & 0 & G_{yaw,44} & 0 & 0 \\ 0 & 0 & 0 & 0 & G_{yaw,55} & 0 \\ 0 & 0 & 0 & 0 & 0 & G_{yaw,66} \end{bmatrix}, \tag{4.91}$$

where

$$G_{yaw,11} = \frac{C_{\psi_e}}{ms(s + c_t)} \tag{4.92}$$

$$G_{yaw,12} = -\frac{S_{\psi_e}}{ms(s + c_t)} \tag{4.93}$$

$$G_{yaw,14} = \frac{gS_{\psi_e}}{(c_t + s)(c_r + J_x s)s^2} \tag{4.94}$$

$$G_{yaw,15} = \frac{gC_{\psi_e}}{(c_t + s)(c_r + J_y s)s^2} \tag{4.95}$$

$$G_{yaw,21} = \frac{S_{\psi_e}}{ms(s + c_t)} \tag{4.96}$$

$$G_{yaw,22} = \frac{C_{\psi_e}}{ms(s + c_t)} \tag{4.97}$$

$$G_{yaw,24} = -\frac{gC_{\psi_e}}{(c_t + s)(c_r + J_x s)s^2} \tag{4.98}$$

$$G_{yaw,25} = \frac{gS_{\psi_e}}{(c_t + s)(c_r + J_y s)s^2} \tag{4.99}$$

$$G_{yaw,33} = \frac{1}{ms(s + c_t)} \tag{4.100}$$

$$G_{yaw,44} = \frac{1}{s(c_r + J_x s)} \tag{4.101}$$

$$G_{yaw,55} = \frac{1}{s(c_r + J_y s)} \tag{4.102}$$

$$G_{yaw,66} = \frac{1}{s(c_r + J_z s)}. \tag{4.103}$$

The modified left interactor (MLI) matrix is obtained as

$$\xi_{m,yaw}(s) = \begin{bmatrix} (s+1)^2 & 0 & 0 & 0 & 0 & 0 \\ 0 & (s+1)^2 & 0 & 0 & 0 & 0 \\ 0 & 0 & (s+1)^2 & 0 & 0 & 0 \\ 0 & 0 & 0 & (s+1)^2 & 0 & 0 \\ 0 & 0 & 0 & 0 & (s+1)^2 & 0 \\ 0 & 0 & 0 & 0 & 0 & (s+1)^2 \end{bmatrix}, \tag{4.104}$$

and the high frequency gain matrix is

$$K_{p,yaw} = \begin{bmatrix} C_{\psi_e}/m & -S_{\psi_e}/m & 0 & 0 & 0 & 0 \\ S_{\psi_e}/m & C_{\psi_e}/m & 0 & 0 & 0 & 0 \\ 0 & 0 & 1/m & 0 & 0 & 0 \\ 0 & 0 & 0 & 1/J_x & 0 & 0 \\ 0 & 0 & 0 & 0 & 1/J_y & 0 \\ 0 & 0 & 0 & 0 & 0 & 1/J_z \end{bmatrix}. \tag{4.105}$$

If ψ_e is in $(-\pi/2, \pi/2)$, then the leading principal minors of K_p are known and nonzero as

$$\Delta_1 > 0, \Delta_2 > 0, \Delta_3 > 0, \Delta_4 > 0, \Delta_5 > 0, \Delta_6 > 0. \tag{4.106}$$

4.2.3   Conditions with Non-Zero Pitch Angle

The parameter matrices for the condition are given as

$$A_t = \begin{bmatrix} 0 & g & 0 \\ -g & 0 & gT_{\theta_e} \\ 0 & -gT_{\theta_e} & 0 \end{bmatrix} \tag{4.107}$$

$$A_r = -c_r \, \mathrm{diag}\left\{ \frac{1}{J_x} \quad \frac{1}{J_y} \quad \frac{1}{J_z} \right\} \tag{4.108}$$

$$A_s = 0_{3\times3} \tag{4.109}$$

$$A_w = \begin{bmatrix} 1 & 0 & T_{\theta_e} \\ 0 & 1 & 0 \\ 0 & 0 & 1/C_{\theta_e} \end{bmatrix} \tag{4.110}$$

$$B_t = \begin{bmatrix} \dfrac{S_{\theta_e}}{m} & 0 & \dfrac{C_{\theta_e}}{m} \end{bmatrix}^T \tag{4.111}$$

$$B_r = \mathrm{diag}\left\{ \frac{1}{J_x} \quad \frac{1}{J_y} \quad \frac{1}{J_z} \right\} \tag{4.112}$$

and the transfer function is

$$
G_{pit}(s) = \begin{bmatrix}
G_{pit,11} & 0 & G_{pit,13} & 0 & G_{pit,15} & 0 \\
0 & G_{pit,22} & 0 & G_{pit,24} & 0 & G_{pit,26} \\
G_{pit,31} & 0 & G_{pit,33} & 0 & G_{pit,35} & 0 \\
0 & 0 & 0 & G_{pit,44} & 0 & G_{pit,46} \\
0 & 0 & 0 & 0 & G_{pit,55} & 0 \\
0 & 0 & 0 & 0 & 0 & G_{pit,66}
\end{bmatrix},
\tag{4.113}
$$

where

$$
G_{pit,11} = \frac{C_{\theta_e}}{ms(s + c_t)}
\tag{4.114}
$$

$$
G_{pit,13} = \frac{S_{\theta_e}}{ms(s + c_t)}
\tag{4.115}
$$

$$
G_{pit,15} = \frac{g}{(c_t + s)(c_r + J_y s)s^2}
\tag{4.116}
$$

$$
G_{pit,22} = \frac{1}{ms(s + c_t)}
\tag{4.117}
$$

$$
G_{pit,24} = -\frac{g}{(c_t + s)(c_r + J_x s)s^2}
\tag{4.118}
$$

$$
G_{pit,26} = \frac{g(T_{\theta_e} - S_{\theta_e})}{C_{\theta_e}(c_t + s)(c_r + J_z s)s^2}
\tag{4.119}
$$

$$
G_{pit,31} = -\frac{S_{\theta_e}}{ms(s + c_t)}
\tag{4.120}
$$

$$
G_{pit,33} = \frac{C_{\theta_e}}{ms(s + c_t)}
\tag{4.121}
$$

$$
G_{pit,35} = -\frac{gT_{\theta_e}}{C_{\theta_e}(c_t + s)(c_r + J_y s)s^2}
\tag{4.122}
$$

$$
G_{pit,44} = \frac{1}{s(c_r + J_x s)}
\tag{4.123}
$$

$$
G_{pit,46} = \frac{T_{\theta_e}}{s(c_r + J_z s)}
\tag{4.124}
$$

$$
G_{pit,55} = \frac{1}{s(c_r + J_y s)}
\tag{4.125}
$$

$$
G_{pit,66} = \frac{1}{C_{\theta_e}s(c_r + J_z s)}.
\tag{4.126}
$$

The modified left interactor (MLI) matrix is obtained as

$$
\xi_{m,pit}(s) = \begin{bmatrix}
(s+1)^2 & 0 & 0 & 0 & 0 & 0 \\
0 & (s+1)^2 & 0 & 0 & 0 & 0 \\
0 & 0 & (s+1)^2 & 0 & 0 & 0 \\
0 & 0 & 0 & (s+1)^2 & 0 & 0 \\
0 & 0 & 0 & 0 & (s+1)^2 & 0 \\
0 & 0 & 0 & 0 & 0 & (s+1)^2
\end{bmatrix},
\qquad (4.127)
$$

and the high frequency gain matrix is

$$
K_{p,pit} = \begin{bmatrix}
C_{\theta_e}/m & 0 & S_{\theta_e}/m & 0 & 0 & 0 \\
0 & 1/m & 0 & 0 & 0 & 0 \\
-S_{\theta_e}/m & 0 & C_{\theta_e}/m & 0 & 0 & 0 \\
0 & 0 & 0 & 1/J_x & 0 & T_{\theta_e}/J_z \\
0 & 0 & 0 & 0 & 1/J_y & 0 \\
0 & 0 & 0 & 0 & 0 & 1/J_z
\end{bmatrix}.
\qquad (4.128)
$$

If θ_e is in $(-\pi/2, \pi/2)$, then the signs of the leading principal minors of K_p are the same as the general hover condition as (4.106), which are known and nonzero. This is a rational constraint that the quadrotor is able to fly either forward or backward with a large enough acceleration.

4.2.4 Conditions with Non-Zero Roll Angle

The parameter matrices for the condition are given as

$$
A_t = \begin{bmatrix} 0 & g & gT_{\phi_e} \\ -\dfrac{g}{C_{\phi_e}} & 0 & 0 \\ -gT_{\phi_e} & 0 & 0 \end{bmatrix} \tag{4.129}
$$

$$
A_r = -c_r \ \mathrm{diag} \left\{ \dfrac{1}{J_x} \quad \dfrac{1}{J_y} \quad \dfrac{1}{J_z} \right\} \tag{4.130}
$$

$$
A_s = 0_{3\times3} \tag{4.131}
$$

$$
A_w = \begin{bmatrix} 1 & 0 & 0 \\ 0 & C_{\phi_e} & -S_{\phi_e} \\ 0 & S_{\phi_e} & C_{\phi_e} \end{bmatrix} \tag{4.132}
$$

$$
B_t = \begin{bmatrix} 0 & -\dfrac{S_{\phi_e}}{m} & \dfrac{C_{\phi_e}}{m} \end{bmatrix}^T \tag{4.133}
$$

$$
B_r = \ \mathrm{diag} \left\{ \dfrac{1}{J_x} \quad \dfrac{1}{J_y} \quad \dfrac{1}{J_z} \right\}. \tag{4.134}
$$

The transfer matrix can be found as

$$
G_{rol}(s) = \begin{bmatrix} G_{rol,11} & 0 & 0 & 0 & G_{rol,15} & 0 \\ 0 & G_{rol,22} & G_{rol,23} & G_{rol,24} & 0 & 0 \\ 0 & G_{rol,32} & G_{rol,33} & G_{rol,34} & 0 & 0 \\ 0 & 0 & 0 & G_{rol,44} & 0 & 0 \\ 0 & 0 & 0 & 0 & \dfrac{C_{\phi_e}}{s(c_r + J_y s)} & -\dfrac{S_{\phi_e}}{s(c_r + J_z s)} \\ 0 & 0 & 0 & 0 & \dfrac{S_{\phi_e}}{s(c_r + J_y s)} & \dfrac{C_{\phi_e}}{s(c_r + J_z s)} \end{bmatrix}, \tag{4.135}
$$

where

$$
G_{rol,11} = \dfrac{1}{ms(s + c_t)} \tag{4.136}
$$

$$G_{rol,15} = \frac{g}{C_{\phi_e}(c_t + s)(c_r + J_y s)s^2} \tag{4.137}$$

$$G_{rol,22} = \frac{C_{\phi_e}}{ms(s + c_t)} \tag{4.138}$$

$$G_{rol,23} = -\frac{S_{\phi_e}}{ms(s + c_t)} \tag{4.139}$$

$$G_{rol,24} = -\frac{g}{C_{\phi_e}(c_t + s)(c_r + J_x s)s^2} \tag{4.140}$$

$$G_{rol,32} = \frac{S_{\phi_e}}{ms(s + c_t)} \tag{4.141}$$

$$G_{rol,33} = \frac{C_{\phi_e}}{ms(s + c_t)} \tag{4.142}$$

$$G_{rol,34} = -\frac{gT_{\phi_e}}{(c_t + s)(c_r + J_x s)s^2} \tag{4.143}$$

$$G_{rol,44} = \frac{1}{s(c_r + J_x s)}. \tag{4.144}$$

The modified left interactor (MLI) matrix is obtained as

$$\xi_{m,rol}(s) = \begin{bmatrix} (s+1)^2 & 0 & 0 & 0 & 0 & 0 \\ 0 & (s+1)^2 & 0 & 0 & 0 & 0 \\ 0 & 0 & (s+1)^2 & 0 & 0 & 0 \\ 0 & 0 & 0 & (s+1)^2 & 0 & 0 \\ 0 & 0 & 0 & 0 & (s+1)^2 & 0 \\ 0 & 0 & 0 & 0 & 0 & (s+1)^2 \end{bmatrix}, \tag{4.145}$$

and the high frequency gain matrix is

$$K_{p,rol} = \begin{bmatrix} 1/m & 0 & 0 & 0 & 0 & 0 \\ 0 & C_{\theta_e}/m & -S_{\theta_e}/m & 0 & 0 & 0 \\ 0 & S_{\theta_e}/m & C_{\theta_e}/m & 0 & 0 & 0 \\ 0 & 0 & 0 & 1/J_x & 0 & 0 \\ 0 & 0 & 0 & 0 & C_{\theta_e}/J_y & -S_{\theta_e}/J_z \\ 0 & 0 & 0 & 0 & S_{\theta_e}/J_y & C_{\theta_e}/J_z \end{bmatrix}. \tag{4.146}$$

If ϕ_e is in $(-\pi/2, \pi/2)$, then the signs of the leading principal minors of K_p are the same as the general hover condition as (4.106), which are known and nonzero.

4.3 Issues with Dynamics Mutation

We have shown that the changeable system parameters at different operating conditions can lead to mutative transfer matrices and interactor matrices. Such dynamics mutation is an obstacle for the design of an adaptive controller with a uniform control parameter updating law. The interactor matrix and the signs of the leading principal minors of the high-frequency gain matrix are important prior information for designing MRAC schemes. Because of the varying interactor matrices, different adaptive laws are needed for different operating conditions.

A possible solution is to construct a control system with multiple controllers for a group of selected operating conditions. As derived in (4.27), the desired attitude is related to the desired cruising speed. So the corresponding guidance system should adjust the reference trajectory to guarantee the quadrotor working around selected operating conditions. However, such a scheme is based on the assumption that the translational drag coefficient in (4.27) as c_t is known. Since the parameter is dependent on the environment and unknown, then a stable and fast estimator for c_t should also be attached to the scheme, which definitely increases the complexity of the system and difficulty of stability analysis.

Chapter 5

Compensable Patterns of Actuator Failure

The emerging NNPPNP rotor arrangement of hexarotors is adopted in this work and is investigated for its capability of tolerating up to two failed actuators and for the design of compensators for individual failure patterns. The compensable failure patterns of the octorotor systems are also investigated, which include patterns of one, two, three, and four actuator failures.

5.1 Hexarotors

5.1.1 NPNPNP Hexarotors

A hexarotor with NPNPNP rotor arrangement as in Figure 5.1 can not tolerate the loss-of-control failure at any actuator [69, 74, 75].

5.1.2 NNPPNP Hexarotors

The controllability investigation in [69] reveals that the hexarotors with an NNPPNP rotor arrangement have better performance than the ones with NPNPNP in tolerating
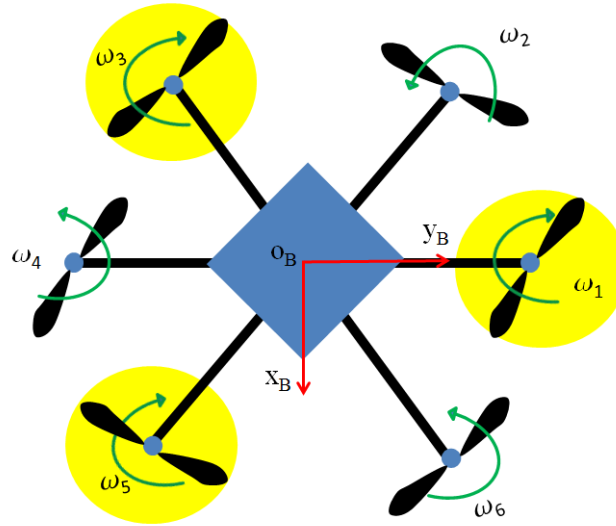
Figure 5.1: The NPNPNP rotor arrangement of a hexarotor.

the loss-of-thrust failure. However, [69] also shows that some of the failure patterns still cannot be compensated even with the NNPPNP arrangement. All the compensable patterns are enumerated and grouped as follows.
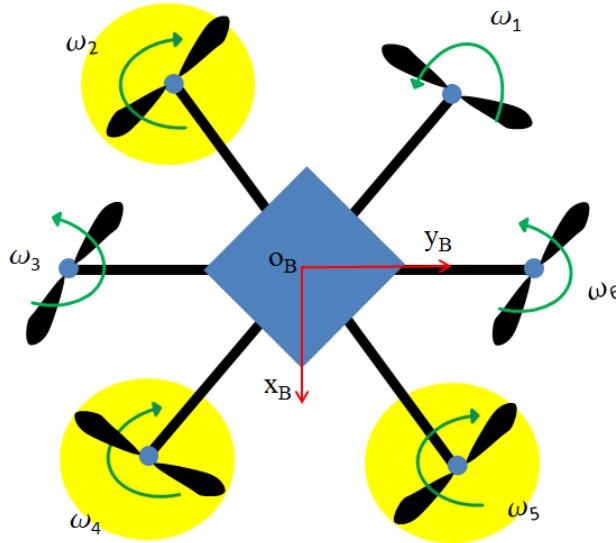
Figure 5.2: The NNPPNP rotor arrangement of a hexarotor.

(i) The pattern with no actuator failure

(0) $\sigma_{(0)} = \mathrm{diag}\{0, 0, 0, 0, 0, 0\}$.

(ii) Patterns with one actuator failure

(1) $\sigma_{(1)} = \text{diag}\{1, 0, 0, 0, 0, 0\}$.

(2) $\sigma_{(2)} = \text{diag}\{0, 0, 0, 1, 0, 0\}$.

(3) $\sigma_{(3)} = \text{diag}\{0, 0, 0, 0, 1, 0\}$.

(4) $\sigma_{(4)} = \text{diag}\{0, 0, 0, 0, 0, 1\}$.

(iii) Patterns with two actuators failures

(5) $\sigma_{(5)} = \text{diag}\{1, 0, 0, 1, 0, 0\}$.

(6) $\sigma_{(6)} = \text{diag}\{1, 0, 0, 0, 1, 0\}$.

(7) $\sigma_{(7)} = \text{diag}\{0, 0, 0, 1, 0, 1\}$.

Remark 4. The compensable patterns with one failure are based on the study in [69], which do not include the failure of rotor 2 or 3. The two-failure patterns presented above are not discussed in [69], which are figured out by us following the controllability analysis procedure in [69]. The hexarotor system in Figure 3.2 cannot bear any loss-of-control failures of rotor 2 or 3. However, the hexarotors with NPNPNP cannot control 4-DOF when there is only one rotor with a loss-of-control failure. Though the compensable patterns are still limited, the NNPPNP rotor arrangement has brought a huge breakthrough in the failure compensation control of hexarotors.   □

5.2   Octorotors

5.2.1   NPNPNPNP Octorotors

(i) Pattern with no actuator failure

(0) $\sigma_{(0)} = \text{diag}\{0, 0, 0, 0, 0, 0, 0, 0\}$.
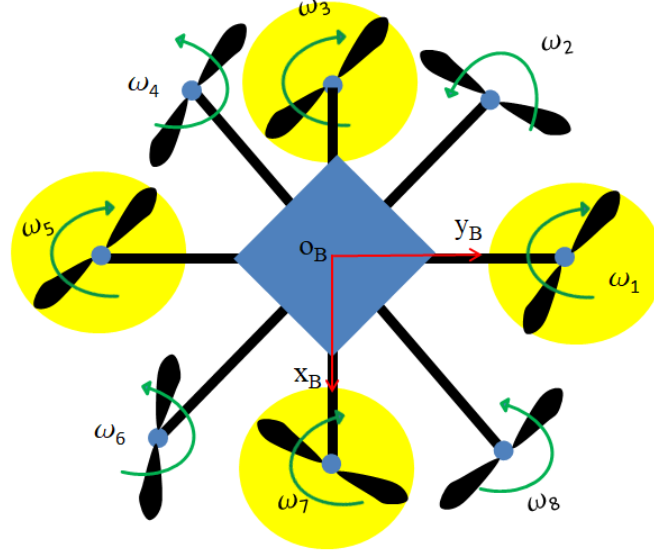
Figure 5.3: The NPNPNPNP rotor arrangement of an octorotor.

(ii) Patterns with one actuator failure

All the eight patterns of single actuator failure are compensable.

(iii) Patterns with two actuators failures

All twenty-eight patterns of two failed actuators are compensable.

(iii) Patterns with three actuators failures

$$\sigma_{(37)} = \sigma_{\overline{124}}, \; \sigma_{(38)} = \sigma_{\overline{125}}, \; \sigma_{(39)} = \sigma_{\overline{126}}, \; \sigma_{(40)} = \sigma_{\overline{127}}, \; \sigma_{(41)} = \sigma_{\overline{134}}, \; \sigma_{(42)} = \sigma_{\overline{136}},$$

$$\sigma_{(43)} = \sigma_{\overline{138}}, \; \sigma_{(44)} = \sigma_{\overline{145}}, \; \sigma_{(45)} = \sigma_{\overline{147}}, \; \sigma_{(46)} = \sigma_{\overline{148}}, \; \sigma_{(47)} = \sigma_{\overline{156}}, \; \sigma_{(48)} = \sigma_{\overline{158}},$$

$$\sigma_{(49)} = \sigma_{\overline{167}}, \; \sigma_{(50)} = \sigma_{\overline{168}}, \; \sigma_{(51)} = \sigma_{\overline{235}}, \; \sigma_{(52)} = \sigma_{\overline{236}}, \; \sigma_{(53)} = \sigma_{\overline{237}}, \; \sigma_{(54)} = \sigma_{\overline{238}},$$

$$\sigma_{(55)} = \sigma_{\overline{245}}, \; \sigma_{(56)} = \sigma_{\overline{247}}, \; \sigma_{(57)} = \sigma_{\overline{256}}, \; \sigma_{(58)} = \sigma_{\overline{257}}, \; \sigma_{(59)} = \sigma_{\overline{258}}, \; \sigma_{(60)} = \sigma_{\overline{267}},$$

$$\sigma_{(61)} = \sigma_{\overline{278}}, \; \sigma_{(62)} = \sigma_{\overline{346}}, \; \sigma_{(63)} = \sigma_{\overline{347}}, \; \sigma_{(64)} = \sigma_{\overline{348}}, \; \sigma_{(65)} = \sigma_{\overline{356}}, \; \sigma_{(66)} = \sigma_{\overline{358}},$$

$$\sigma_{(67)} = \sigma_{\overline{367}}, \; \sigma_{(68)} = \sigma_{\overline{368}}, \; \sigma_{(69)} = \sigma_{\overline{378}}, \; \sigma_{(70)} = \sigma_{\overline{457}}, \; \sigma_{(71)} = \sigma_{\overline{458}}, \; \sigma_{(72)} = \sigma_{\overline{467}},$$

$$\sigma_{(73)} = \sigma_{\overline{478}}, \; \sigma_{(74)} = \sigma_{\overline{568}}, \; \sigma_{(75)} = \sigma_{\overline{578}}.$$

Remark 5. We use a more compact notation formula in this part to represent the failure patterns in this section.

☐

(iii) Patterns with four actuators failures

$\sigma_{(76)} = \sigma_{\overline{1245}}$, $\sigma_{(77)} = \sigma_{\overline{1247}}$, $\sigma_{(78)} = \sigma_{\overline{1256}}$, $\sigma_{(79)} = \sigma_{\overline{1267}}$, $\sigma_{(80)} = \sigma_{\overline{1346}}$, $\sigma_{(81)} = \sigma_{\overline{1348}}$,

$\sigma_{(82)} = \sigma_{\overline{1368}}$, $\sigma_{(83)} = \sigma_{\overline{1458}}$, $\sigma_{(84)} = \sigma_{\overline{1467}}$, $\sigma_{(85)} = \sigma_{\overline{1568}}$, $\sigma_{(86)} = \sigma_{\overline{2356}}$, $\sigma_{(87)} = \sigma_{\overline{2358}}$,

$\sigma_{(88)} = \sigma_{\overline{2367}}$, $\sigma_{(89)} = \sigma_{\overline{2378}}$, $\sigma_{(90)} = \sigma_{\overline{2457}}$, $\sigma_{(91)} = \sigma_{\overline{2578}}$, $\sigma_{(92)} = \sigma_{\overline{3467}}$, $\sigma_{(93)} = \sigma_{\overline{3478}}$,

$\sigma_{(94)} = \sigma_{\overline{3568}}$, $\sigma_{(95)} = \sigma_{\overline{4578}}$.

5.2.2   NNPPNNPP Octorotors

An octorotor with NNPPNNPP rotor arrangement is shown in Figure 5.4.
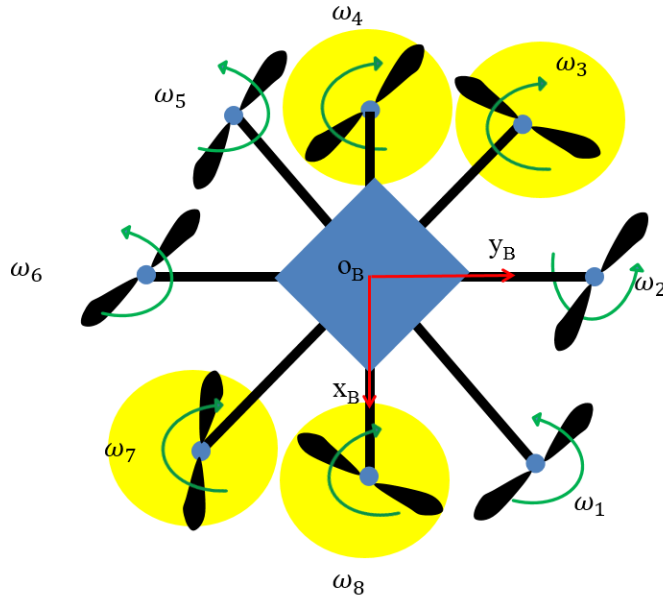
Figure 5.4: The NNPPNNPP rotor arrangement of an octorotor.

(i) Pattern with no actuator failure

(0) $\sigma_{(0)} = \mathrm{diag}\{0, 0, 0, 0, 0, 0, 0, 0\}$.

(ii) Patterns with one actuator failure

All the eight patterns of single actuator failure are compensable.

(iii) Patterns with two actuators failures

$\sigma_{(9)} = \sigma_{\overline{13}}$, $\sigma_{(10)} = \sigma_{\overline{14}}$, $\sigma_{(11)} = \sigma_{\overline{15}}$, $\sigma_{(12)} = \sigma_{\overline{16}}$, $\sigma_{(13)} = \sigma_{\overline{17}}$, $\sigma_{(14)} = \sigma_{\overline{18}}$, $\sigma_{(15)} = \sigma_{\overline{23}}$,

$\sigma_{(16)} = \sigma_{\overline{24}}$, $\sigma_{(17)} = \sigma_{\overline{25}}$, $\sigma_{(18)} = \sigma_{\overline{26}}$, $\sigma_{(19)} = \sigma_{\overline{27}}$, $\sigma_{(20)} = \sigma_{\overline{28}}$, $\sigma_{(21)} = \sigma_{\overline{35}}$, $\sigma_{(22)} = \sigma_{\overline{36}}$,

$\sigma_{(23)} = \sigma_{\overline{37}}$, $\sigma_{(24)} = \sigma_{\overline{38}}$, $\sigma_{(25)} = \sigma_{\overline{45}}$, $\sigma_{(26)} = \sigma_{\overline{46}}$, $\sigma_{(27)} = \sigma_{\overline{47}}$, $\sigma_{(28)} = \sigma_{\overline{48}}$, $\sigma_{(29)} = \sigma_{\overline{57}}$,

$\sigma_{(30)} = \sigma_{\overline{58}}$, $\sigma_{(31)} = \sigma_{\overline{67}}$, $\sigma_{(32)} = \sigma_{\overline{68}}$,

(iii) Patterns with three actuators failures

$\sigma_{(33)} = \sigma_{\overline{457}}$, $\sigma_{(34)} = \sigma_{\overline{458}}$, $\sigma_{(35)} = \sigma_{\overline{467}}$, $\sigma_{(36)} = \sigma_{\overline{468}}$, $\sigma_{(37)} = \sigma_{\overline{135}}$, $\sigma_{(38)} = \sigma_{\overline{136}}$,

$\sigma_{(39)} = \sigma_{\overline{137}}$, $\sigma_{(40)} = \sigma_{\overline{138}}$, $\sigma_{(41)} = \sigma_{\overline{145}}$, $\sigma_{(42)} = \sigma_{\overline{146}}$, $\sigma_{(43)} = \sigma_{\overline{147}}$, $\sigma_{(44)} = \sigma_{\overline{148}}$,

$\sigma_{(45)} = \sigma_{\overline{157}}$, $\sigma_{(46)} = \sigma_{\overline{158}}$, $\sigma_{(47)} = \sigma_{\overline{167}}$, $\sigma_{(48)} = \sigma_{\overline{168}}$, $\sigma_{(49)} = \sigma_{\overline{235}}$, $\sigma_{(50)} = \sigma_{\overline{236}}$,

$\sigma_{(51)} = \sigma_{\overline{237}}$, $\sigma_{(52)} = \sigma_{\overline{238}}$, $\sigma_{(53)} = \sigma_{\overline{245}}$, $\sigma_{(54)} = \sigma_{\overline{246}}$, $\sigma_{(55)} = \sigma_{\overline{247}}$, $\sigma_{(56)} = \sigma_{\overline{248}}$,

$\sigma_{(57)} = \sigma_{\overline{257}}$, $\sigma_{(58)} = \sigma_{\overline{258}}$, $\sigma_{(59)} = \sigma_{\overline{267}}$, $\sigma_{(60)} = \sigma_{\overline{268}}$, $\sigma_{(61)} = \sigma_{\overline{357}}$, $\sigma_{(62)} = \sigma_{\overline{358}}$,

$\sigma_{(63)} = \sigma_{\overline{367}}$, $\sigma_{(64)} = \sigma_{\overline{368}}$.

(iii) Patterns with four actuators failures

$\sigma_{(65)} = \sigma_{\overline{1357}}$, $\sigma_{(66)} = \sigma_{\overline{1358}}$, $\sigma_{(67)} = \sigma_{\overline{1367}}$, $\sigma_{(68)} = \sigma_{\overline{1368}}$, $\sigma_{(69)} = \sigma_{\overline{1457}}$, $\sigma_{(70)} = \sigma_{\overline{1458}}$,

$\sigma_{(71)} = \sigma_{\overline{1467}}$, $\sigma_{(72)} = \sigma_{\overline{1468}}$, $\sigma_{(73)} = \sigma_{\overline{2357}}$, $\sigma_{(74)} = \sigma_{\overline{2358}}$, $\sigma_{(75)} = \sigma_{\overline{2367}}$. $\sigma_{(76)} = \sigma_{\overline{2368}}$,

$\sigma_{(77)} = \sigma_{\overline{2457}}$, $\sigma_{(78)} = \sigma_{\overline{2458}}$, $\sigma_{(79)} = \sigma_{\overline{2467}}$, $\sigma_{(80)} = \sigma_{\overline{2468}}$.

Chapter 6

MRAC for Quadrotors with Non-Diagonal Interactor Matrices

An adaptive control design is presented in this chapter for quadrotor systems working at non-equilibrium operating conditions under parameter uncertainties. The motivation of the part is to handle the situation that existing control schemes are either restricted to the system equilibrium as the hover condition or unable to deal with the system uncertainties. An adaptive controller is constructed to ensures the signal boundedness of the closed-loop system and asymptotic output tracking. The proposed scheme expands the capacity of adaptive control for quadrotors to fly with high speed in the presence of system uncertainties.

The main contributions of the part include:

- A multivariable MRAC scheme is established for quadrotor systems at non-equilibrium operating conditions.

- A state feedback based adaptive controller with rejection of the non-equilibrium offset is developed for uncertain quadrotor systems at non-equilibrium operating conditions.

6.1 Problem Statement

In this section, we investigate the system characteristics over a typical flight conditions and present our control problem. There are three significant differences between the work in this chapter and [47]. First, as shown in following the linearized system is with a non-diagonal interactor matrix. Second, there exists a non-equilibrium offset to be eliminated. Third, the drag effect is considered in the system dynamic model.

6.1.1 Linearized Models at Typical Flight Conditions

In this part, we survey two typical flight conditions to show the interactor matrices and gain matrix signs of different modes may differ from each other.

Generalized hover condition

The hover condition is the condition that the quadrotor is hovering around some arbitrary position with arbitrary yaw angle while all the angular velocities of the drone are zero. The system is at its equilibrium point as

$$x_{\text{hov}} = [x_E, y_E, z_E, 0, 0, 0, 0, 0, \psi_e, 0, 0, 0]^T, \tag{6.1}$$

where x_E, y_E, z_E are arbitrary and ψ_e is a constant, and the input vector is given by

$$u_{\text{hov}} = [mg, 0, 0, 0]^T. \tag{6.2}$$

The modified left interactor (MLI) matrix is obtained as

$$\xi_{m,hov}(s) = \begin{bmatrix} (s+1)^2 & 0 & 0 & 0 \\ 0 & (s+1)^4 & 0 & 0 \\ 0 & 0 & (s+1)^4 & 0 \\ 0 & 0 & 0 & (s+1)^2 \end{bmatrix}, \tag{6.3}$$

and the high frequency gain matrix is

$$K_{p,hov} = \begin{bmatrix} 1/m & 0 & 0 & 0 \\ 0 & -gC_{\psi_e}/J_x & gS_{\psi_e}/J_y & 0 \\ 0 & gS_{\psi_e}/J_x & gC_{\psi_e}/J_y & 0 \\ 0 & 0 & 0 & 1/J_z \end{bmatrix}. \tag{6.4}$$

If ψ_e is in $(-\pi/2, \pi/2)$ as (6.1), then the signs of the leading principal minors of $K_{p,hov}$ are known and nonzero as $\Delta_1 > 0, \Delta_2 < 0, \Delta_3 < 0, \Delta_4 < 0$, where Δ_k is the kth order leading principal minors of $K_{p,hov}$. If ψ_e is in $(\pi/2, 3\pi/2)$ as , then the signs of the leading principal minors of $K_{p,hov}$ are known and nonzero as $\Delta_1 > 0, \Delta_2 > 0, \Delta_3 < 0, \Delta_4 < 0$.

Cruise condition along the direction of x_E

When the quadrotor is flying in the horizontal plane and the velocity direction is along the x_E axis, say, the pitch angle θ is nonzero to generate a propulsion force against the drag effect. The state vector of the cruise condition along the direction of x_E is given by

$$x_{pit} = [x_E, y_E, z_E, \dot{x}_o, 0, 0, 0, \theta_o, 0, 0, 0, 0]^T, \tag{6.5}$$

where x_E, y_E, z_E are arbitrary, $\theta_o, \dot{x}_o$ are constants. Since the speed $\dot{x}_o$ along th x_E axis is a constant, the acceleration $\ddot{x}_E$ along the x_E axis is zero. The input vector is given by

$$u = [mg/C_{\theta_o}, 0, 0, 0]^T. \tag{6.6}$$

For the cruise condition, the interactor matrix can be obtained as

$$\xi_{m,pit}(s) = \begin{bmatrix} (s+1)^2 & 0 & 0 & 0 \\ 0 & (s+1)^4 & 0 & 0 \\ -T_{\theta_o}(s+1)^4 & 0 & (s+1)^4 & 0 \\ 0 & 0 & 0 & (s+1)^2 \end{bmatrix}, \tag{6.7}$$

where $T_{\theta_o} = \tan \theta_o$ is the tangent value of the constant pitch angle θ_o at the given operating point, such that the high frequency gain matrix is

$$K_{p,pit} = \begin{bmatrix} C_{\theta_o}/m & 0 & 0 & 0 \\ 0 & -\frac{g}{J_x} & 0 & \frac{g(T_{\theta_o} - S_{\theta_o})}{C_{\theta_o} J_z} \\ 0 & 0 & \frac{g(T_{\theta_o}^2 + C_{\theta_o})}{J_y C_{\theta_o}} & 0 \\ 0 & 0 & 0 & 1/C_{\theta_o} J_z \end{bmatrix}. \tag{6.8}$$

If θ_o is in $(-\pi/2, \pi/2)$ as (6.5), then the signs of the leading principal minors of $K_{p,pit}$ are known and nonzero as $\Delta_1 > 0, \Delta_2 < 0, \Delta_3 < 0, \Delta_4 < 0$ which are the same as the general hover condition in (6.1). If θ_o is in $(0.77\pi, 1.23\pi)$, then the signs of the leading principal minors of $K_{p,pit}$ are known and nonzero as $\Delta_1 < 0, \Delta_2 > 0, \Delta_3 > 0, \Delta_4 < 0$. If θ_o is in $(\pi/2, 0.77\pi) \cup (1.23\pi, 3\pi/2)$, then the signs of the leading principal minors of $K_{p,pit}$ are known and nonzero as $\Delta_1 < 0, \Delta_2 > 0, \Delta_3 < 0, \Delta_4 > 0$.

6.1.2   Control objective

The system model of the quadrotor with high cruise speed is described as

$$\dot{x}(t) = Ax(t) + Bu(t) + f_o, \quad y(t) = Cx(t), \tag{6.9}$$

where $x(t) \in R^n$ is the state vector, $u(t) \in R^M$ is the input vector, $y(t) \in R^M$ is the output vector, f_o is an unknown constant vector A and B are unknown matrices, C is the known output matrix

$$C = \begin{bmatrix} C_t & 0_{3\times3} & 0_{3\times3} & 0_{3\times3} \\ 0_{1\times3} & 0_{1\times3} & C_r & 0_{1\times3} \end{bmatrix}. \tag{6.10}$$

The objective of this research is to design a multivariable adaptive control scheme for a quadrotor at a non-equilibrium operating condition at which the linearized system model has a non-diagonal interactor matrix. The adaptive control scheme ensures that all signals in the closed-loop system are bounded, and the output of the system $y(t)$ asymptotically tracks a reference signal $y_m(t)$ generated from a reference model system

$$y_m(t) = W_m(s)[r](t), \quad W_m(s) = \xi_m^{-1}(s). \tag{6.11}$$

where $r(t)$ is a bounded reference input signal.

6.2   Adaptive Control Scheme

A multivariable control scheme is developed for the linearized system with input compensator in this section, which can compensate the unknown non-equilibrium offset and the uncertain parameters.

6.2.1 Nominal Controller Design

When the system parameters are known, the nominal controller of state feedback for output tracking is given by

$$u^*(t) = K_x^{*T}x(t) + K_r^*r(t) + k_f^*, \tag{6.12}$$

where the non-equilibrium matching parameter $k_f^* \in R^M$ is used to cancel the effect of the non-equilibrium offset $f_o = f(x_o, u_o)$, and $K_x^{*T} \in R^{M \times n}$ and $K_r^{*T} \in R^{M \times M}$ are for the plant-model output matching:

$$C(sI - A - BK_x^{*T})^{-1}BK_r^* = W_m(s), \; K_r^{*-1} = K_p, \tag{6.13}$$

where K_p is the high-frequency gain matrix in (2.17). The existence of K_x^* and K_r^* is guaranteed by following lemma.

Lemma 2 [27]. *There exist K_x^* and K_r^* such that the plant-model matching condition (6.13) holds.*

Non-equilibrium offset rejection design

Substituting the applied controller (6.12) into the linearized system, the closed-loop system in the frequency domain is

$$y(s) = C(sI - A - BK_x^{*T})^{-1}BK_r^*r(s) + \delta(s), \tag{6.14}$$

where

$$\delta(s) = C(sI - A - BK_x^{*T})^{-1}BK_r^*(B\frac{k_f^*}{s} + \frac{f_o}{s}), \tag{6.15}$$

The we can derive the output-tracking error in s domain from the reference system in (6.11) and the matching conditions as (6.13), which is

$$e(s) = y(s) - y_m(s) = \delta(s). \tag{6.16}$$

Then the final value of the tracking error can be found as

$$\lim_{t \to \infty} e(t) = \lim_{t \to \infty} \delta(t) = \lim_{s \to 0} s\delta(s) = Dk_f^* + d, \tag{6.17}$$

where

$$D = -C(A + BK_x^*)^{-1}B$$

$$d = -C(A + BK_x^*)^{-1}f_o.$$

In order to reject the offset d, the nominal parameter k_f^* should be as

$$k_f^* = -D^{-1}d \tag{6.18}$$

so that $\lim_{t \to \infty} \delta(t) = 0$, where D is nonsingular as the result of Assumption (A1). Then from (6.17) and (6.18), it follows that

$$\lim_{t \to \infty} (y(t) - y_m(t)) = \lim_{t \to \infty} \delta(t) = 0. \tag{6.19}$$

In summary, the following lemma is given for the nominal controller.

Lemma 3. *For the plant (6.9) in the presence of the non-equilibrium offset f_o, there exist matrices K_x^*, K_r^* and k_f^*, with which the state feedback controller (6.12) ensures the closed-loop signal boundedness, nonlinear offset rejection, and output tracking of a chosen reference output $y_m(t)$ by the output $y(t)$.*

6.2.2 Adaptive Controller Design

When the system parameters and the offset vector f_o are unknown, the state-feedback controller structure is given as

$$u(t) = K_x^T(t)x(t) + K_r(t)r(t) + k_f(t), \tag{6.20}$$

where $K_x(t)$, $K_r(t)$ and $k_f(t)$ are the estimates of the nominal controller parameters K_x^*, K_r^* and k_f^* .

Error equation

By substituting the control law as (6.20) into the system model as (6.9), we can write the system dynamic as

$$
\begin{aligned}
\dot{x}(t) =& Ax(t) + B(K_x^T(t)x(t) + K_r(t)r(t) + k_f(t)) + f_o \\
=& (A + BK_x^{*T})x(t) + BK_r^*r(t) + Bk_f^* + f_o \\
& + B(\tilde{K}_x^T(t)x(t) + \tilde{K}_r(t)r(t) + \tilde{k}_f(t))
\end{aligned}
\tag{6.21}
$$

where $\tilde{K}_x(t) = K_x(t) - K_x^*$, $\tilde{K}_r(t) = K_r(t) - K_r^*$, $\tilde{k}_f(t) = k_f(t) - k_f^*$. The tracking error of the system is $e(t) = y(t) - y_m(t)$, by combing the reference model system as (6.11), the matching conditions in(6.13), and the closed-loop system as (6.21), $e(t)$ can be represented as

$$e(t) = y(t) - y_m(t) = W_m(s)K_p[\tilde{\Theta}^T\omega](t) + \delta(t) \tag{6.22}$$

where $\tilde{\Theta}(t) = \Theta(t) - \Theta^*$, $\Theta(t) = [K_x^T(t), K_r(t), k_f(t)]^T$, $\Theta^* = [K_x^{*T}, K_r^*, k_f^*]^T$, $\omega(t) = [x^T(t), r^T(t), 1]^T$. To deal with the uncertainty of K_p, the LDS decomposition [27] is used as

$$K_p = L_s D_s S, \tag{6.23}$$

where $S \in R^{M \times M}$ is a symmetric positive definite matrix, $L_s \in R^{M \times M}$ is a unity lower triangular matrix, and

$$D_s = \{\text{sign}[\Delta_1]\gamma_1, \text{sign}\left[\frac{\Delta_2}{\Delta_1}\right]\gamma_2, \ldots, \text{sign}\left[\frac{\Delta_M}{\Delta_{M-1}}\right]\gamma_M\} \tag{6.24}$$

such that $\gamma_i \geq 0$, $i = 1, \ldots, M$, may be chosen to be arbitrary.

Estimation error

The next step is to parameterize the tracking-error signal and establish the model of estimation error which is crucial for deriving the adaptive laws of the controller parameters. By substituting the LDS decomposition of K_p as (6.23) in to the parameterized tracking error as (6.22), we have

$$L_s^{-1}\xi_m(s)[e](t) = D_s S \tilde{\Theta}^T(t)\omega(t). \tag{6.25}$$

The term δ is omitted because it is exponentially decaying according to the choice of k_f^* in (6.18). A parameter matrix is introduced as

$$\Theta_0^* = L_s^{-1} - I = \begin{bmatrix} 0 & 0 & 0 & \cdots & 0 \\ \theta_{21}^* & 0 & 0 & \cdots & 0 \\ \theta_{31}^* & \theta_{32}^* & 0 & \cdots & 0 \\ \vdots & \vdots & \vdots & \vdots & \vdots \\ \theta_{M-11}^* & \cdots & \theta_{M-1M-2}^* & 0 & 0 \\ \theta_{M1}^* & \cdots & \theta_{MM-2}^* & \theta_{MM-1}^* & 0 \end{bmatrix} \in R^{M \times M}. \tag{6.26}$$

Consider a stable and monic polynomial $f_h(s)$, whose degree is equal to the maximum degree of $\xi_m(s)$. Operating both sides of (6.25) by $I_M/f_h(s)$, we obtain the filtered

tracking error

$$\bar{e}(t) + [0, \theta_2^{*T}\eta_2(t), \theta_3^{*T}\eta_3(t), \ldots, \theta_M^{*T}\eta_M(t)]^T = D_s Sh(s)[\tilde{\Theta}^T\omega](t), \qquad (6.27)$$

where $\bar{e}(t) = \xi_m(s)h(s)[e](t) = [\bar{e}_1(t), \ldots, \bar{e}_M(t)]^T$, $\eta_i(t) = [\bar{e}_1(t), \ldots, \bar{e}_{i-1}(t)]^T$, for $i = 2, \ldots, M$, $\theta_i^* = [\theta_{i1}^*, \ldots, \theta_{ii-1}^*]^T$, for $i = 2, \ldots, M$. Based on this error equation, we construct the estimation error vector signal:

$$\epsilon(t) = \bar{e}(t) + [0, \theta_2^T(t)\eta_2(t), \theta_3^T(t)\eta_3(t), \ldots, \theta_M^T(t)\eta_M(t)]^T + \Psi(t)\xi(t), \qquad (6.28)$$

where $\theta_i(t)$ are the estimates of θ_i^*, $\Psi(t)$ is the estimate of $\Psi^* = D_s S$, and $\xi(t) = \Theta^T(t)\zeta(t) - h(s)[\Theta^T\omega](t)$, $\zeta(t) = h(s)[\omega](t)$. From (6.27) and (6.28), it then follows that

$$\epsilon(t) = [0, \tilde{\theta}_2^T(t)\eta_2(t), \tilde{\theta}_3^T(t)\eta_3(t), \ldots, \tilde{\theta}_M^T(t)\eta_M(t)]^T + \tilde{\Psi}(t)\xi(t) + D_s S\tilde{\Theta}^T(t)\zeta(t), (6.29)$$

where $\tilde{\theta}_i(t) = \theta_i(t) - \theta_i^*$ and $\tilde{\Psi}(t) = \Psi(t) - \Psi^*$ are the related parameter errors.

Adaptive laws

With the estimation error model (6.29), we choose the adaptive laws

$$\dot{\theta}_i(t) = -\frac{\Gamma_{\theta_i}\epsilon_i(t)\eta_i(t)}{m^2(t)}, i = 2, 3, \ldots, M \qquad (6.30)$$

$$\dot{\Theta}^T(t) = -\frac{D_s\epsilon(t)\zeta^T(t)}{m^2(t)}, \qquad (6.31)$$

$$\dot{\Psi}(t) = -\frac{\Gamma\epsilon(t)\xi^T(t)}{m^2(t)} \qquad (6.32)$$

where the signal $\epsilon(t) = [\epsilon_1(t), \epsilon_2(t), \ldots, \epsilon_M(t)]^T$ is computed from (6.29), $\Gamma_{\theta_i} = \Gamma_{\theta_i}^T > 0$ and $\Gamma = \Gamma^T > 0$ are adaptation gain matrices, and

$$m(t) = \sqrt{1 + \zeta^T(t)\zeta(t) + \xi^T(t)\xi(t) + \Sigma_{i=2}^M \eta_i^T(t)\eta_i(t)}, \tag{6.33}$$

is a standard normalization signal.

6.2.3   Stability analysis

The desired properties of the adaptive laws for the linearized system at each operating condition is established in this part. Then the closed-loop system stability is analyzed.

Lemma 4. *The adaptive laws (6.30)-(6.32) ensure the following desired properties:*

1. $\theta_i(t) \in L^\infty (i = 2, 3, \ldots, M), \Theta(t) \in L^\infty, \Psi \in L^\infty, \frac{\epsilon(t)}{m(t)} \in L^2 \cap L^\infty$; *and*

2. $\dot{\theta}_i(t) \in L^2 \cap L^\infty (i = 2, 3, \ldots, M), \dot{\Theta}(t) \in L^2 \cap L^\infty, \dot{\Psi}(t) \in L^2 \cap L^\infty$.

Based on Lemma 4, we can derive the following properties of closed-loop system for each linearized system model:

Theorem 1. *The multivariable MRAC scheme with the state feedback control law (6.20) updated by the adaptive laws (6.30)-(6.32), when applied to the system (6.9), guarantees the closed-loop signal boundedness and asymptotic output tracking:* $\lim_{t \to \infty} (\Delta y(t) - \Delta y_m(t)) = 0$, *for any initial conditions.*

The key step of proving Lemma 4 is to choose a positive definite Lyapunov function candidate as

$$V = \frac{1}{2}(\sum_{i=2}^M \tilde{\theta}_i^T \Gamma_{\theta_i}^{-1} \tilde{\theta}_i + \text{tr}[\tilde{\Psi}^T \Gamma^{-1} \tilde{\Psi}] + \text{tr}[\tilde{\Theta} S \tilde{\Theta}^T]) > 0. \tag{6.34}$$

Then proof of Theorem 1 is in a similar way to that derived in [27].

6.3 Simulation Study

Table 6.1: Parameter values for simulation

Parameter	Value	Unit
c_m	0.0025	m·s
c_r	0.001	N·m·s
c_t	0.25	N·m·s
d	0.2	m
g	9.8	m/s^2
J_x	0.005	kg·m^2
J_y	0.005	kg·m^2
J_z	0.009	kg·m^2
m	2	kg

The quadrotor system is linearized at the high speed cruise condition in the x_E direction with pitch angle $\theta = 0.3$ rad and velocity $\dot{x}_E = 12$ m/s. For $t \in [0, 20) \cap [40, 50]$, $r = [0, 0, 12t, 0]^T$, the quadrotor is flying along x_E direction with the speed as $12m/s$. For $t \in [20, 40)$, $r = [\sin(1.5t), 2\cos(0.96t), 12t, 0]^T$, the quadrotor is flying along a circular path in $y_E - z_E$ plane in addition to the uniform motion along x_E.

The simulation results can be found in Figure 6.1. The tracking error $e_z(t) = z_E(t) - z_m(t)$ is relatively large in the first 10 seconds. With the proposed MRAC design, the output tracking error $e_z(t)$ decreases exponentially as the time increases. The simulation results have verified that the proposed approach is effective at the non-equilibrium operating conditions of linearized quadrotor systems.

6.4 Summary

In this chapter, we developed a linearization-based model reference adaptive control scheme for a multivariable quadrotor system. The proposed adaptive design can reject
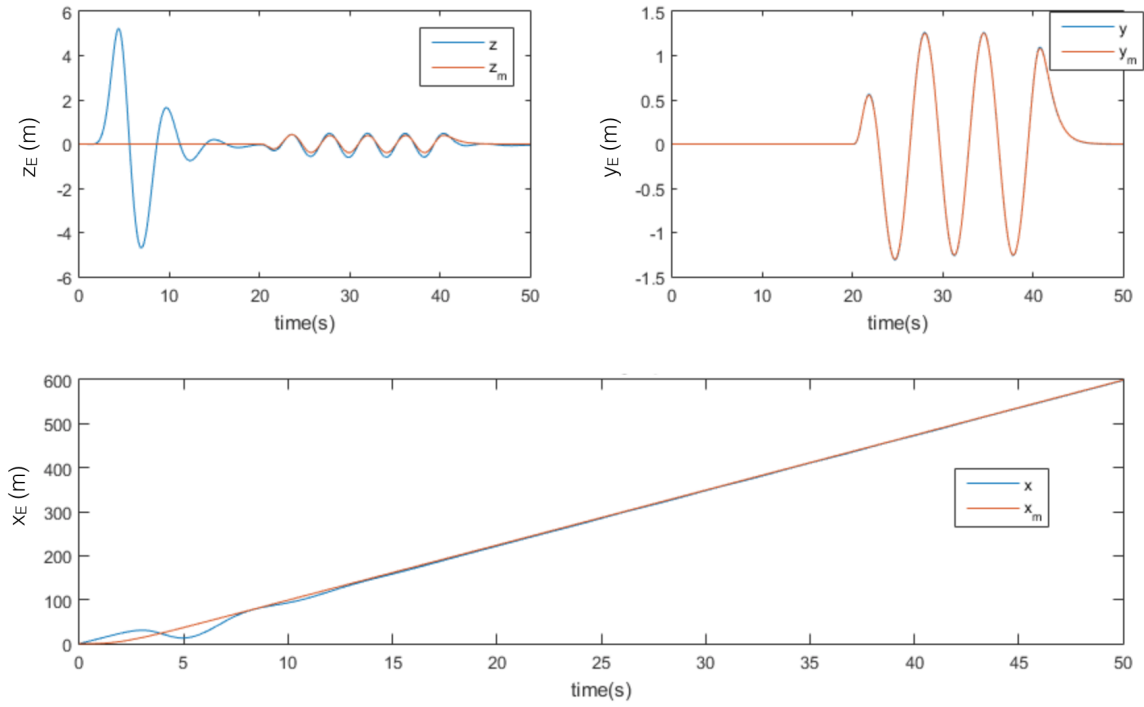
Figure 6.1: System responses for high speed cruise condition.

the non-equilibrium offset and make the closed-loop system signals bounded and the outputs track the chosen reference signals asymptotically.

Chapter 7

Input Compensation Design for Quadrotors

This chapter presents an adaptive controller design framework with input compensation for quadrotor systems, which is expected to work at different system operating conditions with a uniform updating law for the controller parameters. The motivation of the part is to handle the situations that existing adaptive control schemes are either restricted to the system equilibrium as at the hover condition or unable to deal with the full system uncertainties, which cause system interactor matrix and high frequency gain matrix to change. An adaptive control scheme with an input compensator is constructed for a uniform interactor matrix and a consistent pattern of the gain matrix signs over different operating conditions, which are key prior design conditions for model reference adaptive control. To deal with the uncertain system high-frequency gain matrix, a gain matrix decomposition technique is employed to parametrize an error system model in terms of the parameter and tracking errors, for the design of an adaptive parameter update law with reduced system knowledge. Stability analysis shows that all closed-loop system signals are bounded, and the system output tracks a reference output asymptotically despite the system parameter

uncertainties and the uncertain offsets at non-equilibrium operating points. The proposed scheme expands the capacity of adaptive control for quadrotors to operate at multiple operating conditions in the presence of system uncertainties. Simulation results of a quadrotor system with the proposed adaptive control scheme are presented to show the desired system performance.

The main contributions of this part are summarized as follows.

- A unified framework of multivariable adaptive control schemes with a uniform interactor matrix for quadrotor systems of multiple operating conditions is established to meet desired asymptotic output tracking in addition to system stability.

- A thorough study of the system characteristic for a quadrotor system with input compensator is performed, whose interactor matrices and gain matrix signs are consistent for multiple typical operating conditions.

- Adaptive state feedback based control with rejection of non-equilibrium offset is developed for uncertain quadrotor systems that may work at non-equilibrium points, including key design condition specification, nominal plant-model matching control design and its adaptive version with adaptive laws and stability analysis.

- Extensive simulation results are obtained through a quadrotor model with multiple operating conditions, to verify the effectiveness of our proposed adaptive control algorithm.

7.1 Problem Statement

Consider a quadrotor dynamic model

$$\dot{x}_p(t) = f(x_p(t), u_p(t)) \tag{7.1}$$

$$y_p(t) = C_p x_p(t), \tag{7.2}$$

where $x_p(t)$ is the state vector, $u_p(t)$ is the input vector, $y_p(t)$ is the output vector, f and h represent the system dynamics with unknown parameters, C_p is a known output matrix. As discussed in last section, most of the control methods on quadrotors are based on linearization approaches. We can linearize the system at an arbitrary operating point (x_o, u_o) as

$$\Delta\dot{x}_p(t) = A_p \Delta x_p(t) + B_p \Delta u_p(t) + f_{op} \tag{7.3}$$

$$\Delta y_p(t) = C_p \Delta x_p(t), \tag{7.4}$$

where $\Delta x_p(t) = x_p(t) - x_o$, $\Delta u_p(t) = u_p(t) - u_o$, A_p, B_p are system matrices with unknown parameters, and $f_{op} = f(x_o, u_o)$ is the non-equilibrium offset of the system at the chosen operating point. Among the linearization based designs, the PID controllers [18–20] are most widely used to control quadrotors at the equilibrium point for tasks around hover condition. However, the PID controller can only work with constant reference signals and can not deal with high order systems with parameter uncertainties like a quadrotor.

MRAC is an effective control method dealing with parameter uncertainty of systems. It has been used on quadrotor systems with random reference signals in [47] and [58]. When $f_{op} = 0$, the linearized quadrotor system can be expressed as

$$\Delta y_p(t) = G_0(s)[\Delta u_p](t) \triangleq \mathcal{L}^{-1}\{G_0(s)\Delta U_p(s)\}, \tag{7.5}$$

where $\mathcal{L}^{-1}\{*\}$ is the inverse Laplace transform operator. The notation (7.5) represents that $\Delta y_p(t)$ is the output of a system with transfer matrix $G_0(s)$ by the input $\Delta u_p(t)$, where the transfer matrix is defined as $G_0(s) = C_p(sI - A_p)^{-1}B_p$.

For the multivariable MRAC for output tracking , the goal is to design a control signal $\Delta u_p(t)$ such that all signals in the closed-loop system are bounded, and the output of the linearized system $\Delta y_p(t)$ asymptotically tracks a reference signal $y_m(t)$, with $y_m(t)$ generated from a reference model system

$$y_m(t) = \xi_m^{-1}(s)[r](t), \tag{7.6}$$

where $r(t)$ is a bounded reference signal, $\xi_m(s)$ is the modified left interactor matrix of the transfer matrix $G_0(s)$. The updating law of $\Delta u_p(t)$ requires the information of the signs of the leading principal minors of the high-frequency matrix K_p.

The quadrotor system should be able to work at different operating points for different tasks. However, the quadrotor system may have different linearized models at different operating points, which may lead to different transfer matrices. In this part, we investigate the system characteristics over two typical flight conditions and present our control problem of quadrotor systems at multiple operating conditions.

Control objective

In this paper, a sequential linear system with unknown non-equilibrium offset is used to represent the linearized quadrotor system models under multiple operating conditions, and such a system model is described as

$$\Delta \dot{x}_p(t) = \bar{A}(t)\Delta x_p(t) + \bar{B}(t)\Delta u(t) + \bar{f}_o(t) \tag{7.7}$$

$$\Delta y_p(t) = C_p \Delta x_p(t), \tag{7.8}$$

where $\bar{A}(t)$ and $\bar{B}(t)$ are unknown piecewise-constant matrices, and $\bar{f}_o(t)$ is an unknown piecewise-constant vector, C_p is the known output matrix as

$$C_p = \begin{bmatrix} C_t & 0_{3\times3} & 0_{3\times3} & 0_{3\times3} \\ 0_{1\times3} & 0_{1\times3} & C_r & 0_{1\times3} \end{bmatrix} \tag{7.9}$$

with the submatrices

$$C_t = \begin{bmatrix} 0 & 0 & 1 \\ 0 & 1 & 0 \\ 1 & 0 & 0 \end{bmatrix}, \quad C_r = \begin{bmatrix} 0 & 0 & 1 \end{bmatrix}.$$

There are a finite number of unknown operating conditions of the quadrotor system, and the ith operating condition of the system is characterized as $(A_{oi}, B_{oi}, f_{opi})$, $i = 1, 2, \ldots, N$. For a given time t, the system is at an unknown operating condition j with the system parameter matrices $\bar{A}(t) = A_{pj}$, $\bar{B}(t) = B_{pj}$, and $\bar{f}_o(t) = f_{opj}$.

Our objective is to design a multivariable adaptive control scheme for a quadrotor operating at different conditions at which the linearized system models have different and uncertain interactor matrices and gain matrix signs, in the presence of system parameter uncertainties. The adaptive control scheme uses an input compensator to result in a uniform interactor matrix $\xi_m(s)$ for system models over multiple operating conditions, and ensures that all signals in the closed-loop system are bounded, and the output of the system $\Delta y_p(t)$ asymptotically tracks a reference signal $y_m(t)$ generated from a reference model system

$$y_m(t) = W_m(s)[r](t), \tag{7.10}$$

where $r(t)$ is a bounded reference input signal, and $W_m(s) = \xi_m^{-1}(s)$.

Remark 6. In this chapter, we assume that the system stays at an operating condition

for some sufficient time before switching to another such that the model switching cause no fatal problem for the stability. This is because the main goal of this work is to solve the quadrotor control problem of inconsistent interactor matrices and gain matrix signs under multiple operating conditions. Due to space limit, the problem of the switch of system stability will be not considered in this paper.   □

7.2   Input Compensation for Quadrotors with Dynamics Mutation

In order to design a uniform adaptive controller for different operating conditions, we introduce the control design as input compensation. The technique can modify the system so that the prior information are not changed at different operating conditions.

7.2.1   Input Compensation Technique

From last section, it is learned that there is a uniform interactor matrix at some operating points. Though they do not share a same high-frequency gain matrix, the signs of the leading principal minors are the same if some realistic conditions are applied. However, there are also many operating points without a diagonal interactor matrix. As shown in Section IV.B, the interactor matrices of those operating points are even depended on the state. In order to remain the advantage of the MRAC scheme, we wish to obtain diagonal interactor matrices via additional controller structure.

A dynamic input compensator is studied in [128] to make its Hermite normal form diagonal for a MIMO plant with the knowledge of the relative degrees of the plant transfer matrix. It is demonstrated that a diagonal input compensator can be designed such that the transfer matrix with compensation has a diagonal Hermite form. The following lemma is based on the work in [128]:

Lemma 5. *For any $m \times m$ strictly proper and full rank matrix $G_0(s)$ with the knowledge of the relative degrees of its elements, there exist a diagonal polynomial matrix $\xi_m(s)$ and a stable diagonal nonsingular input compensator $W_c(s)$ such that the high frequency gain matrix with input compensation of $G_0(s)$ as $K_{pc} = \lim_{s \to \infty} \xi_m(s) G_0(s) W_c(s)$ is nonsingular.*

As shown in the previous section, the relative degrees of the elements in $G_0(s)$ remain the same among the typical operating points. Then according to Lemma 1, there exists an input compensator for the linearized quadrotor models at the typical operating points.

7.2.2   Input Compensation for Quadrotor Systems

Equipped by the theory of input compensation, a stable diagonal nonsingular input compensator can be designed for the typical operating conditions of the quadrotor system as

$$
W_c(s) = \begin{bmatrix} \dfrac{1}{(s+b)^2} & 0 & 0 & 0 \\ 0 & 1 & 0 & 0 \\ 0 & 0 & 1 & 0 \\ 0 & 0 & 0 & 1 \end{bmatrix},
\tag{7.11}
$$

where b is a positive constant. For the typical operating conditions with the input compensator as in (7.11), the corresponding uniform modified left interactor matrix is

$$
\xi_m(s) = \begin{bmatrix} (s+a)^4 & 0 & 0 & 0 \\ 0 & (s+a)^4 & 0 & 0 \\ 0 & 0 & (s+a)^4 & 0 \\ 0 & 0 & 0 & (s+a)^2 \end{bmatrix}
\tag{7.12}
$$

such that the high-frequency gain matrix

$$K_{pc} = \lim_{s \to \infty} \xi_m(s)G(s) \tag{7.13}$$

is nonsingular, where a is a positive constant and the compensated system is

$$G(s) = G_0(s)W_c(s). \tag{7.14}$$

For the conditions with diagonal interactor matrices in Section 4.1.1, the high-frequency gain matrix with input compensation K_{pc} remains the same as the original high-frequency matrix K_p. The results for the signs of the leading principal minors remains, if the conditions on attitude still hold. The results of the operating points with non-diagonal interactor matrices as Section 4.1.2 will change as following:

Uniform motion condition along the x_E axis

$$K_{pc,pit} = \begin{bmatrix} C_{\theta_o}/m & 0 & -\dfrac{gT_{\theta_o}}{C_{\theta_o}J_y} & 0 \\ 0 & -g/J_x & 0 & \dfrac{g(T_{\theta_o} - S_{\theta_o})}{C_{\theta_o}J_z} \\ S_{\theta_o}/m & 0 & g/J_y & 0 \\ 0 & 0 & 0 & 1/(C_{\theta_o}J_z) \end{bmatrix}. \tag{7.15}$$

If θ_o satisfies

$$\theta_o \in (-\pi/2, \pi/2), \tag{7.16}$$

then the signs of the leading principal minors of $K_{pc,pit}$ are the same as $\Delta_1 > 0, \Delta_2 < 0, \Delta_3 < 0, \Delta_4 < 0$, which are known and nonzero.

Uniform motion condition along the y_E axis

$$
K_{pc,rol} = \begin{bmatrix}
C_{\phi_e}/m & -gT_{\phi_e}/J_x & 0 & 0 \\
-S_{\phi_e}/m & -g/C_{\phi_e}J_x & 0 & 0 \\
0 & 0 & g/J_y & 0 \\
0 & 0 & S_{\phi_e}/J_y & C_{\phi_e}/J_z
\end{bmatrix}.
\tag{7.17}
$$

If ϕ_o satisfies

$$
\phi_0 \in (-\pi/2, \pi/2),
\tag{7.18}
$$

then the signs of the leading principal minors of $K_{pc,rol}$ are the same as $\Delta_1 > 0, \Delta_2 < 0, \Delta_3 < 0, \Delta_4 < 0$, which are known and nonzero.

We can integrate the conditions for attitude as following:

$$
\phi_o \in (-\tfrac{\pi}{2}, \tfrac{\pi}{2}), \quad \theta_o \in (-\tfrac{\pi}{2}, \tfrac{\pi}{2}), \quad \psi_o \in (-\tfrac{\pi}{2}, \tfrac{\pi}{2})
$$
$$
\phi_o\theta_o = 0, \quad \phi_o\psi_o = 0, \quad \theta_o\psi_o = 0.
\tag{7.19}
$$

By summarizing Lemma 5 together with our compensator design in (7.11), we can build a proposition for the quadrotor system in (3.1)-(3.9), which is at one of those different operating conditions satisfying (7.19), as follows:

Proposition 3. *There exists a nonsingular input compensator $W_c(s)$ as in (7.11) such that the compensated system $G(s)$ in (7.14) have a uniform diagonal interactor matrix $\xi_m(s)$ as in (7.12) and signs of the leading principal minors of K_{pc} as (7.13) are known and nonzero as $\Delta_1 > 0, \Delta_2 < 0, \Delta_3 < 0, \Delta_4 < 0$.*

7.2.3 System Model with Input Compensator

The adaptive control proposed in this paper consists two parts, which are an input compensator and an adaptive controller. The control input signal with input

compensation can be denoted as

$$\Delta u(t) = W_c(s)[v](t),\tag{7.20}$$

where $v(t)$ is the applied control signal from the adaptive controller, whose parameters are updated by the adaptive laws designed next. Consider the linearized quadrotor system with the input compensator as the new plant, whose transfer function is $G(s) = G_0(s)W_c(s)$, the input-output form of the system is obtained as

$$\Delta y_p(t) = G(s)[v](t) + G_f(s)[f_o](t).\tag{7.21}$$

We denote the state vector for the plant with input compensator as

$$x(t) = \begin{bmatrix} \Delta x_p(t) \\ x_c(t) \end{bmatrix},\tag{7.22}$$

where $\Delta x_p(t) = x_p(t) - x_o$, and $x_c(t)$ is the state vector of the input compensator. For the particular design of $W_c(s)$ in (7.11), we have

$$x_c(t) = \begin{bmatrix} \Delta u_1(t) \\ \Delta \ddot{u}_1(t) \end{bmatrix},\tag{7.23}$$

where $\Delta u_1(t)$ is the first element of $\Delta u(t)$.

The model of the new total plant, which is the combination of the linearized model at (x_o, u_o) and the input compensator $W_c(s)$ in (7.11), is denoted as

$$\dot{x}(t) = Ax(t) + Bv(t) + f_o, \quad y(t) = Cx(t),\tag{7.24}$$

where $x(t)$ is the state vector denoted in (7.22), $v(t)$ is the applied control signal, $y(t) = \Delta y_p(t)$, C is the known output matrix as

$$C = \begin{bmatrix} C_p & 0_{4\times2} \end{bmatrix}, \tag{7.25}$$

and the parameter matrices are

$$A = \begin{bmatrix} 0_{3\times3} & I_{3\times3} & 0_{3\times3} & 0_{3\times3} & 0_{3\times1} & 0_{3\times1} \\ 0_{3\times3} & -c_t I_{3\times3} & A_t & 0_{3\times3} & B_t & 0_{3\times1} \\ 0_{3\times3} & 0_{3\times3} & A_s & A_w & 0_{3\times1} & 0_{3\times1} \\ 0_{3\times3} & 0_{3\times3} & 0_{3\times3} & A_r & 0_{3\times1} & 0_{3\times1} \\ 0_{1\times3} & 0_{1\times3} & 0_{1\times3} & 0_{1\times3} & 0 & 1 \\ 0_{1\times3} & 0_{1\times3} & 0_{1\times3} & 0_{1\times3} & -b^2 & -2b \end{bmatrix} \tag{7.26}$$

$$B = \begin{bmatrix} 0_{3\times1} & 0_{3\times3} \\ 0_{3\times1} & 0_{3\times3} \\ 0_{3\times1} & 0_{3\times3} \\ 0_{3\times1} & B_r \\ 0 & 0_{1\times3} \\ 1 & 0_{1\times3} \end{bmatrix} \tag{7.27}$$

$$f_o = \begin{bmatrix} f_{op} \\ 0_{2\times1} \end{bmatrix}. \tag{7.28}$$

The transfer function can also be derived from the above system matrices by

$$G(s) = C(sI - A)^{-1}B, \tag{7.29}$$

from which the high-frequency gain with input compensation can be found. As the dynamics mutation under different operating conditions is well treated by the input

compensator, the remaining task is to design an adaptive control frame work dealing with the system uncertainties.

7.3   Adaptive Control Scheme

In this section, a state feedback adaptive controller is developed for the quadrotor system under multiple operating conditions in the presence of uncertain system parameters and non-equilibrium offset. The proposed controller consists two parts: a feedforward input compensator and a feedback adaptive controller. The input compensation technique assures that there exists a uniform interactor matrix for multiple operating points, for the design of a reference model system. The parameters of the adaptive controller are updated with the sign information of the corresponding gain matrix K_p.

In this section, a multivariable state feedback model reference adaptive control scheme for the linearized system with input compensator will be developed to compensate the unknown non-equilibrium offset and the uncertainties of system parameters. The nominal nonlinear offset rejection design is first developed for the system with known parameters, and then an adaptive design is developed using decomposition of the gain matrix K_{pc}.

Remark 7. Like other linearization based designs, the adaptive controller proposed in this section is designed for linearized models at operating points and expected to work around the operating points.   □

7.3.1   Output Tracking Control Framework

We have shown that there exists a uniform input compensator for the typical operating conditions we studied. The interactor matrices and the signs of the leading principal minors of the high-frequency gain matrices keep consistent with the designed input

compensator. Then only one controller parameter update law is needed to control the quadrotor to work at a operating condition within the typical operating conditions. The adaptive control design procedure for quadrotors can be proposed as follows.

Compensated plant

Consider a linearized quadrotor system at a typical operating point (x_o, u_o), whose transfer matrix $G_0(s)$ is as (3.16). We can design an input compensator $W_c(s)$ as (7.11) such that the uniform interactor matrix with input compensation $\xi_m(s)$ is as (7.12) with the high-frequency gain matrix with input compensation K_{pc} as (7.13).

We can rewrite the system model of the compensated system in (7.24) as

$$y(t) = G(s)[v](t) + G_f(s)[f_o](t), \tag{7.30}$$

where

$$G(s) = C(sI - A)^{-1}B \tag{7.31}$$

$$G_f(s) = C(sI - A)^{-1}, \tag{7.32}$$

$y(t)$ is the output of the new plant, $v(t)$ is the applied input signal to be designed, f_o is the offset in (7.28).

Controller structure

The input signal of the new plant with input compensation can be denoted as

$$v(t) = K_x(t)x(t) + K_r(t)r(t) + k_f(t), \tag{7.33}$$

where the adaptive parameters K_x, K_r and k_f will be updated from adaptive laws using the knowledge of the signs of leading principal minor Δ_k of the high frequency

gain matrix with input compensation K_{pc}. The relationship between the $\Delta u_p(t)$ of the original linearized quadrotor system and the input of the new plant with input compensation $v(t)$ is

$$\Delta u_p(t) = W_c(s)[v](t), \tag{7.34}$$

where $W_c(s)$ is the input compensator designed as in (7.11).

Control problem

The control objective is to design a state feedback control signal $v(t)$ such that all signals in the closed-loop system are bounded and the output signal of the new plant with input compensation $y(t)$, as in (7.30), asymptotically tracks a given reference vector signal $y_m(t)$, which is generated by a reference system

$$y_m(t) = W_m(s)[r](t), \tag{7.35}$$

where the reference model is selected as $W_m(s) = \xi_m^{-1}(s)$, and $\xi_m(s)$ is the interactor matrix of the system with input compensation as (7.12).

Design condition verification

The plant assumptions for MRAC scheme design is introduced in Section 2.3, it is necessary to verify the linearized quadrotor system before further discussions. If the quadrotor system is linearized at a operating condition in (7.19), then the plant assumptions (A1)-(A4) are satisfied. To deal with the dynamics mutation, an input compensator is designed for the system, whose existence is guaranteed by Proposition 3.

It can be shown from the results in Section 7.2.2 and Section 7.2.3 that the system after compensation still satisfies all the assumptions. For the integrity of the

design procedure, we conclude that the system in (7.30) satisfies the following design conditions:

(C1) all zeros of $G(s)$ have negative real parts;

(C2) (A, B) is stabilizable and (A, C) is detectable;

(C3) the input compensator $W_c(s)$ of the system is known;

(C4) $G(s)$ has full rank and its modified left interactor matrix $\xi_m(s)$ is known; and

(C5) all leading principal minors Δ_k of the high-frequency gain matrix K_{pc} of $G(s)$ are nonzero and their signs are known.

7.3.2 Nominal controller design

When the parameters of the system are known, the nominal controller structure is given by

$$v(t) = K_x^{*T} x(t) + K_r^* r(t) + k_f^*, \tag{7.36}$$

where $k_f^* \in R^M$ is used to cancel the effect of the constant offset f_o, and $K_x^{*T} \in R^{M \times n}$ and $K_r^{*T} \in R^{M \times M}$ are for the plant-model output matching. The existence of the controller parameters have been proved in [84]. The value of them are also derived in [84] as

$$C(sI - A - BK_x^{*T})^{-1} BK_r^* = W_m(s), \qquad K_r^{*-1} = K_{pc}, \qquad k_f^* = -D^{-1}d, \tag{7.37}$$

where

$$D = - C(A + BK_x^*)^{-1} B$$

$$d = - C(A + BK_x^*)^{-1} f_o,$$

and the high-frequency gain matrix is

$$K_{pc} = \lim_{s \to \infty} \xi_m(s) C(sI - A)^{-1} B. \tag{7.38}$$

In summary, the following lemma is given for the nominal controller.

Lemma 6. *For the plant (7.24) in the presence of the non-equilibrium offset f_o, there exist matrices K_x^*, K_r^* and k_f^*, with which the state feedback controller (7.36) ensures the closed -loop signal boundedness of all s, nonlinear offset rejection, and output tracking of a chosen reference output $y_m(t)$ by the output $y(t)$.*

7.3.3 Adaptive Law Design

When the system parameters and the offset vector f_o are unknown, the state-feedback controller structure is given as

$$v(t) = K_x^T(t) x(t) + K_r(t) r(t) + k_f(t), \tag{7.39}$$

where $K_x(t)$, $K_r(t)$ and $k_f(t)$ are the estimates of the nominal controller parameters K_x^*, K_r^* and k_f^* .

Error equation

Substituting the control law (7.39) into the the system dynamic (7.24), we obtain

$$\dot{x}(t) = Ax(t) + B(K_x^T(t) x(t) + K_r(t) r(t) + k_f(t)) + f_o$$

$$= (A + BK_x^{*T}) x(t) + BK_r^* r(t) + Bk_f^* + f_o + B(\tilde{K}_x^T(t) x(t) + \tilde{K}_r(t) r(t) + \tilde{k}_f(t)) \tag{7.40}$$

where

$$\tilde{K}_x(t) = K_x(t) - K_x^*$$

$$\tilde{K}_r(t) = K_r(t) - K_r^*$$

$$\tilde{k}_f(t) = k_f(t) - k_f^*.$$

In view of the reference model system, matching conditions (7.37), and the closed-loop system (7.40), the output-tracking error is given as

$$e(t) = y(t) - y_m(t) = W_m(s)K_p[\tilde{\Theta}^T\omega](t) + \delta(t) \qquad (7.41)$$

where

$$\tilde{\Theta}(t) = \Theta(t) - \Theta^*$$

$$\Theta(t) = [K_x^T(t), K_r(t), k_f(t)]^T$$

$$\Theta^* = [K_x^{*T}, K_r^*, k_f^*]^T$$

$$\omega(t) = [\bar{x}^T(t), r^T(t), 1]^T.$$

To deal with the uncertainty of K_{pc}, the LDS decomposition [27] is used as

$$K_{pc} = L_s D_s S, \qquad (7.42)$$

where $S \in R^{M \times M}$ is a symmetric positive definite matrix, $L_s \in R^{M \times M}$ is a unity lower triangular matrix, and

$$D_s = \text{diag}\{s_1^*, s_2^*, \ldots, s_M^*\}$$

$$= \{\text{sign}[\Delta_1]\gamma_1, \text{sign}\left[\frac{\Delta_2}{\Delta_1}\right]\gamma_2, \ldots, \text{sign}\left[\frac{\Delta_M}{\Delta_{M-1}}\right]\gamma_M\} \qquad (7.43)$$

such that $\gamma_i \geq 0, i = 1, \ldots, M$, may be chosen to be arbitrary.

Remark 8. In the adaptive law design, the D_s matrix will be used as a gain matrix. Although K_{pc} is unknown and may vary among different operating conditions, based on previous discussion, a uniform D_s is known for the multiple operating conditions under consideration, which is crucial for deriving stable the adaptive laws.   □

Error parameterization

To obtain the adaptive laws for $K_x(t)$, $K_r(t)$, and $k_f(t)$, a well parameterized tracking-error model is needed. Substituting the LDS decomposition of K_{pc} in (7.42) and ignoring the exponentially decaying term $\delta(t)$, the error equation can be parameterized as

$$L_s^{-1}\xi_m(s)[e](t) = D_s S \tilde{\Theta}^T(t)\omega(t). \tag{7.44}$$

To parameterize the unknown matrix L_s, a parameter matrix is introduced as

$$\Theta_0^* = L_s^{-1} - I, \tag{7.45}$$

which has a special form as

$$\Theta_0^* = \begin{bmatrix} 0 & 0 & 0 & \cdots & 0 \\ \theta_{21}^* & 0 & 0 & \cdots & 0 \\ \theta_{31}^* & \theta_{32}^* & 0 & \cdots & 0 \\ \vdots & \vdots & \vdots & \vdots & \vdots \\ \theta_{M-11}^* & \cdots & \theta_{M-1M-2}^* & 0 & 0 \\ \theta_{M1}^* & \cdots & \theta_{MM-2}^* & \theta_{MM-1}^* & 0 \end{bmatrix} \in R^{M \times M}. \tag{7.46}$$

We introduce a filter $h(s) = 1/f_h(s)$, where $f_h(s)$ is a stable and monic polynomial whose degree is equal to the maximum degree of $\xi_m(s)$. Operating both sides of (7.44)

by $h(s)I_M$ leads to the filtered tracking error

$$\bar{e}(t) + [0, \theta_2^{*T}\eta_2(t), \theta_3^{*T}\eta_3(t), \ldots, \theta_M^{*T}\eta_M(t)]^T = D_s Sh(s)[\tilde{\Theta}^T\omega](t), \qquad (7.47)$$

where

$$\bar{e}(t) = \xi_m(s)h(s)[e](t) = [\bar{e}_1(t), \ldots, \bar{e}_M(t)]^T \qquad (7.48)$$

$$\eta_i(t) = [\bar{e}_1(t), \ldots, \bar{e}_{i-1}(t)]^T \text{ for } i = 2, \ldots, M \qquad (7.49)$$

$$\theta_i^* = [\theta_{i1}^*, \ldots, \theta_{ii-1}^*]^T \text{ for } i = 2, \ldots, M. \qquad (7.50)$$

Based on this error equation, we construct the estimation error vector signal:

$$\epsilon(t) = \bar{e}(t) + [0, \theta_2^T(t)\eta_2(t), \theta_3^T(t)\eta_3(t), \ldots, \theta_M^T(t)\eta_M(t)]^T + \Psi(t)\xi(t), \qquad (7.51)$$

where $\theta_i(t)$ are the estimates of θ_i^*, $\Psi(t)$ is the estimate of $\Psi^* = D_s S$, and

$$\xi(t) = \Theta^T(t)\zeta(t) - h(s)[\Theta^T\omega](t) \qquad (7.52)$$

$$\zeta(t) = h(s)[\omega](t). \qquad (7.53)$$

From (7.47) and (7.51), it then follows that

$$\epsilon(t) = [0, \tilde{\theta}_2^T(t)\eta_2(t), \tilde{\theta}_3^T(t)\eta_3(t), \ldots, \tilde{\theta}_M^T(t)\eta_M(t)]^T + \tilde{\Psi}(t)\xi(t) + D_s S\tilde{\Theta}^T(t)\zeta(t), \quad (7.54)$$

where $\tilde{\theta}_i(t) = \theta_i(t) - \theta_i^*$ and $\tilde{\Psi}(t) = \Psi(t) - \Psi^*$ are the related parameter errors.

Adaptive laws

With the estimation error model (7.54), we choose the adaptive laws

$$\dot{\theta}_i(t) = -\frac{\Gamma_{\theta_i}\epsilon_i(t)\eta_i(t)}{m^2(t)}, \quad i = 2, 3, \dots, M \tag{7.55}$$

$$\dot{\Theta}^T(t) = -\frac{D_s\epsilon(t)\zeta^T(t)}{m^2(t)} \tag{7.56}$$

$$\dot{\Psi}(t) = -\frac{\Gamma\epsilon(t)\xi^T(t)}{m^2(t)} \tag{7.57}$$

where the signal $\epsilon(t) = [\epsilon_1(t), \epsilon_2(t), \dots, \epsilon_M(t)]^T$ is computed from (7.54), $\Gamma_{\theta_i} = \Gamma_{\theta_i}^T > 0$ and $\Gamma = \Gamma^T > 0$ are adaptation gain matrices, and

$$m(t) = \sqrt{1 + \zeta^T(t)\zeta(t) + \xi^T(t)\xi(t) + \sum_{i=2}^{M}\eta_i^T(t)\eta_i(t)}, \tag{7.58}$$

is a standard normalization signal.

Stability analysis

To analyze the closed-loop system stability, we first establish some desired properties of the aforementioned adaptive parameter update laws for the linearized system models at each operating condition.

Lemma 7. *The adaptive laws (7.55)-(7.57) ensure the following desired properties:*

1. $\theta_i(t) \in L^\infty(i = 2, 3, \dots, M), \Theta(t) \in L^\infty, \Psi \in L^\infty, \frac{\epsilon(t)}{m(t)} \in L^2 \cap L^\infty$; and

2. $\dot{\theta}_i(t) \in L^2 \cap L^\infty(i = 2, 3, \dots, M), \dot{\Theta}(t) \in L^2 \cap L^\infty, \dot{\Psi}(t) \in L^2 \cap L^\infty$.

Proof. For each linearized system model, consider the positive-definite function

$$V = \frac{1}{2}(\sum_{i=2}^{M}\tilde{\theta}_i^T\Gamma_{\theta_i}^{-1}\tilde{\theta}_i + \text{tr}[\tilde{\Psi}^T\Gamma^{-1}\tilde{\Psi}] + \text{tr}[\tilde{\Theta}S\tilde{\Theta}^T]) > 0. \tag{7.59}$$

From the adaptive laws, the time derivative of V at each operating condition is obtained to as

$$\dot{V} = -\sum_{i=2}^{M} \frac{\tilde{\theta}_i^T(t)\epsilon_i(t)\eta_i(t)}{m^2(t)} - \frac{\xi^T(t)\tilde{\Psi}^T(t)\epsilon(t)}{m^2(t)} - \frac{\zeta^T(t)\tilde{\Theta}(t)SD_s\epsilon(t)}{m^2(t)}$$
$$= -\frac{\epsilon^T(t)\epsilon(t)}{m^2(t)} \leq 0. \tag{7.60}$$

From (7.59) and (7.60), it can be concluded that $\theta_i(t) \in L^\infty(i = 2, 3, \ldots, M), \Theta(t) \in L^\infty, \Psi(t) \in L^\infty$, and $\frac{\epsilon(t)}{m(t)} \in L^2$. Summing up the boundedness of $\theta_i(t)(i = 2, 3, \ldots, M), \Theta(t)$, and $\Psi(t)$ with (7.54) and (7.58), we have $\frac{\epsilon(t)}{m(t)} \in L^\infty$. Since the normalized signals $\frac{\eta_i(t)}{m(t)}(i = 2, 3, \ldots, M), \frac{\zeta(t)}{m(t)}, \frac{\xi(t)}{m(t)} \in L^\infty$, it can be concluded that $\dot{\theta}_i(t) \in L^2 \cap L^\infty(i = 2, 3, \ldots, M), \dot{\Theta}(t) \in L^2 \cap L^\infty$, and $\dot{\Psi}(t) \in L^2 \cap L^\infty$. $\qquad\square$

Based on Lemma 3, the following desired closed-loop system properties for each linearized system model can be established:

Theorem 2. *The multivariable MRAC scheme with the state feedback control law (7.39) updated by the adaptive laws (7.55)-(7.57), when applied to the system (7.24), guarantees the closed-loop signal boundness and asymptotic output tracking:* $\lim_{t\to\infty}(\Delta y(t) - \Delta y_m(t)) = 0$, *for any initial conditions.*

The proof of Theorem 1 can be carried out in a similar way to that described in [129] for multivariable MRAC for linearized systems with constant non-equilibrium offset. The key step of such an analysis procedure is to express a filtered version of the plant output in a feedback framework that has a small gain due to the L^2 properties of $\dot{\Theta}(t), \dot{\theta}(t)$ and $\epsilon(t)/m(t)$. The state feedback control signal is required to be expressed in terms of the output. This can be done using a state-observer of the plant. Then the analysis procedure in [126] can be used to conclude the closed-loop signal boundedness and output tracking. For the adaptive control scheme of this paper,

an input compensator has been used, whose effect can be handled in the stability analysis.

Remark 9. The nominal controller can only work at a given operating condition of the quadrotor, since it needs the exact parameter information. While the proposed adaptive controller can be applied to the quadrotor system of multiple operating points, because the only information needed is the interactor matrix $\xi_m(s)$ and the sign matrix D_s, which are uniform over the multiple operating conditions.   □

7.4   Simulation Study

In this section, the proposed linearization-based adaptive control design is applied to a quadrotor model with multiple operating conditions. To test the performance of the proposed control scheme, a MATLAB model of the quadrotor system is used. The simulation model offers a realistic representation of a quadrotor, and the simulation results provide a credible assessment of the proposed control design.

7.4.1   Simulation System

The quadrotor system is linearized at three typical operating conditions, which are chosen from the operable domain. The operating conditions studied in this section are as follows:

1. special hover condition with all attitude angles being zero;

2. low speed cruise condition in the x_E direction with pitch angle $\theta = 0.1$ rad and velocity $\dot{x}_E = 4$ m/s;

3. high speed cruise condition in the x_E direction with pitch angle $\theta = 0.3$ rad and velocity $\dot{x}_E = 12$ m/s.

According to

In our simulation, the input compensator is chosen as

$$
W_c(s) = \begin{bmatrix} \dfrac{1}{(s+2)^2} & 0 & 0 & 0 \\ 0 & 1 & 0 & 0 \\ 0 & 0 & 1 & 0 \\ 0 & 0 & 0 & 1 \end{bmatrix},
\tag{7.61}
$$

which satisfies the structure (7.11). It follows that the uniform interactor matrix for all three operating conditions is chosen as

$$
\xi_m(s) = \begin{bmatrix} (s+1)^4 & 0 & 0 & 0 \\ 0 & (s+1)^4 & 0 & 0 \\ 0 & 0 & (s+1)^4 & 0 \\ 0 & 0 & 0 & (s+1)^2 \end{bmatrix},
\tag{7.62}
$$

and the signs of the leading principal minors of the high-frequency gain matrices at the three operating conditions are the same as $\Delta_1 > 0, \Delta_2 < 0, \Delta_3 < 0, \Delta_4 < 0$. The numerical parameter values used for building the aircraft simulation models and verifying the design assumptions are given as follows, which are not used for the control design.

Special hover condition

The system parameter matrices are described as

$$
A = \begin{bmatrix}
0 & 0 & 0 & 1 & 0 & 0 & 0 & 0 & 0 & 0 & 0 & 0 & 0 & 0 \\
0 & 0 & 0 & 0 & 1 & 0 & 0 & 0 & 0 & 0 & 0 & 0 & 0 & 0 \\
0 & 0 & 0 & 0 & 0 & 1 & 0 & 0 & 0 & 0 & 0 & 0 & 0 & 0 \\
0 & 0 & 0 & -0.25 & 0 & 0 & 0 & 9.8 & 0 & 0 & 0 & 0 & 0 & 0 \\
0 & 0 & 0 & 0 & -0.25 & 0 & -9.8 & 0 & 0 & 0 & 0 & 0 & 0 & 0 \\
0 & 0 & 0 & 0 & 0 & -0.25 & 0 & 0 & 0 & 0 & 0 & 0 & 0.5 & 0 \\
0 & 0 & 0 & 0 & 0 & 0 & 0 & 0 & 0 & 1 & 0 & 0 & 0 & 0 \\
0 & 0 & 0 & 0 & 0 & 0 & 0 & 0 & 0 & 0 & 1 & 0 & 0 & 0 \\
0 & 0 & 0 & 0 & 0 & 0 & 0 & 0 & 0 & 0 & 0 & 1 & 0 & 0 \\
0 & 0 & 0 & 0 & 0 & 0 & 0 & 0 & 0 & -0.2 & 0 & 0 & 0 & 0 \\
0 & 0 & 0 & 0 & 0 & 0 & 0 & 0 & 0 & 0 & -0.2 & 0 & 0 & 0 \\
0 & 0 & 0 & 0 & 0 & 0 & 0 & 0 & 0 & 0 & 0 & -0.1111 & 0 & 0 \\
0 & 0 & 0 & 0 & 0 & 0 & 0 & 0 & 0 & 0 & 0 & 0 & 0 & 1 \\
0 & 0 & 0 & 0 & 0 & 0 & 0 & 0 & 0 & 0 & 0 & 0 & -4 & -4
\end{bmatrix}
$$

$$B = \begin{bmatrix} 0 & 0 & 0 & 0 \\ 0 & 0 & 0 & 0 \\ 0 & 0 & 0 & 0 \\ 0 & 0 & 0 & 0 \\ 0 & 0 & 0 & 0 \\ 0 & 0 & 0 & 0 \\ 0 & 0 & 0 & 0 \\ 0 & 0 & 0 & 0 \\ 0 & 0 & 0 & 0 \\ 0 & 200 & 0 & 0 \\ 0 & 0 & 200 & 0 \\ 0 & 0 & 0 & 111.1111 \\ 0 & 0 & 0 & 0 \\ 1 & 0 & 0 & 0 \end{bmatrix},$$

the interactor matrix is chosen as (7.62) such that the high-frequency gain matrix is

$$K_{pc} = \lim_{s \to \infty} \xi_m(s)G(s) = \begin{bmatrix} 0.5 & 0 & 0 & 0 \\ 0 & 1960 & 0 & 0 \\ 0 & 0 & 1960 & 0 \\ 0 & 0 & 0 & 111.1 \end{bmatrix} \quad (7.63)$$

and the signs of its leading principle minors are: $\Delta_1 > 0, \Delta_2 < 0, \Delta_3 < 0, \Delta_4 < 0$.

Low speed cruise condition

The system parameter matrices are described as

$$
A = \begin{bmatrix}
0 & 0 & 0 & 1 & 0 & 0 & 0 & 0 & 0 & 0 & 0 & 0 & 0 & 0 \\
0 & 0 & 0 & 0 & 1 & 0 & 0 & 0 & 0 & 0 & 0 & 0 & 0 & 0 \\
0 & 0 & 0 & 0 & 0 & 1 & 0 & 0 & 0 & 0 & 0 & 0 & 0 & 0 \\
0 & 0 & 0 & -0.25 & 0 & 0 & 0 & 9.8 & 0 & 0 & 0 & 0 & 0.0499 & 0 \\
0 & 0 & 0 & 0 & -0.25 & 0 & -9.8 & 0 & 0.9833 & 0 & 0 & 0 & 0 & 0 \\
0 & 0 & 0 & 0 & 0 & -0.25 & 0 & -0.9833 & 0 & 0 & 0 & 0 & 0.4975 & 0 \\
0 & 0 & 0 & 0 & 0 & 0 & 0 & 0 & 0 & 1 & 0 & 0.1003 & 0 & 0 \\
0 & 0 & 0 & 0 & 0 & 0 & 0 & 0 & 0 & 0 & 1 & 0 & 0 & 0 \\
0 & 0 & 0 & 0 & 0 & 0 & 0 & 0 & 0 & 0 & 0 & 1.005 & 0 & 0 \\
0 & 0 & 0 & 0 & 0 & 0 & 0 & 0 & 0 & -0.2 & 0 & 0 & 0 & 0 \\
0 & 0 & 0 & 0 & 0 & 0 & 0 & 0 & 0 & 0 & -0.2 & 0 & 0 & 0 \\
0 & 0 & 0 & 0 & 0 & 0 & 0 & 0 & 0 & 0 & 0 & -0.1111 & 0 & 0 \\
0 & 0 & 0 & 0 & 0 & 0 & 0 & 0 & 0 & 0 & 0 & 0 & 0 & 1 \\
0 & 0 & 0 & 0 & 0 & 0 & 0 & 0 & 0 & 0 & 0 & 0 & -4 & -4
\end{bmatrix},
$$

and the input matrix B is same as (7.63), the interactor matrix is chosen as (7.62) such that the high-frequency gain matrix

$$
K_{pc} = \lim_{s \to \infty} \xi_m(s)G(s) = \begin{bmatrix}
0.4975 & 0 & -197.6 & 0 \\
0 & -1960 & 0 & 0.5 \\
0.1478 & 0 & 1960 & 0 \\
0 & 0 & 0 & 111.7
\end{bmatrix}
\tag{7.64}
$$

is finite and nonsingular, the signs of its leading principle minors are: $\Delta_1 > 0, \Delta_2 < 0, \Delta_3 < 0, \Delta_4 < 0$.

High speed cruise condition

The system parameter matrices are described as

$$
A = \begin{bmatrix}
0 & 0 & 0 & 1 & 0 & 0 & 0 & 0 & 0 & 0 & 0 & 0 & 0 & 0 \\
0 & 0 & 0 & 0 & 1 & 0 & 0 & 0 & 0 & 0 & 0 & 0 & 0 & 0 \\
0 & 0 & 0 & 0 & 0 & 1 & 0 & 0 & 0 & 0 & 0 & 0 & 0 & 0 \\
0 & 0 & 0 & -0.25 & 0 & 0 & 0 & 9.8 & 0 & 0 & 0 & 0 & 0.1478 & 0 \\
0 & 0 & 0 & 0 & -0.25 & 0 & -9.8 & 0 & 3.0315 & 0 & 0 & 0 & 0 & 0 \\
0 & 0 & 0 & 0 & 0 & -0.25 & 0 & -3.0315 & 0 & 0 & 0 & 0 & 0.4777 & 0 \\
0 & 0 & 0 & 0 & 0 & 0 & 0 & 0 & 0 & 1 & 0 & 0.3093 & 0 & 0 \\
0 & 0 & 0 & 0 & 0 & 0 & 0 & 0 & 0 & 0 & 1 & 0 & 0 & 0 \\
0 & 0 & 0 & 0 & 0 & 0 & 0 & 0 & 0 & 0 & 0 & 1.0468 & 0 & 0 \\
0 & 0 & 0 & 0 & 0 & 0 & 0 & 0 & 0 & -0.2 & 0 & 0 & 0 & 0 \\
0 & 0 & 0 & 0 & 0 & 0 & 0 & 0 & 0 & 0 & -0.2 & 0 & 0 & 0 \\
0 & 0 & 0 & 0 & 0 & 0 & 0 & 0 & 0 & 0 & 0 & -0.1111 & 0 & 0 \\
0 & 0 & 0 & 0 & 0 & 0 & 0 & 0 & 0 & 0 & 0 & 0 & 0 & 1 \\
0 & 0 & 0 & 0 & 0 & 0 & 0 & 0 & 0 & 0 & 0 & 0 & -4 & -4
\end{bmatrix},
$$

and the input matrix B is same as (7.63), the interactor matrix is chosen as (7.62) such that the high-frequency gain matrix

$$
K_{pc} = \lim_{s \to \infty} \xi_m(s)G(s) = \begin{bmatrix}
0.4777 & 0 & -634.6 & 0 \\
0 & -1960 & 0 & 28.3 \\
0.0499 & 0 & 1960 & 0 \\
0 & 0 & 0 & 106.1
\end{bmatrix}
\tag{7.65}
$$

is finite and nonsingular, the signs of its leading principle minors are: $\Delta_1 > 0, \Delta_2 < 0, \Delta_3 < 0, \Delta_4 < 0$.

7.4.2   Simulation Results

Three simulation cases were conducted to verify the effectiveness of our control method. The simulation Case I shows the system response at the special hover condition, which is widely studied in literature. The simulation Case II illustrates the behavior of the quadrotor at the cruise condition with a relatively high speed and attitude angle, which is not well studied before. The last simulation as Case III is a comprehensive study to show that the proposed controller is able to work at different operating conditions without changing the adaptive laws.

Case I

In this case, the system is simulated at the special hover condition of the linearized system model that all attitude angles are zero. For $t \in [0, 10)$, $r = [2, 0, 0, 0]^T$, the quadrotor is taking off and then hovering at a given position. For $t \in [10, 20)$, $r = [2, 0, 0, 0.1 \sin(t)]^T$, the quadrotor is changing its yaw angle for some tasks. For $t \in [20, 30)$, $r = [2, 1.2 \sin(1.5t), 1.2 \cos(1.1t), 0]^T$, the quadrotor is flying along circular path. For $t \in [40, 50]$, $r = [0, 0, 0, 0]^T$, the quadrotor is landing. The simulation result is shown in Figure 7.1. Compared to the results in [47] and [58], we observe that the input compensator in our controller does not affect the system performance of the quadrotor at hover condition.

Case II

In this case, the system is simulated at multiple operating conditions of the linearized model of the quadrotor system, which are the special hover condition, low speed cruise condition and high speed hover condition. The simulation results are shown in Figure 7.2. For $t \in [0, 100)$, $r = [2, 0, 0, 0]^T$, the quadrotor is taking off and then hovering at a given position. For $t \in [100, 200)$, $r = [2, 0, 4(t - 100), 0 \sin(t)]^T$, the quadrotor is flying along the x_E axis with a low speed as $4m/s$. For $t \in [200, 300)$,
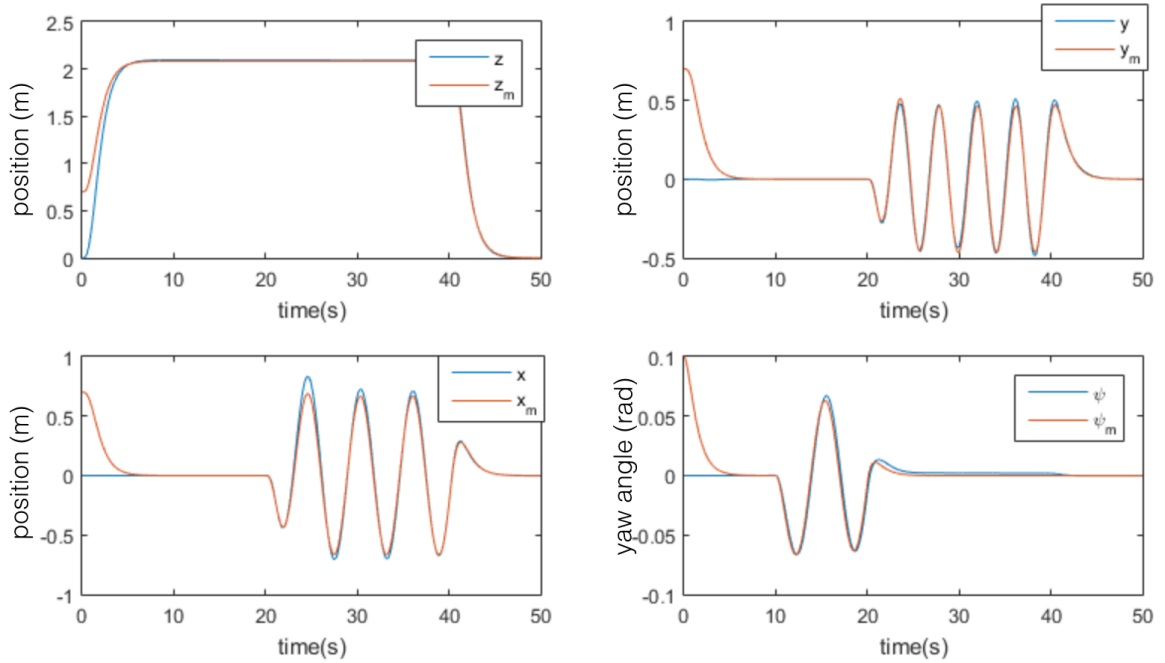
Figure 7.1: System responses for Case I.

$r = [2, 0, 12(t - 200) + 400, 0]^T$, the quadrotor is flying along x_E with a high speed as $12m/s$. For $t \in [300, 400)$, $r = [2, 0, 4(t - 300) + 1600, 0\sin(t)]^T$, the quadrotor is flying along x_E with a low speed as $4m/s$. For $t \in [400, 500]$, $r = [2, 0, 2000, 0]^T$, the quadrotor is hovering at its destination of the flight. The simulation results show that the proposed adaptive control scheme with input compensator can solve the problem of multiple operating conditions of linearized quadrotor systems without changing the controller parameter adaptive laws and reference model systems.

7.5   Summary

We studied the MRAC problem of quadrotors in this chapter by extending the flight conditions from the special hover condition to a group of typical flight conditions. The transfer matrix, interactor matrix and high frequency gain matrix were investigated at each operating condition. Then an input compensator was designed to guarantee the uniform diagonal interactor matrix and the same pattern of the signs of the

Figure 7.2: System responses for Case II.

leading principal minors of the high frequency gain matrices. The input compensator can reduce the difficulty of the design of model reference adaptive controller, since the interactor matrices are the same among the different operating conditions.. A framework of output tracking control is constructed dealing with the dynamics mutatio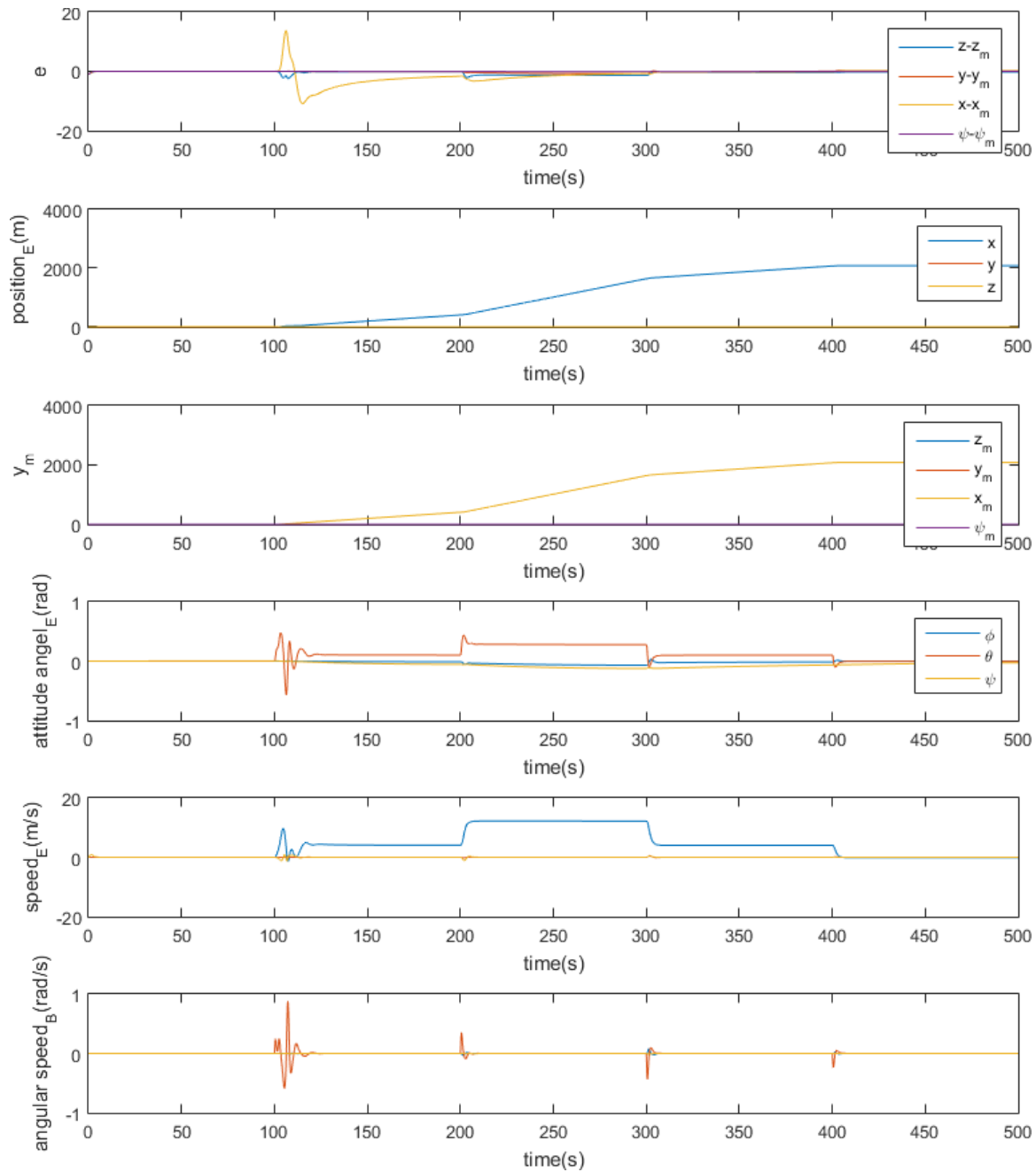n under different operating conditions, which is equipped with the input compensation technique. A nominal controller is designed for the case that the system parameters are known. Because of the achievable plant-model matching conditions, the proposed nominal control design can reject the non-equilibrium offset and make the signals of the closed-loop system bounded and the output signals track some chosen reference signals . For the non-equilibrium operating conditions, the constant term in the linearized model requires new update law of the controller and corresponding analysis of the stability. Complete design of the MRAC scheme with input compensator is still under investigation and will be presented in our future work.

In this chapter, a linearization-based multivariable adaptive control scheme for a nonlinear quadrotor model has been developed. The nonlinear quadrotor system is linearized at given typical operating conditions, and a sequential linear model with parameter uncertainties and a non-equilibrium offset is obtained to represent the linearized system at different operating conditions. With the use of an input compensator, a uniform interactor matrix and identical gain matrix signs are obtained. As a result of the achievable plant-model matching conditions, the proposed MRAC design can reject the non-equilibrium offset and make the closed-loop system signals bounded and the output signals track some chosen reference signals over different operating conditions. Simulation results from the linearized quadrotor system have demonstrated certain desired system performance.

Chapter 8

Adaptive Actuator Failure Compensation for Hexarotors

This chapter develops an adaptive scheme for compensation of uncertain actuator failures in a hexarotor system, which can be combined with a feedback control law to achieve desired closed-loop system stability and asymptotic output tracking in the presence of uncertainties of failure time, values and patterns. Such an adaptive control scheme is based on adaptive integration of individual failure compensators for different failure situations. It can adaptively update its parameters, without explicit failure detection or failure isolation, to deal with uncertain failures. The emerging NNPPNP rotor arrangement of hexarotors is adopted in this work and is investigated for its capability of tolerating up to two failed actuators and for the design of compensators for individual failure patterns. A state feedback model reference control law is chosen as the baseline controller to be combined with the failure compensators to form a nominal actuator failure compensation scheme. To deal with uncertain actuator failures, the nominal controller is parametrized and integrated and its adaptive version is developed by forming an error model and developing an adaptive scheme to update the parameters of the integrated failure compensation controller. Stability analysis

shows that all closed-loop system signals are bounded, and the system output tracks a reference output asymptotically despite the actuator failure uncertainties. Simulation results of a hexarotor system with the proposed adaptive control scheme are to be presented to show the desired system performance.

The main contributions of the chapter are as follows.

- A hexarotor model with NNPPNP rotor arrangement is linearized and studied, which has the potential of dealing with up to two failed actuators.

- The compensable failure patterns of the hexarotor system are investigated, which include one pattern of no actuator failure, four patterns of one actuator failure, and three patterns of two actuator failures.

- A uniform nominal control scheme with proved parameter existence is designed for the compensable failure patterns when the failure information is known, which is a combination of high-level motion control and control allocation.

- An adaptive compensation controller with guaranteed stability is constructed for the compensable patterns, when the failure pattern, failure time and failure value are all unknown.

The rest of the chapter is organized as follows. In Section 8.1, we formulate the control problem of the paper with the explanation of the actuator failure model and the control objective. In Section 8.2, the compensable failure patterns are systematically surveyed; and a nominal controller is designed for the nominal case in which the knowledge of failure is known. In Section 8.3, we derive an adaptive compensation scheme with detailed stability proof for the case of uncertain actuator failure. In Section 8.4, the performance of the proposed adaptive approach is verified by simulation results. In Section 8.5, the concluding remarks are presented.

8.1   Problem Statement

Consider the linearized dynamic model of a hexarotor system as

$$\dot{x}(t) = Ax(t) + Bw(t), \quad w(t) = C_a u(t), \quad y(t) = Cx(t), \tag{8.1}$$

where $x(t) = \Delta x_p(t) \in R^n$ is the state vector of the linearized system, $w(t) = \Delta w_p(t) \in R^m$ is the intermediate input vector of the linearized system, $u(t) = \Delta u_p(t) \in R^M$ is the input vector of the linearized system, $y(t) \in R^m$ is the output vector of the linearized system, the system parameter matrices A, B and C_a are known, the output matrix is

$$C = \begin{bmatrix} C_t & 0_{3\times3} & 0_{3\times3} & 0_{3\times3} \\ 0_{1\times3} & 0_{1\times3} & C_r & 0_{1\times3} \end{bmatrix} \tag{8.2}$$

with the submatrices

$$C_t = \begin{bmatrix} 0 & 0 & 1 \\ 0 & 1 & 0 \\ 1 & 0 & 0 \end{bmatrix}, \quad C_r = \begin{bmatrix} 0 & 0 & 1 \end{bmatrix}.$$

To articulate our control objective of failure compensation, next we introduce an actuator failure model to describe the failures of the system.

Control Objective

The control goal is to design an adaptive controller to generate $v(t)$ for system (8.1) under loss-of-control failures with unknown failure time instants t_j, failure pattern σ (or failure index j) and unknown failure values $\bar{u}_j(t)$, to guarantee that the remaining actuators can still ensure boundedness of the closed-loop signals and asymptotic

tracking of a given reference output signal

$$y_m(t) = W_m(s)[r](t) \tag{8.3}$$

by the system output $y(t)$, where $W_m(s)$ is the reference model system transfer matrix, and $r(t)$ is a bounded reference signal.

The basic procedure for the design of an adaptive failure compensation scheme for the system (21) with $w(t) = C_a u(t)$ has three steps:

Step 1: A desired feedback control law $w_d(t) = K_x^{*T} x(t) + K_r^* r(t)$ is derived for $w(t)$, which is a state feedback model reference controller designed with the knowledge of the system parameters A, B, C (which are assumed to be available for this study, with the main focus given on how to deal with the actuator failure uncertainties). The goal of actuator failure compensation design is to choose the applied control signal $v(t)$ to make $w(t) = w_d(t)$ in the nominal case with the knowledge of actuator failures, or to make $\lim_{t \to \infty} (y(t) - y_m(t)) = 0$ in the adaptive case without the knowledge of actuator failures.

Step 2: A nominal failure compensation control scheme is constructed which consists of a set of failure compensators, each for an individual actuator failure pattern. For each failure pattern, a nominal control signal $v_{(i)}^*(t)$ is designed such that for $v(t) = v_{(i)}^*(t)$ the desired motion control action $w(t) = w_d(t)$ is ensured so that the desired closed-loop stability and tracking performance can be achieved. For each nominal control law, a fixed control allocation matrix Λ_i is chosen, for realizing the control goal of making $w(t) = w_d(t)$. Each such control law contains a failure compensation term which depends on the failure value of each failure pattern. It will be shown that the control signal $v_{(i)}^*(t)$ indeed leads to $w(t) = w_d(t)$. Then, the set of nominal control laws (for all failure patterns from a failure pattern set of interest)

are integrated by using failure indicator functions, to form a unified nominal failure compensation control law or controller structure.

Step 3: Such a nominal controller structure is parametrized in terms of the unknown actuator failure parameters for all possible failure patterns from the failure pattern set. An adaptive failure compensation controller structure is then constructed, for which an adaptive parameter update scheme is developed. The uncertain indicator functions are to be estimated, and so are the unknown failure parameters, for which a linearly and completely parametrized error model is to be derived.

8.2   Nominal Compensation Design

In this section, we study the case that the failure information is known. We derive the corresponding nominal controller and specify its desired performance. Then the nominal control scheme is developed for the no failure and known failure cases. A composite design is also given to construct a uniform controller for different cases.

8.2.1   Design for the No Failure Case

For this case, the failure pattern indicator is $\sigma(t) = \sigma_{(0)}$, the system input of the linearized system is $u(t) = v(t)$. We use a model reference controller for the high-level motion control of the hexarotor system. A control allocation scheme is also designed to generate the input signals for individual rotors.

Model reference control design

Since the parameters of the system are known, the desired state feedback for output tracking control scheme can be constructed for the system (8.1) as

$$w_d(t) = K_x^{*T} x(t) + K_r^* r(t), \tag{8.4}$$

where $w_d(t)$ is the desired intermediate control input of the linearized system in (8.1), and the nominal parameters $K_x^* \in R^{n \times M}$ and $K_r^* \in R^{M \times M}$ are chosen for the plant-model output matching:

$$C(sI - A - BK_x^{*T})^{-1}BK_r^* = W_m(s) = \xi_m^{-1}(s), K_r^{*-1} = K_p, \tag{8.5}$$

with the non-singular high-frequency gain matrix

$$K_p = \lim_{s \to \infty} \xi_m(s)C(sI - A)^{-1}B, \tag{8.6}$$

for the modified left interactor matrix $\xi_m(s)$ [84] is specified as

$$\xi_m(s) = \begin{bmatrix} (s+1)^2 & 0 & 0 & 0 \\ 0 & (s+1)^4 & 0 & 0 \\ 0 & 0 & (s+1)^4 & 0 \\ 0 & 0 & 0 & (s+1)^2 \end{bmatrix}. \tag{8.7}$$

The existence of such control parameter matrices K_x^* and K_r^* for high-level motion control is established in [125].

Controller design and verification

The next step is to construct a proper control allocation design for the linearized system in (8.1). Since there exists actuation redundancy for the no failure case, different designs can be carried out for different focuses. For this work, we use the control allocation matrix Λ_0 in (3.41). With such choice, the applied control input is designed as

$$v_{(0)}^*(t) = \Lambda_0 K_x^{*T} x(t) + \Lambda_0 K_r^* r(t), \tag{8.8}$$

where $x(t)$ and $r(t)$ are the state vector and the bounded reference signal of the linearized system.

With the knowledge that $C_a\Lambda_0 = I$ and $u(t) = v(t)$, we can derive the intermediate control input of the linearized system as

$$w^*_{(0)}(t) = C_a u(t) = C_a v^*_{(0)}(t) = K_x^{*T} x(t) + K_r^* r(t) = w_d(t), \qquad (8.9)$$

then the desired state feedback for output tracking control scheme in (8.4) is achieved.

8.2.2   Designs for Known Failure Cases

There are seven possible failure patterns that can be compensated. In this research, we deal with the loss-of-control failures of the linearized system in (8.1). For the nominal case that the failure value, failure pattern and failure time are all known, the system input is

$$u(t) = (I - \sigma_{(i)})v^*_{(i)}(t) + \bar{u}_{(i)}(t), \quad i \in \{1, 2, \ldots, 7\}, \qquad (8.10)$$

where $v^*_{(i)}(t)$ is the applied control input to be designed for failure pattern (i), the failure value for failure pattern (i) is

$$\bar{u}_{(i)}(t) = \sigma_{(i)}\bar{u}(t) = \sigma_{(i)}\tau\theta(t), \qquad (8.11)$$

where τ is a scalar matrix, $\theta(t)$ is a known bounded signal vector. The desired state feedback for output tracking control scheme for the system in (8.1) is $w_d(t) = K_x^{*T} x(t) + K_r^* r(t)$ as in (8.4).

Nominal controller structure

The state feedback controller structure for $v_{(i)}^*(t)$ is given as

$$v_{(i)}^*(t) = \Lambda_i(K_x^{*T}x(t) + K_r^*r(t) + K_{\theta(i)}^*\theta(t)), \tag{8.12}$$

where K_x^* and K_r^* are the nominal parameters for the plant-model output matching in (8.5), Λ_i is a control allocation matrix to be designed, $K_{\theta(i)}^*$ is the nominal parameter to be designed for compensating the loss-of-control failure $\bar{u}_{(i)}(t)$ of the linearized system.

A design rule is set up for the control allocation matrix Λ_i in this work as

$$C_a(I - \sigma_{(i)})\Lambda_i = I. \tag{8.13}$$

We will show the designs of such control allocation matrices Λ_i for all the compensable patterns after deriving the nominal failure compensation parameter matrix $K_{\theta(i)}^*$.

Compensation design for loss-of-control failures

Consider the output of the closed-loop system in s domain

$$y(s) = C(sI - A - BK_x^{*T})^{-1}BK_r^*r(s) + \delta(s), \tag{8.14}$$

where

$$\delta(s) = C(sI - A - BK_x^{*T})^{-1}BC_a[(I - \sigma_{(i)})\Lambda_i K_{\theta(i)}^* + \bar{u}_{(i)}]\theta(s). \tag{8.15}$$

By plugging (8.13) into (8.15), we have

$$\delta(s) = C(sI - A - BK_x^{*T})^{-1}B[K_{\theta(i)}^* + C_a\bar{u}_{(i)}]\theta(s). \tag{8.16}$$

Then the output tracking error in the s domain is

$$e(s) = y(s) - y_m(s) = \delta(s). \tag{8.17}$$

From the final value theorem, we have $\lim\limits_{t\to\infty} e(t) = \lim\limits_{s\to 0} s\delta(s)$. In order to compensate the failure and guarantee $\lim\limits_{t\to\infty} e(t) = 0$, we choose the nominal failure compensation parameter as

$$K^*_{\theta(i)} = -C_a \bar{u}_{(i)} = -C_a \sigma_{(i)} \tau. \tag{8.18}$$

Then it follows that

$$\lim\limits_{t\to\infty} (y(t) - y_m(t)) = \lim\limits_{t\to\infty} \delta(t) = 0. \tag{8.19}$$

With the nominal parameters $K^*_{\theta(i)}$ given by (8.18), K^*_x and K^*_r given by (8.5), the design of the applied control input in (8.12) will be completed by proper control allocation matrix Λ_i for failure pattern (i).

Designs for two actuator failures cases

We start with the failure patterns with two failed actuators. For these cases, the hexarotor system has no actuation redundancy for 4-DOF output tracking. Then the control allocation matrix is unique for each pattern as follows.

Failure pattern (5): in this case failures happen in actuator 1 and 4, the corresponding control allocation matrix is

$$\Lambda_5 = \begin{bmatrix} 0 & 0 & 0 & 0 \\ \frac{1}{4} & \frac{\sqrt{3}}{6d} & \frac{1}{2d} & \frac{1}{4c_m} \\ \frac{1}{4} & -\frac{\sqrt{3}}{6d} & \frac{1}{2d} & -\frac{1}{4c_m} \\ 0 & 0 & 0 & 0 \\ \frac{1}{4} & -\frac{\sqrt{3}}{6d} & -\frac{1}{2d} & \frac{1}{4c_m} \\ \frac{1}{4} & \frac{\sqrt{3}}{6d} & -\frac{1}{2d} & -\frac{1}{4c_m} \end{bmatrix}. \tag{8.20}$$

Failure pattern (6): in this case failures happen in actuator 1 and 5, the corresponding control allocation matrix is

$$
\Lambda_6 =
\begin{bmatrix}
0 & 0 & 0 & 0 \\
0.1830 & \frac{0.3660}{d} & \frac{0.6340}{d} & \frac{0.1830}{c_m} \\
0.1585 & -\frac{0.1830}{d} & \frac{0.6830}{d} & -\frac{0.3415}{c_m} \\
0.3170 & -\frac{0.3660}{d} & -\frac{0.6340}{d} & \frac{0.3170}{c_m} \\
0 & 0 & 0 & 0 \\
0.3415 & \frac{0.1830}{d} & -\frac{0.6830}{d} & -\frac{0.1585}{c_m}
\end{bmatrix} .
\tag{8.21}
$$

Failure pattern (7): in this case failures happen in actuator 4 and 6, the corresponding control allocation matrix is

$$
\Lambda_7 =
\begin{bmatrix}
0.3170 & \frac{0.3660}{d} & -\frac{0.6340}{d} & -\frac{0.3170}{c_m} \\
0.1585 & \frac{0.1830}{d} & \frac{0.6830}{d} & \frac{0.3415}{c_m} \\
0.1830 & -\frac{0.3660}{d} & \frac{0.6340}{d} & -\frac{0.1830}{c_m} \\
0 & 0 & 0 & 0 \\
0.3415 & -\frac{0.1830}{d} & -\frac{0.6830}{d} & \frac{0.1585}{c_m} \\
0 & 0 & 0 & 0
\end{bmatrix} .
\tag{8.22}
$$

Designs for one actuator failure cases

For the one failure cases, the control allocation matrix is not unique. Designs can be made based on different requirements. In this paper, we follow the principle that all the actuators are with equal priority. The control allocation matrices are as follows.

Failure pattern (1): in this case the failure happens in rotor 1, the corresponding control allocation matrix is chosen as Λ_1 in (3.42). The matrices in (8.20) and (8.21) are also valid candidates for this case.

Failure pattern (2): in this case the failure happens in rotor 4, the corresponding control allocation matrix is

$$
\Lambda_2 = \begin{bmatrix}
\frac{3}{22} & \frac{2}{11d} & 0 & -\frac{3}{22c_m} \\
\frac{11-\sqrt{3}}{44} & \frac{3\sqrt{3}}{22d} & \frac{1}{2d} & \frac{11+\sqrt{3}}{44c_m} \\
\frac{8+\sqrt{3}}{44} & -\frac{2+3\sqrt{3}}{22d} & \frac{1}{2d} & -\frac{8+\sqrt{3}}{44c_m} \\
0 & 0 & 0 & 0 \\
\frac{11+\sqrt{3}}{44} & -\frac{3\sqrt{3}}{22d} & -\frac{1}{2d} & \frac{11-\sqrt{3}}{44c_m} \\
\frac{8-\sqrt{3}}{44} & \frac{-2+3\sqrt{3}}{22d} & -\frac{1}{2d} & \frac{-8+\sqrt{3}}{44c_m}
\end{bmatrix} . \tag{8.23}
$$

The matrices in (8.20) and (8.22) are also valid candidates for this case.

Failure pattern (3): in this case failures happen in actuator 5, the corresponding control allocation matrix is

$$
\Lambda_3 = \begin{bmatrix}
0.1278 & \frac{0.1825}{d} & \frac{0.1167}{d} & -\frac{0.1447}{c_m} \\
0.1362 & \frac{0.2992}{d} & \frac{0.5913}{d} & \frac{0.2360}{c_m} \\
0.1180 & -\frac{0.2409}{d} & \frac{0.6460}{d} & -\frac{0.2956}{c_m} \\
0.3638 & -\frac{0.2992}{d} & -\frac{0.5913}{d} & \frac{0.2640}{c_m} \\
0 & 0 & 0 & 0 \\
0.2542 & \frac{0.0583}{d} & -\frac{0.7627}{d} & -\frac{0.0597}{c_m}
\end{bmatrix} . \tag{8.24}
$$

The matrix in (8.21) is also a valid candidate for this case.

Failure pattern (4): in this case failures happen in actuator 6, the corresponding control allocation matrix is

$$\Lambda_4 = \begin{bmatrix} 0.3638 & \frac{0.2992}{d} & -\frac{0.5913}{d} & -\frac{0.2640}{c_m} \\ 0.1180 & -\frac{0.2409}{d} & \frac{0.6460}{d} & \frac{0.2956}{c_m} \\ 0.1362 & -\frac{0.2992}{d} & \frac{0.5913}{d} & -\frac{0.2360}{c_m} \\ 0.1278 & -\frac{0.1825}{d} & \frac{0.1167}{d} & \frac{0.1447}{c_m} \\ 0.2542 & -\frac{0.0583}{d} & -\frac{0.7627}{d} & \frac{0.0597}{c_m} \\ 0 & 0 & 0 & 0 \end{bmatrix}. \tag{8.25}$$

The matrix in (8.22) is also a valid candidate for this case.

Remark 10. Due to the actuation redundancy, the choice of Λ_0 is also not unique. All the Λ_i presented in this section can serve as an alternate for Λ_0. There are many considerations in determining such a control allocation matrix, like energy efficiency, emphasis on the agility of a selected output. Since the loss-of-thrust failure of rotor 2 and 3 are not compensable, one may increase their priorities. The main objective is to design adaptive control scheme for unknown failure pattern and time. So we do not discuss the control allocation problem in-depth, which is investigated in detail in [127] and [130]. □

Controller performance verification

Consider the nominal intermediate control law for the linearized system with failure pattern (i):

$$w_{(i)}^*(t) = C_a[(I - \sigma_{(i)})v_{(i)}^*(t) + \bar{u}_{(i)}]. \tag{8.26}$$

By plugging (8.12), (8.13) and (8.18) into (8.26), we have

$$w_{(i)}^*(t) = C_a(I - \sigma_{(i)})\Lambda_i(K_x^{*T}x(t) + K_r^*r(t) + K_{\theta(i)}^*) + C_a\bar{u}_{(i)} = w_d(t). \qquad (8.27)$$

Thus, it is verified that the desired motion control action in (8.4) has been met for the cases with known failure.

8.2.3   Composite Control Design

Introducing the indicator functions

$$\chi_i^* = \begin{cases} 1 & \text{if failure patter } (i) \text{ happens} \\ 0 & \text{otherwise} \end{cases} \text{, for } i = 0, 1, \dots, 7. \qquad (8.28)$$

With the nominal controller design for the no actuator failure case, four cases of one actuator failure, and three cases of two actuators failure, a composite controller structure can be given as

$$\begin{aligned}
v^*(t) &= \sum_{i=0}^{7} \chi_i^*(t)v_{(i)}^*(t) \\
&= \sum_{i=0}^{7} \chi_i^*(t)\Lambda_i(K_x^{*T}(t)x(t) + K_r^*(t)r(t) + K_{\theta(i)}^*\theta(t)), \qquad (8.29)
\end{aligned}$$

where the nominal failure compensation parameter for the no failure case is $K_{\theta(0)}^* = 0$.

By summarizing (8.9) and (8.27), we present the performance of the nominal controller in (8.29) as follows.

Lemma 8. *For the system in (8.1) under known compensable failures, there exist matrices K_x^*, K_r^*, $K_{\theta(i)}^*$ and Λ_i such that $w_{(i)}^*(t) = w_d(t)$, with which the state feedback controller (8.29) ensures the closed-loop signal boundedness, and asymptotic output tracking of the reference output $y_m(t)$ by the system output $y(t)$.*

8.3 Adaptive Compensation Design

The nominal controller presented in last section requires the full knowledge of the failures. When the failure pattern, failure time, and failure value are unknown, the given nominal controller can not guarantee closed-loop performance and stability anymore. In this section, we develop an adaptive actuator failure compensation scheme for the system in the presence of uncertain actuator failures.

8.3.1 Adaptive Controller Structure

When the failure information of actuators is unknown, the state-feedback controller structure is given as

$$v(t) = \sum_{i=0}^{7} \chi_i(t) v_i(t) = \sum_{i=0}^{7} \chi_i(t) \Lambda_i [K_x^{*T} x(t) + K_r^* r(t) + K_{\theta(i)}(t) \theta(t)], \qquad (8.30)$$

where $\chi_i(t)$ is the estimation of χ_i^*, Λ_i is the known control allocation matrix for failure pattern (i), and $K_{\theta(i)}(t)$ is the estimation of $K_{\theta(i)}^*$. We can rewrite (8.30) in a more compact form as

$$v(t) = [\sum_{i=0}^{N} \chi_i(t) \Lambda_i \Theta^{*T} \omega(t)] + \Upsilon(t) \theta(t) \qquad (8.31)$$

where

$$\Theta^* = [K_x^{*T}, K_r^*]^T$$

$$\omega(t) = [x^T(t), r^T(t)]^T,$$

the controller parameter matrix for failure compensation

$$\Upsilon(t) = \sum_{i=0}^{N} \chi_i(t) \Lambda_i K_{\theta(i)}(t) \qquad (8.32)$$

is the estimation of

$$\Upsilon^* = \sum_{i=0}^{N} \chi_i^* \Lambda_i K_{\theta(i)}^*, \tag{8.33}$$

and $\theta(t)$ is a vector of known bounded signals.

Substituting the controller structure (8.31), the failure model (3.43), and the design rule of the control allocation matrix (8.13) into the linearized hexarotor system model in (8.1), we obtain

$$\dot{x}(t) = Ax(t) + BC_a[(I - \sigma(t))\sum_{i=0}^{7} \chi_i(t)\Lambda_i(K_x^{*T}x(t) + K_r^*r(t) + K_{\theta(i)}(t)\theta(t)) + \sigma(t)\bar{u}(t)]$$

$$= (A + BK_x^{*T})x(t) + BK_r^*r(t) + B[C_a(I - \sigma(t))\sum_{i=0}^{7} \chi_i^*\Lambda_i K_{\theta(i)}^* + C_a\sigma(t)\bar{u}(t)]$$

$$+ BC_a(I - \sigma(t))[\sum_{i=0}^{7} \widetilde{\chi}_i(t)\Lambda_i\Theta^{*T}\omega(t) + \widetilde{\Upsilon}(t)\theta(t)] \tag{8.34}$$

where

$$\widetilde{\chi}_i(t) = \chi_i(t) - \chi_i^* \tag{8.35}$$

$$\widetilde{\Upsilon}(t) = \Upsilon(t) - \Upsilon^*. \tag{8.36}$$

8.3.2   Error Parameterization

To obtain the adaptive law for $\chi_i(t)$, a well parameterized tracking error model is needed. In view of the reference model system (8.3), matching conditions (8.5), and the closed-loop system (8.34), the output-tracking error is given as

$$e(t) = y(t) - y_m(t) = W_m(s)[K_p C_a(I - \sigma)(\sum_{i=0}^{7} \widetilde{\chi}_i\Lambda_i\Theta^{*T}\omega + \widetilde{\Upsilon}\theta)](t) + \delta(t), \quad (8.37)$$

where

$$\delta(t) = \mathcal{L}^{-1}\{C(sI - A - BK_x^{*T})^{-1}B[C_a(I - \sigma(t))\sum_{i=0}^{7}(\chi_i^*\Lambda_i K_{\theta(i)}^* + C_a\sigma(t)\bar{u}(t))]\}. \quad (8.38)$$

Ignoring the exponentially decaying term $\delta(t)$ in (8.38), we can rewrite (8.37) as

$$K_p^{-1}\xi_m(s)[e](t) = C_a(I - \sigma(t))[\sum_{i=0}^{7}\Lambda_i\widetilde{\chi}_i(t)\Theta^{*T}\omega(t) + \widetilde{\Upsilon}(t)\theta(t)], \quad (8.39)$$

where the interactor matrix $\xi_m(s) = W_m^{-1}(s)$ is specified in (8.7).

Then we introduce a filter $h(s) = 1/f_h(s)$, where $f_h(s)$ is a stable and monic polynomial whose degree is equal to the maximum degree of $\xi_m(s)$. Operating both sides of (8.39) by $h(s)I_m$, the filtered tracking error can be denoted as

$$\bar{e}(t) = K_p^{-1}\xi_m(s)h(s)[e](t) = C_a h(s)[(I - \sigma)(\sum_{i=0}^{7}\widetilde{\chi}_i\Lambda_i\Theta^{*T}\omega + \widetilde{\Upsilon}\theta)](t). \quad (8.40)$$

Based on (8.40), we construct the estimation error vector signal:

$$\epsilon(t) = \bar{e}(t) + C_a\lambda(t)\xi(t), \quad (8.41)$$

where the parameter matrix

$$\lambda(t) = \text{diag}\{\lambda_1, \lambda_2, \ldots, \lambda_M\} \quad (8.42)$$

is the estimation of $(I - \sigma(t))$ and

$$\xi(t) = \sum_{i=0}^{7}[\chi_i(t)\Lambda_i\Theta^{*T}\eta(t)] + \Upsilon(t)\zeta(t) - h(s)[\sum_{i=0}^{7}\chi_i\Lambda_i\Theta^{*T}\omega + \Upsilon\theta](t) \quad (8.43)$$

with the signal vectors

$$\eta(t) = h(s)[\omega](t) \tag{8.44}$$

$$\zeta(t) = h(s)[\theta](t). \tag{8.45}$$

It then follows from (8.40), (8.41), and (8.43) that

$$\epsilon(t) = C_a\widetilde{\lambda}(t)\xi(t) + C_a(I - \sigma(t))[\sum_{i=0}^{7} \Lambda_i\widetilde{\chi}_i(t)\Theta^{*T}\eta(t) + \widetilde{\Upsilon}(t)\zeta(t)], \tag{8.46}$$

where

$$\widetilde{\lambda}(t) = \lambda(t) - \lambda^*. \tag{8.47}$$

8.3.3   Adaptive Laws

With the parameterized error model, the adaptive laws are chosen as

$$\dot{\lambda}_j(t) = -\frac{\gamma_{\lambda j}C_{aj}^T\epsilon(t)\xi_j^T(t)}{m^2(t)}, \quad j = 1, 2, \ldots, M \tag{8.48}$$

$$\dot{\chi}_i(t) = -\frac{\gamma_{\chi i}\eta^T(t)\Theta^*\Lambda_i^T C_a^T\epsilon(t)}{m^2(t)}, \quad i = 0, 1, \ldots, N \tag{8.49}$$

$$\dot{\Upsilon}(t) = -\frac{C_a^T\epsilon(t)\zeta^T(t)}{m^2(t)}, \tag{8.50}$$

where $\lambda_j(t)$ is the jth diagonal element of $\lambda(t)$ in (8.42), $\gamma_{\lambda j} > 0 \, (j = 1, 2, \ldots, M)$ and $\gamma_{\chi i} > 0 \, (i = 0, 1, \ldots, N)$ are adaptive gains, C_{aj} is the jth column of C_a, $\xi_j(t)$ is the jth element of $\xi(t)$, and

$$m(t) = \sqrt{1 + \xi^T(t)\xi(t) + \eta^T(t)\eta(t) + \zeta^T(t)\zeta(t)} \tag{8.51}$$

is a standard normalization signal.

8.3.4 Stability Analysis

For the adaptive laws (8.48)-(8.50), we have following desired stability properties.

Lemma 9. *The adaptive laws (8.48)-(8.50) guarantee the following desired properties:*

1) $\lambda_j(t) \in L^\infty$ $(j = 1, 2, \ldots, M)$, $\chi_i(t) \in L^\infty$ $(i = 0, 1, \ldots, N)$, $\Upsilon(t) \in L^\infty$, $\frac{\epsilon(t)}{m(t)} \in L^2 \cap L^\infty$; *and*

2) $\dot{\lambda}_j(t) \in L^\infty \cap L^2$ $(j = 1, 2, \ldots, M)$, $\dot{\chi}_i(t) \in L^\infty \cap L^2$ $(i = 0, 1, \ldots, N)$, $\dot{\Upsilon}(t) \in L^\infty \cap L^2$.

Proof. Consider the positive-definite function

$$V = \frac{1}{2}(\text{tr}[\widetilde{\lambda}^T(t)\Gamma_\lambda^{-1}\widetilde{\lambda}(t)] + \text{tr}[\sum_{i=0}^{N} \gamma_{\chi i}^{-1}\widetilde{\chi}_i^2(t)(I - \sigma(t))] + \text{tr}[\widetilde{\Upsilon}^T(t)(I - \sigma(t))\widetilde{\Upsilon}(t)]) > 0,$$

$$(8.52)$$

where the adaptive gain matrix

$$\Gamma_\lambda = \text{diag}\{\gamma_{\lambda 1}, \gamma_{\lambda 2}, \ldots, \gamma_{\lambda M}\}. \tag{8.53}$$

From the adaptive laws (8.48)-(8.50), the time derivative of V at each operating condition is obtained to as

$$\dot{V} = -\frac{\epsilon^T(t)C_a\widetilde{\lambda}(t)\xi(t)}{m^2(t)} - \frac{\epsilon^T(t)C_a(I - \sigma(t))\sum_{i=0}^{N}\widetilde{\chi}_i(t)\Lambda_i\Theta^{*T}\eta(t)}{m^2(t)} - \frac{\epsilon^T(t)C_a(I - \sigma(t))\widetilde{\Upsilon}(t)\zeta(t)}{m^2(t)}$$

$$= -\frac{\epsilon^T(t)\epsilon(t)}{m^2(t)} \leq 0. \tag{8.54}$$

From (8.52) and (8.54), it can be concluded that $\lambda(t)$, $\chi_i(t) \in L^\infty$ $(i = 0, 1, \ldots, N)$, $\Upsilon(t) \in L^\infty$, $\frac{\epsilon(t)}{m(t)} \in L^2$. Summing up the boundedness of $\lambda(t)$, $\chi_i(t)$ $(i = 0, 1, \ldots, N)$ and $\Upsilon(t)$, with (8.46) and (8.51), we have $\frac{\epsilon(t)}{m(t)} \in L^\infty$. Since the normalized signals $\frac{\eta(t)}{m(t)}, \frac{\zeta(t)}{m(t)}, \frac{\xi(t)}{m(t)} \in L^\infty$, it can be concluded that $\dot{\lambda}(t) \in L^\infty \cap L^2$, $\dot{\chi}_i(t) \in L^\infty \cap L^2$ $(i = 0, 1, \ldots, N)$ and $\dot{\Upsilon}(t) \in L^\infty \cap L^2$. $\square$

Based on Lemma 2, the following desired closed-loop system properties for each linearized system model can be established:

Theorem 3. *The multivariable MRAC scheme with the state feedback control law (8.31) updated by the adaptive laws (8.48)-(8.50), when applied to the system (8.1), guarantees the closed-loop signal boundness and asymptotic output tracking:* $\lim\limits_{t\to\infty}(\Delta y(t) - \Delta y_m(t)) = 0$, *for any initial conditions.*

8.4   Simulation Study

The simulation results are shown in Figure 3. Rotor 1 is failed at $t = 10$. Both rotor 1 and 3 are failed at $t = 30$. All of the failures are loss-of control failure.
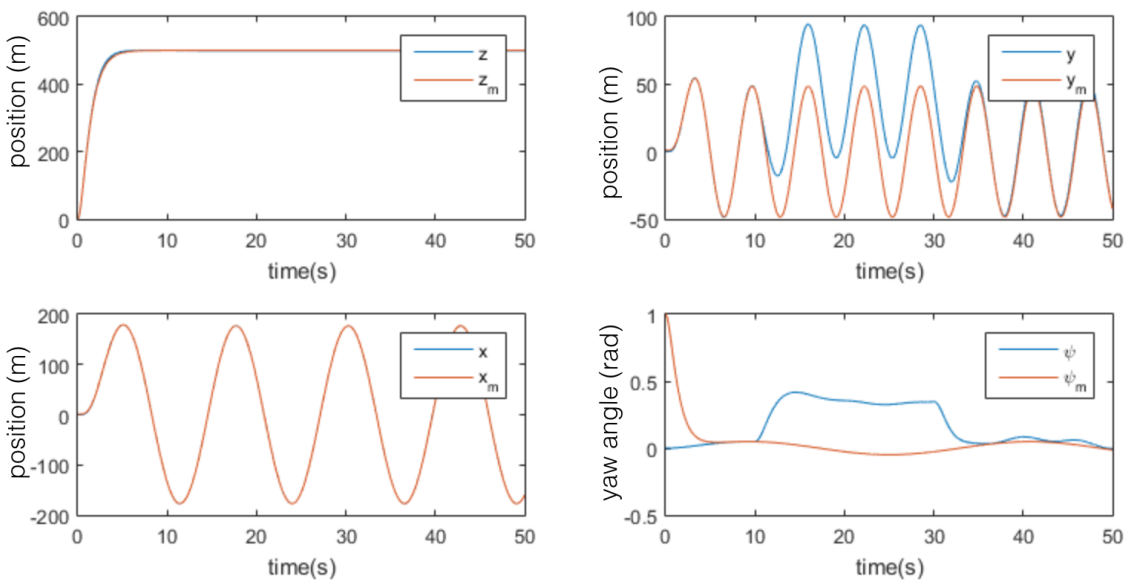
Figure 8.1: System response with loss-of-control failures.

8.5   Summary

In this chapter, we studied the adaptive actuator failure compensation scheme of a hexarotor system with NNPPNP rotor arrangement. Our research shows that,

with a complete parameterization of failure patterns and system parameters, desired closed-loop stability and asymptotic tracking of the system can be achieved, despite uncertain actuator failures whose failure index, failure time, and failure value are unknown. The simulation results also verify the performance of the adaptive failure compensation algorithm when applied to the linearized hexarotor model subject to uncertain actuator failures.

Chapter 9

Designs for Hexarotors with Failure and Parameter Uncertainties

In this chapter, an adaptive control design is developed for hexarotor systems subject to uncertain parameters and unknown actuator failures. The developed control scheme consists of a control signal distributor and a state feedback controller equipped with adaptive laws. It is verified that the control distribution matrix ensures that under different uncertain actuator failure patterns the controlled system has high frequency gain matrices whose equivalent signs are invariant. This property is crucial for the design of a multivariable adaptive controller which has the capability to ensure desired stability and asymptotic output tracking of an arbitrary time-varying reference signal for the high-order hexarotor dynamics with unknown parameters and with actuator failures whose failure patterns, values and time instants are uncertain. A nominal control scheme is first constructed for the case of known parameters and failures, to demonstrate the existence of the plant and reference model matching parameters. A multivariable model reference adaptive controller is developed to deal

with system and failure uncertainties, using an LDS gain matrix decomposition based parametrization for the derivation of the estimation error and adaptive law. Such a control design effectively utilizes the controller adaptation and system actuation redundancy to compensate for possible uncertain actuator failures in the presence of system uncertainties. Simulation results are presented to verify the desired performance of the adaptive compensation scheme developed for hexarotor systems.

The main contributions of the part are as follows.

- A control signal distribution matrix is proposed to deal with uncertainties of the control allocation scheme for a 4-DOF hexarotor, which includes additive and manipulative parameters uncertainties.

- The important prior information for adaptive control design, as interactor matrix and gain matrix signs, are investigated and shown to be fixed with the distributor against up to two actuator failures with unknown failure time, failure pattern and failure value.

- A nominal compensation scheme is derived to deal with the compensable failure patterns.

- An adaptive controller equipped with control signal distributor is developed for the hexarotor system with parameter and failure uncertainties.

The chapter is organized as follows. The control problem of the paper is formulated in Section 9.1. Some background information is also introduced in the section, which includes the nonlinear and linearized model of the hexarotor system, the actuator failure model, and the basics of model reference adaptive control. In Section 9.2, the design and function of the control signal distributor are explained in detail. The nominal controller for the problem is presented and proved in Section 9.3, which is for the case that the parameters and failures are known. Then in Section 9.4, the adaptive

control laws are constructed for the cases that the information is unknown, which is validated by rigorous stability analysis. Some numerical results of the proposed approach are shown in Section 9.5.

9.1 Problem Statement

In this chapter, we study the output tracking problem. The output signal is chosen as

$$y = [z_E, y_E, x_E, \psi]. \tag{9.1}$$

The linearized hexarotor system model at an operating condition $(x_o.u_o)$ with actuator failure can be represented as

$$\dot{x}(t) = Ax(t) + \bar{B}v_c(t) + B_{\bar{u}}\bar{u}(t) + f_o, \ y(t) = Cx(t), \tag{9.2}$$

where $x(t) = \Delta x_p(t) \in R^n$ is the state vector, $v_c(t) \in R^M$ is the applied control input to be designed, $y(t) \in R^m$ is the output vector; $f_o = f(x_o.u_o)$ is the non-equilibrium offset, $A = A_p$, $\bar{B} = B_pC_a(I - \sigma(t))$, $B_{\bar{u}} = B_pC_a\sigma(t)$ are unknown matrices, the control effectiveness matrix is

$$C_a = \begin{bmatrix} 1 & 1 & 1 & 1 & 1 & 1 \\ d & \frac{\sqrt{3}}{2}d & -\frac{\sqrt{3}}{2}d & -d & -\frac{\sqrt{3}}{2}d & \frac{\sqrt{3}}{2}d \\ 0 & \frac{1}{2}d & \frac{1}{2}d & 0 & -\frac{1}{2}d & -\frac{1}{2}d \\ -c_m & -c_m & c_m & -c_m & c_m & c_m \end{bmatrix}, \tag{9.3}$$

the known output matrix is

$$C = \begin{bmatrix} C_t & 0_{3\times3} & 0_{3\times3} & 0_{3\times3} \\ 0_{1\times3} & 0_{1\times3} & C_r & 0_{1\times3} \end{bmatrix} \tag{9.4}$$

with the submatrices

$$C_t = \begin{bmatrix} 0 & 0 & 1 \\ 0 & 1 & 0 \\ 1 & 0 & 0 \end{bmatrix}, \quad C_r = \begin{bmatrix} 0 & 0 & 1 \end{bmatrix}.$$

The control goal is to design an adaptive controller to generate $v_c(t)$ for system (9.2) under loss-of-control failures with unknown failure time instants t_j, failure pattern σ (or failure index j) and unknown failure values $\bar{u}_j(t)$, to guarantee that the remaining actuators can still ensure boundedness of the closed-loop signals and asymptotic tracking of a given reference output signal

$$y_m(t) = W_m(s)[r](t)^1 \tag{9.5}$$

by the system output $y(t)$, where $W_m(s)$ is the reference model system transfer matrix, and $r(t)$ is a bounded reference signal.

Remark 11. In this chapter, we work on the failure compensation problem for the loss-of-control failure in the original nonlinear hexarotor system and the linearized system in (9.2). For this case, denote the jth element of u_o as u_{oj}. Recall that $\Delta u_f(t) = u_f(t) - u_o$, the failure value $\bar{u}(t)$ in the linearized system is connected to the failure value $\bar{u}_f(t)$ in the original nonlinear system through $\bar{u}(t) = \bar{u}_f(t) - u_o$. Thus, we can conclude that the unknown loss-of-control failure in the original nonlinear system is still an unknown loss-of-control failure in the linearized system. □

---

[1] The notation $G(s)[u](t)$ is short for

$$\mathscr{L}^{-1}\{G(s)\mathscr{L}[u(t)]\}. \tag{9.6}$$

9.2 Control Distribution Scheme

In order to design a MRAC scheme, the system has to satisfy the design conditions. When a system does not fully meet the requirements, we may apply some treatment to it to derive the invariant system characteristics and make control design upon the new system. In this part, a control signal distributor is proposed for 4-DOF hexarotors under parameter and failure uncertainties.

9.2.1 Control Signal Distribution Matrix

The process of control signal distribution is to generate the applied control input $v_c(t) \in R^M$ from the control input $u_c(t) \in R^m$ by

$$v_c(t) = C_d u_c(t), \tag{9.7}$$

where $C_d \in R^{M \times m}$ is the control distribution matrix to be designed. For systems with $m = M$, like a quadrotor, the control distribution matrix C_d is the inverse of C_a. However, for the systems with redundant actuation that $M > m$, like the 4-DOF hexarotors, the control distribution matrix is not unique. Different methods are proposed to figure out C_d from C_a and performance requirement as discussed in [127].

In this part, we propose a fixed control signal distribution matrix as

$$C_d = \begin{bmatrix} \frac{1}{6} & \frac{2}{13} & 0 & -\frac{3}{26} \\ \frac{1}{6} & \frac{3\sqrt{3}}{26} + \frac{1}{13} & \frac{1}{2} & \frac{\sqrt{3}}{26} + \frac{5}{26} \\ \frac{1}{6} & -\frac{3\sqrt{3}}{26} - \frac{1}{13} & \frac{1}{2} & -\frac{\sqrt{3}}{26} - \frac{5}{26} \\ \frac{1}{6} & -\frac{2}{13} & 0 & \frac{3}{26} \\ \frac{1}{6} & -\frac{3\sqrt{3}}{26} + \frac{1}{13} & -\frac{1}{2} & -\frac{\sqrt{3}}{26} + \frac{5}{26} \\ \frac{1}{6} & \frac{3\sqrt{3}}{26} - \frac{1}{13} & -\frac{1}{2} & \frac{\sqrt{3}}{26} - \frac{5}{26} \end{bmatrix} c_d, \tag{9.8}$$

where $c_d = \text{diag}\{1, d^{-1}, d^{-1}, c_m^{-1}\}$. It can be easily verified that the distribution matrix in (9.8) and the control effectiveness matrix in (9.3) satisfies

$$C_a C_d = I. \tag{9.9}$$

So for the case that there is no actuator failure, which means $I - \sigma(t) = I - \sigma_{(0)} = I$, we can derive the following property:

$$C_a(I - \sigma(t))C_d = I. \tag{9.10}$$

Such property is crucial to verify the plant assumptions in Section 2.3 and design a MRAC scheme. We will verify the design conditions for the cases with actuator failure in next part.

9.2.2 Design Condition Verification

In this part, we show that the plant assumptions in Section 2.3 still stands when the system with actuator failure is equipped with the control distribution scheme in (9.8).

System model with control distribution

By plugging (9.8) and (9.7) into (9.2), we have

$$\dot{x}(t) = Ax(t) + Bu_c(t) + B_{\bar{u}}\bar{u}(t) + f_o, \tag{9.11}$$

where the unknown parameter matrix

$$B = B_p C_a (I - \sigma) C_d. \tag{9.12}$$

The transfer function of the new system is

$$G(s) = C(sI - A)^{-1}B. \tag{9.13}$$

The first step of the verification is to show the property as below.

Proposition 4. *The control signal distribution matrix C_d in (9.8) guarantees that*

$$rank(C_a(I - \sigma(t))C_d) = m, \tag{9.14}$$

for the control effectiveness matrix C_a in (9.3) and all the compensable failure patterns in Section 6.1.2.

Proof. We can derive the determine of $C_a(I - \sigma(t))C_d$ for each compensable pattern:

$$\det(C_a(I - \sigma_{(1)})C_d) = 0.5641$$

$$\det(C_a(I - \sigma_{(2)})C_d) = 0.5641$$

$$\det(C_a(I - \sigma_{(3)})C_d) = 0.3512$$

$$\det(C_a(I - \sigma_{(4)})C_d) = 0.3512$$

$$\det(C_a(I - \sigma_{(5)})C_d) = 0.3077$$

$$\det(C_a(I - \sigma_{(6)})C_d) = 0.1914$$

$$\det(C_a(I - \sigma_{(7)})C_d) = 0.0893.$$

Since the determines are all nonzero, so $C_a(I - \sigma(t))C_d$ is nonsingular and full rank for each compensable pattern. □

From [66], we know that the linearized system without control distribution as $G_0 = C_p(sI - A_p)^{-1}B_p$ satisfies the plant assumptions. Then the design conditions for the system $G(s) = G_0(s)C_a(I - \sigma(t))C_d$ are verified as following.

1. Since the zeros of a transfer matrix are the zeros make the transfer matrix lose rank. So the constant matrix $C_a(I - \sigma(t))C_d$ does not bring any new zeros to the transfer matrix.

2. We know that (A_p, B_p) is stabilizable; and $C_a(I - \sigma(t))C_d$ is full rank. Then $(A_p, B_p C_a(I - \sigma(t))C_d)$ is also stabilizable.

3. Because $C_a(I - \sigma(t))C_d$ is full rank and $G_0(s)$ is full rank, so $G(s) = G_0(s)C_a(I - \sigma(t))C_d$ is full rank.

   It can be verified numerically that the interactor matrices of $G_0(s)$ still work for $G(s)$. For example, for the hover condition

$$\xi_{m,hov}(s) = \begin{bmatrix} (s+1)^2 & 0 & 0 & 0 \\ 0 & (s+1)^4 & 0 & 0 \\ 0 & 0 & (s+1)^4 & 0 \\ 0 & 0 & 0 & (s+1)^2 \end{bmatrix}, \tag{9.15}$$

   and for the cruise condition

$$\xi_{m,pit}(s) = \begin{bmatrix} (s+1)^2 & 0 & 0 & 0 \\ 0 & (s+1)^4 & 0 & 0 \\ -T_{\theta_o}(s+1)^4 & 0 & (s+1)^4 & 0 \\ 0 & 0 & 0 & (s+1)^2 \end{bmatrix}. \tag{9.16}$$

4. This condition can also be verified numerically. Limited by the paper length, the trivial derivation process is not shown here.

By summarizing the above analysis, we can build a lemma for the linearized hexarotor system with control signal distributor as follows:

Lemma 10. *There exists a control signal distributor C_d as in (9.8) such that the system $G(s)$ in (9.13) satisfies the design conditions in Section 2.3.*

9.3 Nominal Controller Design

When the parameters of the system are known, the nominal controller structure is

$$u_c^*(t) = K_x^{*T}x(t) + K_r^*r(t) + K_\beta^*\beta(t) + k_f^*, \tag{9.17}$$

where $\beta(t)$ is a known signal vector with element $\beta_k(t)$ defined in (3.51), $K_x^{*T} \in R^{M \times n}$ and $K_r^{*T} \in R^{M \times m}$ are for the plant-model output matching:

$$C(sI - A - BK_x^{*T})^{-1}BK_r^* = W_m(s), \quad K_r^* = K_p^{-1}, \tag{9.18}$$

and the high-frequency gain matrix is $K_p = \lim_{s \to \infty} \xi_m G(s)$.

The existence of K_x^* and K_r^* is guaranteed by following lemma, whose proof is in [125].

Lemma 11. *There exist K_x^* and K_r^* such that the plant-model matching condition (9.18) holds.*

The nominal parameter k_f^* for rejecting the non-equilibrium offset f_o is derived in [50] as

$$k_f^* = -D^{-1}d \tag{9.19}$$

where

$$D = -C(A + BK_x^*)^{-1}B, \quad d = -C(A + BK_x^*)^{-1}f_o.$$

For the nominal case that the failure value, failure pattern and failure time are all known, the system input is

$$\Delta u_f(t) = (I - \sigma_{(i)})v_{(i)}^*(t) + \bar{u}_{(i)}(t), \quad i \in \{1, 2, \dots, 7\}, \tag{9.20}$$

where $v_{(i)}^*(t)$ is the applied control input to be designed for failure pattern (i), the failure value for failure pattern (i) is

$$\bar{u}_{(i)}(t) = \sigma_{(i)}\bar{u}(t). \tag{9.21}$$

Compensation design for actuator failures

Consider the output of the closed-loop system in s domain

$$y(s) = C(sI - A - BK_x^{*T})^{-1}BK_r^*r(s) + \delta(s) \tag{9.22}$$

where

$$\delta(s) = C(sI - A - BK_x^{*T})^{-1}[BK_\beta^* + B_pC_a\sigma_{(i)}\bar{u}]\beta(s). \tag{9.23}$$

Then the output tracking error in the s domain is

$$e(s) = y(s) - y_m(s) = \delta(s). \tag{9.24}$$

From the final value theorem, we have $\lim_{t\to\infty} e(t) = \lim_{s\to 0} s\delta(s)$. Recall that $B = B_pC_a(I - \sigma_{(i)})C_d$; and as shown in Proposition 1 that $C_a(I - \sigma_{(i)})C_d$ is full rank. So there exists the matrix $(C_a(I - \sigma_{(i)})C_d)^{-1}$. In order to compensate the failure and guarantee $\lim_{t\to\infty} e(t) = 0$, we choose the nominal failure compensation parameter as

$$K_{\beta(i)}^* = -(C_a(I - \sigma_{(i)})C_d)^{-1}C_a\sigma_{(i)}\bar{u}(t) \tag{9.25}$$

Then it follows that

$$\lim_{t\to\infty}(y(t) - y_m(t)) = \lim_{t\to\infty}\delta(t) = 0. \tag{9.26}$$

In summary, we have the following theorem.

Theorem 4. *For the plant (9.11), there exist matrices K_x^*, K_r^*, k_f^* and K_β^*, with which*

the state feedback controller (9.17) ensures the closed -loop signal boundedness of all s, nonlinear offset rejection, and output tracking of a chosen reference output $y_m(t)$ by the output $y(t)$.

9.4 Adaptive Control Design

The nominal controller presented in last section requires the full knowledge of the failures. When the failure pattern, failure time, and failure value are all unknown, the given nominal controller can not guarantee closed-loop performance and stability anymore. In this section, an adaptive actuator failure compensation scheme is developed for the system in the presence of uncertain actuator failures.

9.4.1 Adaptive Law Design

When the system parameters are unknown, the state-feedback controller structure is

$$u_c(t) = \Theta^T(t)\omega(t), \tag{9.27}$$

where

$$\omega(t) = [x^T(t), r^T(t), \beta(t)^T, 1]^T, \tag{9.28}$$

the controller parameter matrix $\Theta(t)$ is an estimation of the nominal parameters

$$\Theta^* = [K_x^{*T}, K_r^*, K_\beta^*, k_f^*]^T. \tag{9.29}$$

Error equation

Substituting the control law (9.27) into the the system dynamic , we obtain

$$\dot{x}(t) = Ax(t) + B\Theta^T(t)\omega(t) + B_{\bar{u}}\bar{u}(t)$$
$$= (A + BK_x^{*T})x(t) + BK_r^*r(t) + BK_\beta^*\beta(t) + B_{\bar{u}}\bar{u}(t)$$
$$+ B\tilde{\Theta}(t)\omega(t), \tag{9.30}$$

where

$$\tilde{\Theta}(t) = \Theta(t) - \Theta^*. \tag{9.31}$$

In view of the reference model system (9.5), matching conditions (9.18), and the closed-loop system (9.30), the output-tracking error is given as

$$e(t) = y(t) - y_m(t) = W_m(s)K_p[\tilde{\Theta}^T\omega](t) + \delta(t). \tag{9.32}$$

To deal with the uncertainty of K_p, the LDS decomposition [27] is used as

$$K_p = L_s D_s S, \tag{9.33}$$

where $S \in R^{M \times M}$ is a symmetric positive definite matrix, $L_s \in R^{M \times M}$ is a unity lower triangular matrix, and

$$D_s = \text{diag}\{s_1^*, s_2^*, \ldots, s_M^*\}$$
$$= \{\text{sign}[\Delta_1]\gamma_1, \text{sign}\left[\frac{\Delta_2}{\Delta_1}\right]\gamma_2, \ldots, \text{sign}\left[\frac{\Delta_M}{\Delta_{M-1}}\right]\gamma_M\} \tag{9.34}$$

such that $\gamma_i \geq 0, i = 1, \ldots, M$, may be chosen to be arbitrary.

Error parameterization

To obtain the adaptive laws for $K_x(t)$, $K_r(t)$, and $K_\beta(t)$, a well parameterized tracking-error model is needed. Substituting the LDS decomposition of K_p and ignoring the exponentially decaying term $\delta(t)$, the error equation can be parameterized as

$$L_s^{-1}\xi_m(s)[e](t) = D_s S\tilde{\Theta}^T(t)\omega(t). \tag{9.35}$$

To parameterize the unknown matrix L_s, a parameter matrix is introduced as

$$\Theta_0^* = L_s^{-1} - I, \tag{9.36}$$

which has a special form as

$$\Theta_0^* = \begin{bmatrix} 0 & 0 & 0 & \cdots & 0 \\ \theta_{21}^* & 0 & 0 & \cdots & 0 \\ \theta_{31}^* & \theta_{32}^* & 0 & \cdots & 0 \\ \vdots & \vdots & \vdots & \vdots & \vdots \\ \theta_{M-11}^* & \cdots & \theta_{M-1M-2}^* & 0 & 0 \\ \theta_{M1}^* & \cdots & \theta_{MM-2}^* & \theta_{MM-1}^* & 0 \end{bmatrix} \in R^{M\times M}. \tag{9.37}$$

We introduce a filter $h(s) = 1/f_h(s)$, where $f_h(s)$ is a stable and monic polynomial whose degree is equal to the maximum degree of $\xi_m(s)$. Operating both sides of (9.35) by $h(s)I_M$ leads to the filtered tracking error

$$\bar{e}(t) + [0, \theta_2^{*T}\eta_2(t), \theta_3^{*T}\eta_3(t), \ldots, \theta_M^{*T}\eta_M(t)]^T$$

$$= D_s Sh(s)[\tilde{\Theta}^T\omega](t), \tag{9.38}$$

where

$$\bar{e}(t) = \xi_m(s)h(s)[e](t) = [\bar{e}_1(t), \ldots, \bar{e}_M(t)]^T \tag{9.39}$$

$$\eta_i(t) = [\bar{e}_1(t), \ldots, \bar{e}_{i-1}(t)]^T \text{ for } i = 2, \ldots, M \tag{9.40}$$

$$\theta_i^* = [\theta_{i1}^*, \ldots, \theta_{ii-1}^*]^T \text{ for } i = 2, \ldots, M. \tag{9.41}$$

Based on this error equation, we construct the estimation error vector signal:

$$\epsilon(t) = \bar{e}(t) + [0, \theta_2^T(t)\eta_2(t), \theta_3^T(t)\eta_3(t), \ldots, \theta_M^T(t)\eta_M(t)]^T + \Psi(t)\xi(t), \tag{9.42}$$

where $\theta_i(t)$ are the estimates of θ_i^*, $\Psi(t)$ is the estimate of $\Psi^* = D_s S$, and

$$\xi(t) = \Theta^T(t)\zeta(t) - h(s)[\Theta^T \omega](t) \tag{9.43}$$

$$\zeta(t) = h(s)[\omega](t). \tag{9.44}$$

Adaptive laws

With the estimation error model, we choose the adaptive laws

$$\dot{\theta}_i(t) = -\frac{\Gamma_{\theta_i}\epsilon_i(t)\eta_i(t)}{m^2(t)}, \quad i = 2, 3, \ldots, M \tag{9.45}$$

$$\dot{\Theta}^T(t) = -\frac{D_s\epsilon(t)\zeta^T(t)}{m^2(t)} \tag{9.46}$$

$$\dot{\Psi}(t) = -\frac{\Gamma\epsilon(t)\xi^T(t)}{m^2(t)} \tag{9.47}$$

where $\Gamma_{\theta_i} = \Gamma_{\theta_i}^T > 0$ and $\Gamma = \Gamma^T > 0$ are adaptation gain matrices, and

$$m^2(t) = 1 + \zeta^T(t)\zeta(t) + \xi^T(t)\xi(t) + \sum_{i=2}^{M} \eta_i^T(t)\eta_i(t), \tag{9.48}$$

is a standard normalization signal.

9.4.2 Stability Analysis

To analyze the closed-loop system stability, we first establish some desired properties of the aforementioned adaptive parameter update laws for the linearized system models at each operating condition.

Lemma 12. *The adaptive laws (9.45)-(9.47) ensure the following desired properties:*

1. $\theta_i(t) \in L^\infty (i = 2, 3, \ldots, M), \Theta(t) \in L^\infty, \Psi \in L^\infty, \frac{\epsilon(t)}{m(t)} \in L^2 \cap L^\infty$; and

2. $\dot{\theta}_i(t) \in L^2 \cap L^\infty (i = 2, 3, \ldots, M), \dot{\Theta}(t) \in L^2 \cap L^\infty, \dot{\Psi}(t) \in L^2 \cap L^\infty$.

Proof. For the linearized system model, consider the positive-definite function

$$V = \frac{1}{2}(\sum_{i=2}^{M} \tilde{\theta}_i^T \Gamma_{\theta_i}^{-1} \tilde{\theta}_i + \text{tr}[\tilde{\Psi}^T \Gamma^{-1} \tilde{\Psi}] + \text{tr}[\tilde{\Theta} S \tilde{\Theta}^T]) > 0. \tag{9.49}$$

From (9.38) and (9.42), it then follows that

$$\epsilon(t) = [0, \tilde{\theta}_2^T(t)\eta_2(t), \tilde{\theta}_3^T(t)\eta_3(t), \ldots, \tilde{\theta}_M^T(t)\eta_M(t)]^T$$
$$+ \tilde{\Psi}(t)\xi(t) + D_s S \tilde{\Theta}^T(t)\zeta(t), \tag{9.50}$$

where $\tilde{\theta}_i(t) = \theta_i(t) - \theta_i^*$ and $\tilde{\Psi}(t) = \Psi(t) - \Psi^*$ are the related parameter errors.

From the adaptive laws, the time derivative of V can be obtained to as

$$\dot{V} = -\sum_{i=2}^{M} \frac{\tilde{\theta}_i^T(t)\epsilon_i(t)\eta_i(t)}{m^2(t)} - \frac{\xi^T(t)\tilde{\Psi}^T(t)\epsilon(t)}{m^2(t)}$$
$$- \frac{\zeta^T(t)\tilde{\Theta}(t)SD_s\epsilon(t)}{m^2(t)}$$
$$= -\frac{\epsilon^T(t)\epsilon(t)}{m^2(t)} \leq 0. \tag{9.51}$$

From (9.49) and (9.51), it can be concluded that $\theta_i(t) \in L^\infty (i = 2, 3, \ldots, M), \Theta(t) \in L^\infty, \Psi(t) \in L^\infty$, and $\frac{\epsilon(t)}{m(t)} \in L^2$. Summing up the boundedness of $\theta_i(t)(i = 2, 3, \ldots, M), \Theta(t)$,

and $\Psi(t)$ with (9.50) and (9.48), we have $\frac{\epsilon(t)}{m(t)} \in L^\infty$. Since the normalized signals $\frac{\eta_i(t)}{m(t)}(i = 2, 3, \ldots, M), \frac{\zeta(t)}{m(t)}, \frac{\xi(t)}{m(t)} \in L^\infty$, it can be concluded that $\dot{\theta}_i(t) \in L^2 \cap L^\infty (i = 2, 3, \ldots, M), \dot{\Theta}(t) \in L^2 \cap L^\infty$, and $\dot{\Psi}(t) \in L^2 \cap L^\infty$. $\qquad \square$

Based on Lemma 4, the following desired closed-loop system properties for each linearized system model can be established:

Theorem 5. *The multivariable MRAC scheme with the state feedback control law (9.27) updated by the adaptive laws (9.45)-(9.47), when applied to the system , guarantees the closed-loop signal boundness and asymptotic output tracking:* $\lim\limits_{t \to \infty}(\Delta y(t) - \Delta y_m(t)) = 0$*, for any initial conditions.*

The proof of Theorem 1 is similar to that explained in [125] for MRAC design for MIMO systems. The key step is to formulate a filtered output signal. The state feedback control signal is required to be expressed in terms of the output. Since the state feedback control input $u_c(t)$ depends on the state $x(t)$, we need to express it in terms of the output y(t), which can be done using a state-observer of the plant. Then the analysis procedure in [126] can be used to conclude the closed-loop signal boundedness and output tracking.

9.5   Simulation Study

The proposed adaptive controller has been verified analytically in last section. In this section, we show its performance by simulation.

9.5.1   Simulation System

The simulation is based on the data of a real hexarotor system. The details of the parameters we use is shown in Table 9.1. The reference output signal $y_m(t)$ is chosen

to be: $y_m(t) = [500, 50\sin(t), 180\sin(0.5t), 0]^T$, for $t \in [0, 80)$; $y_d(t) = [20, 0, 0, 0]^T$, for $t \in [80, 100)$.

Table 9.1: Parameter values for simulation

Parameter	Value	Unit
c_m	0.0025	m·s
c_r	0.001	N·m·s
c_t	0.25	N·m·s
d	0.2	m
g	9.8	m/s^2
J_x	0.005	kg·m^2
J_y	0.005	kg·m^2
J_z	0.009	kg·m^2
m	2	kg

9.5.2   Simulation Results

Case I

A loss-of-effectiveness failure happens at rotor 1 from $t = 20s$. The rotor can only perform 80% of command input. The results are shown in Figure 9.1.

Case II

A lock-in-place failure happens at rotor 1 from $t = 20s$. The rotor stops receiving commands and keeps rotating at the same speed. The results are shown in Figure 9.2.

Case III

A loss-of control failure happens at rotor 1 from $t = 10s$, the rotor stops working after the failure. Then a loss-of control failure happens at rotor 4 from $t = 30s$, the rotor stops working after the failure. The results are shown in Figure 9.3.
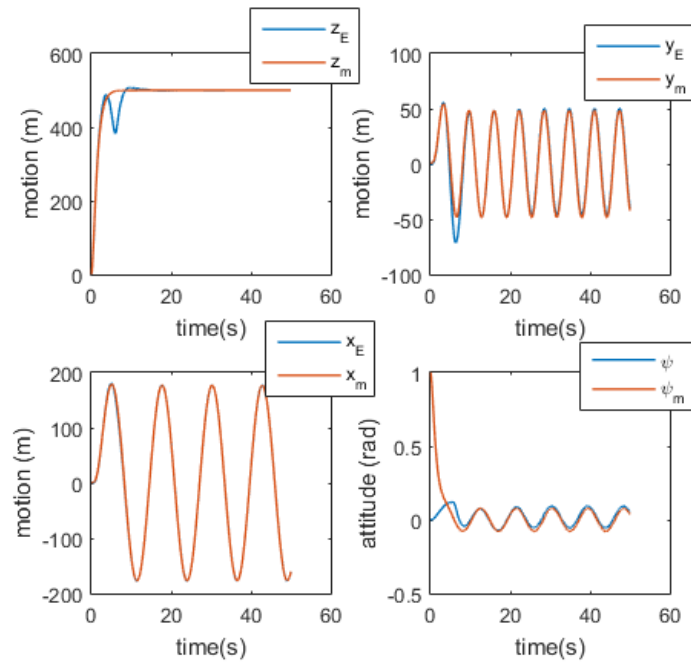
Figure 9.1: Simulation results for loss-of-effectiveness failure compensation.
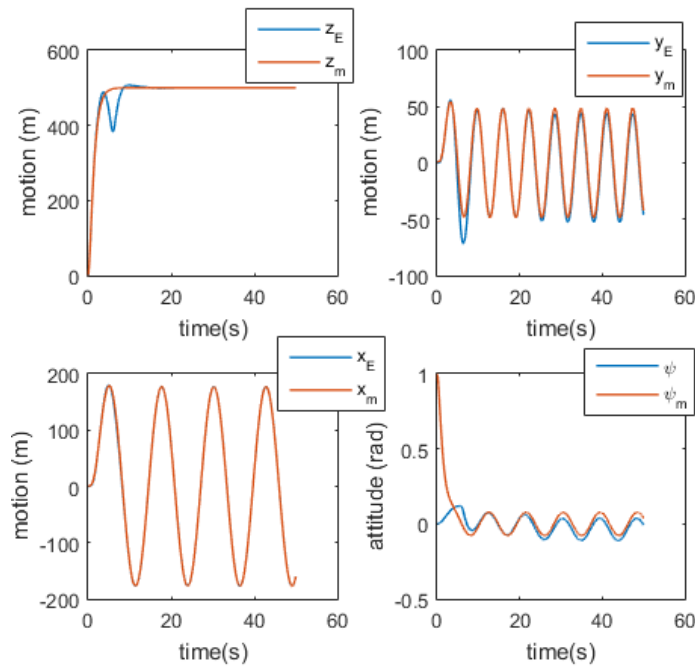
Figure 9.2: Simulation results for lock-in-place failure compensation.
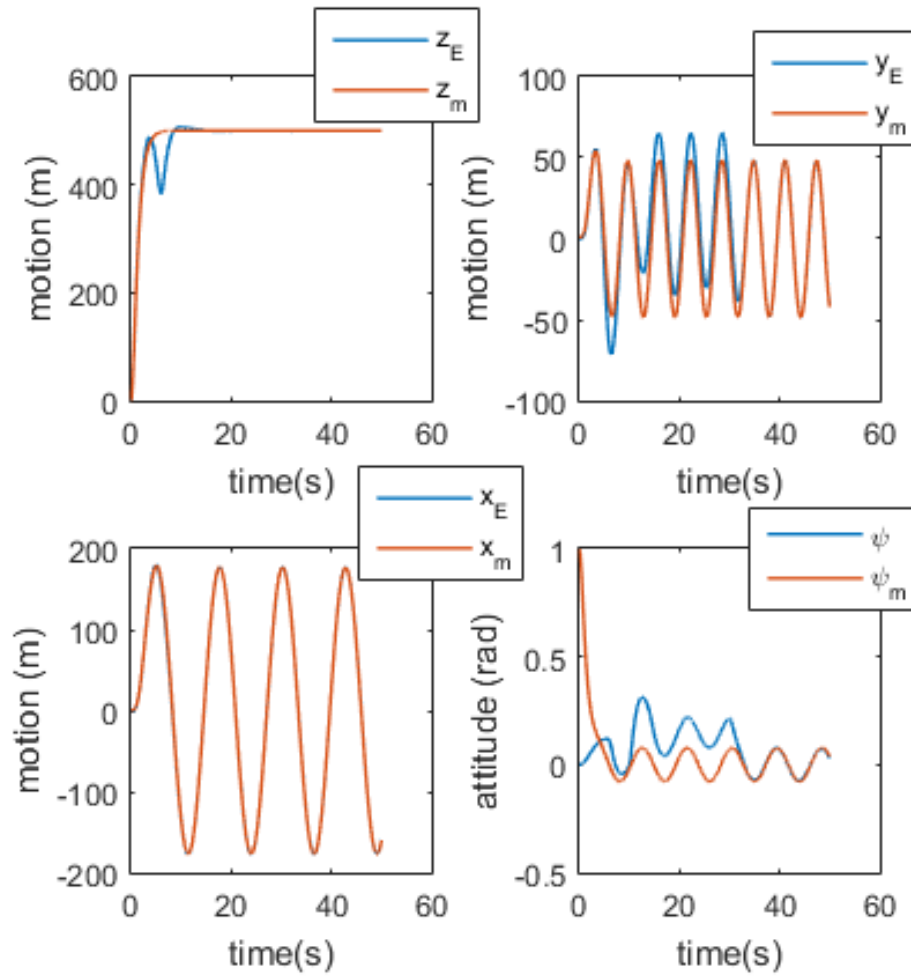
Figure 9.3: Simulation results for loss-of-control failures compensation.

Case IV

In this case, both failures are loss-of-control failure. The results is shown in Figure 9.4.
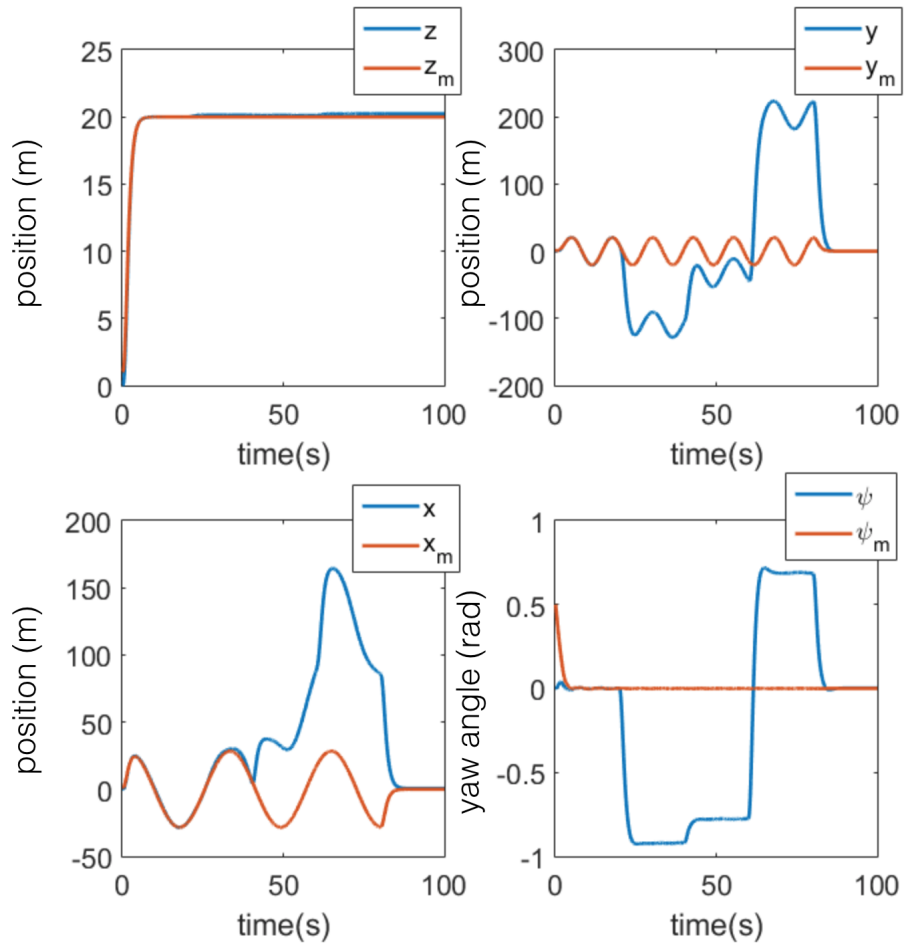
Figure 9.4: Simulation results for loss-of control failure.

Case V

In this case, the first failure is lock in place failure, the second failure is loss-of-effectiveness . The results is shown in Figure 9.5.
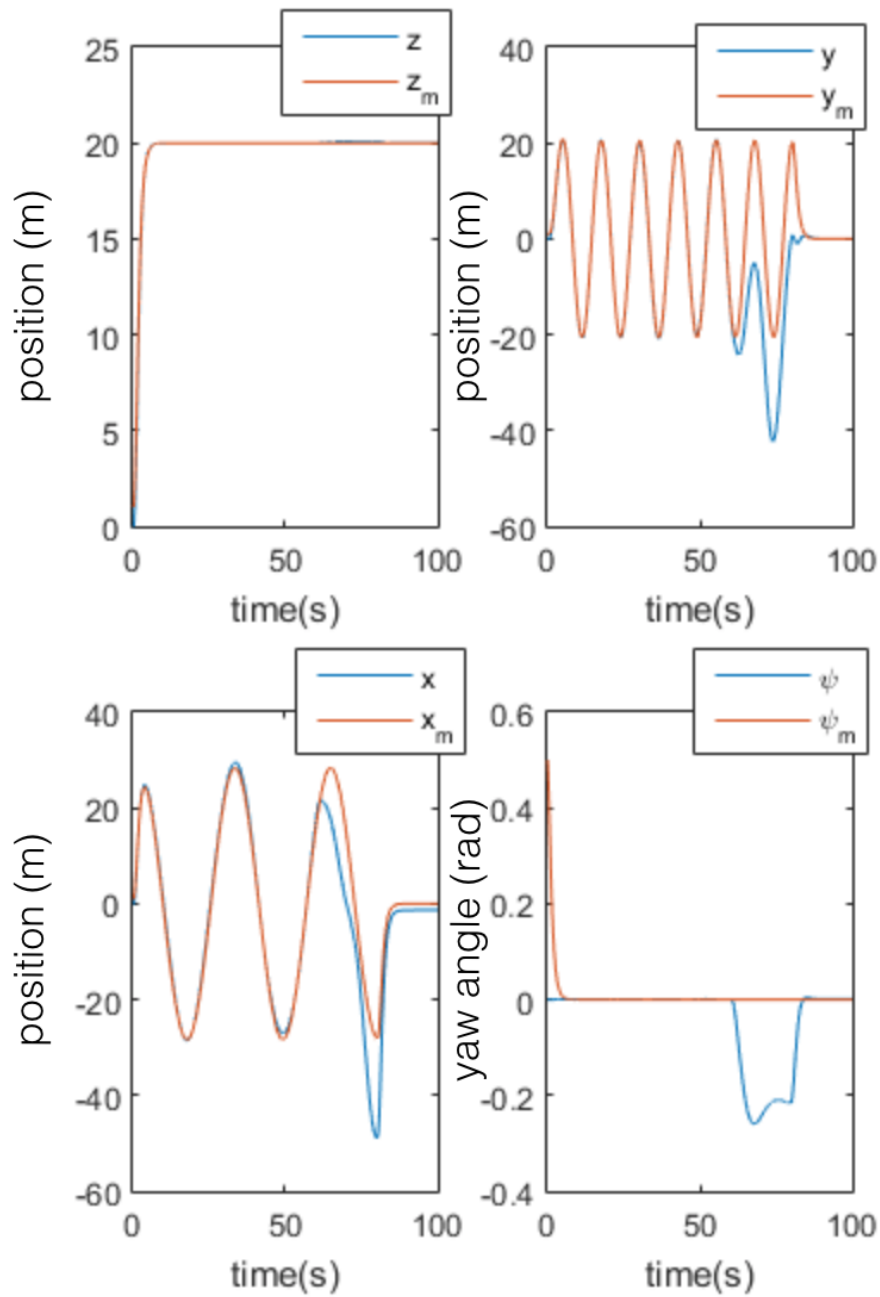
Figure 9.5: Simulation results for loss-of-effectiveness and lock-in-place failures.

Case VI

In this case, the desired output $y_d(t)$ is chosen as: $y_d(t) = [20, 20\sin(0.5t), 30\cos(0.2t), 0]^T$, for $t \in [0, 10000)$; The results is shown in Figure 9.6.
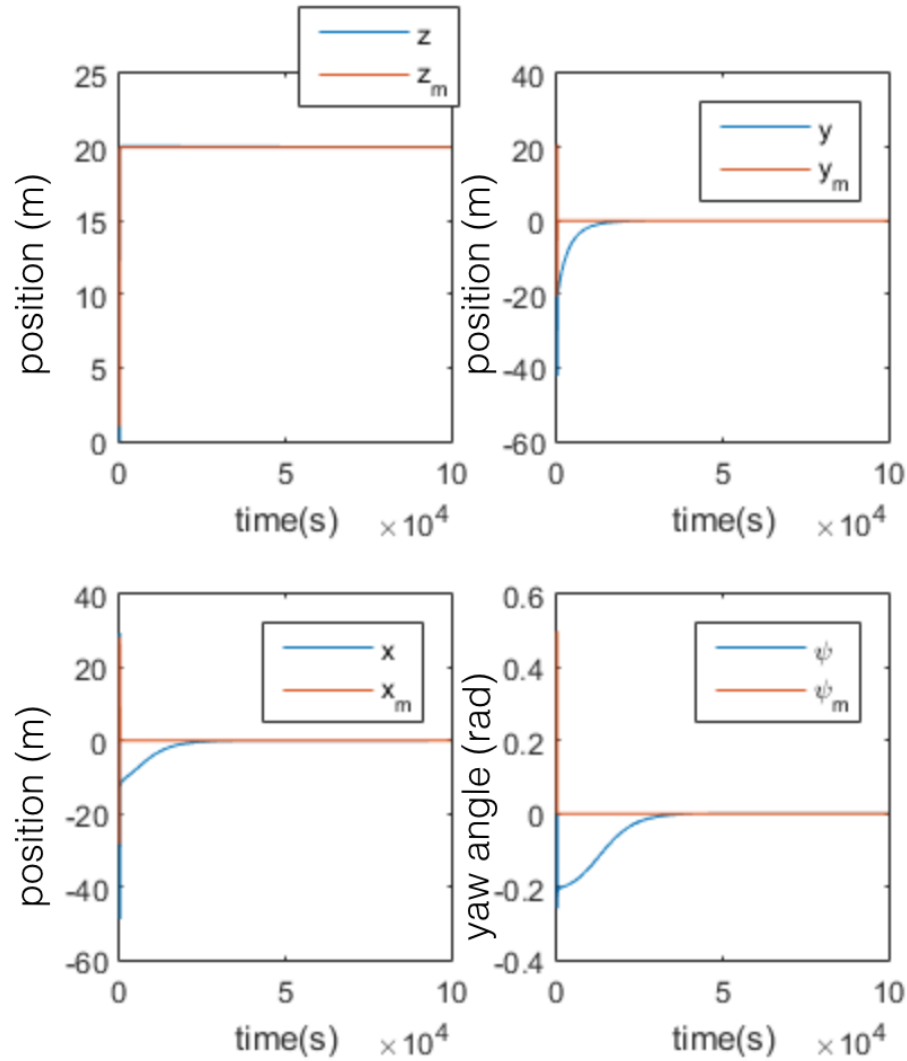
Figure 9.6: Verification of the asymptotic stability of the output.

9.6   Summary

In this chapter, we studied the adaptive actuator failure compensation scheme for a hexarotor system. The work shows that, with a complete parameterization of failure

patterns and system parameters, desired closed-loop stability and asymptotic tracking of the system can be achieved, despite uncertain actuator failures whose failure pattern, failure time, and failure value are all unknown. The simulation results also verified the performance of the adaptive control algorithm when applied to the hexarotor system.

Chapter 10

Conclusions and Future Work

10.1 Conclusions

Given the importance of multirotors and the current lacking of effective control techniques for the next generation of autonomous multirotors (which are expected to have guaranteed stability and tracking properties for sophisticated fast maneuvers and under system parameter and fault uncertainties, without the human manipulation), this dissertation research developed advanced adaptive control techniques to meet the needs of next generation multirotors: robust stability, asymptotic tracking, and adaptive fault accommodation, in the presence of system and environment uncertainties. Such advanced adaptive control methods for multirotors are effective for dealing with system parameter uncertainties and system faults.

In Chapter 6, we developed a linearization-based model reference adaptive control scheme for a multivariable quadrotor system. The proposed adaptive design can reject the non-equilibrium offset and make the closed-loop system signals bounded and the outputs track the chosen reference signals asymptotically.

In Chapter 7, a linearization-based multivariable adaptive control scheme for a nonlinear quadrotor model has been developed. The nonlinear quadrotor system

is linearized at given typical operating conditions, and a sequential linear model with parameter uncertainties and a non-equilibrium offset is obtained to represent the linearized system at different operating conditions. With the use of an input compensator, a uniform interactor matrix and identical gain matrix signs are obtained. As a result of the achievable plant-model matching conditions, the proposed MRAC design can reject the non-equilibrium offset and make the closed-loop system signals bounded and the output signals track some chosen reference signals over different operating conditions.

Chapter 8, we studied the adaptive actuator failure compensation scheme of a hexarotor system with NNPPNP rotor arrangement. It is shown that, with a complete parameterization of failure patterns and system parameters, desired closed-loop stability and asymptotic tracking of the system can be achieved, despite uncertain actuator failures whose failure index, failure time, and failure value are unknown.

In Chapter 9, we developed an adaptive controller for hexarotor systems subject to parameter uncertainty and actuator failures. A control signal distribution matrix is proposed to deal with uncertainties of the control allocation scheme for a 4-DOF hexarotor, which includes additive and manipulative parameters uncertainties. The design conditions are verified for the distributor under up to two actuator failures with unknown failure time, failure pattern and failure value. An adaptive controller equipped with control signal distributor is developed for the hexarotor system with parameter and failure uncertainties.

The control designs for multirotors under uncertainties and faults obtained in this dissertation research will be the basis for resilient control not only in multirotor systems but also in a broad range of other performance-critical cyber-physical systems such as intelligent and collaborative robots.

10.2 Future Work

In this dissertation, an adaptive control framework is presented for different multirotor systems under various abnormal conditions. There are still some potential directions for future research work. We would like investigate the non-equilibrium conditions of omni-directional multirotor systems to reach more sophisticated flight maneuvers. The compensable actuator failures summarized in Chapter 5 are obtained through numerical methods, so an analytical study of failure compensability or fault tolerance should be conducted. The center of gravity variation problem is still unsolved, it affects both the dynamics and actuation of the system and requires special treatment.

Bibliography

[1] Joseph Flynt. 21 types of drones. `https://3dinsider.com/types-of-drones/`.

[2] Ascending Technologies. Renewable uk: Cyberhawk launches special wind turbine inspection service. `http://www.asctec.de/en/renewable-uk-cyberhawk-drone-wind-turbine-service/`.

[3] KRISTIN HOUSER. Ups is now using drones to deliver blood to a hospital. `https://futurism.com/the-byte/ups-drone-delivery-blood-hospital`.

[4] Day_Dreamer. Earthbound robots today need to take flight. `https://forum.dji.com/thread-82587-1-1.html`.

[5] S. Bouabdallah and R. Siegwart. Full control of a quadrotor. In *2007 IEEE/RSJ International Conference on Intelligent Robots and Systems*, pages 153–158, Oct 2007.

[6] Alessandro Freddi, Alexander Lanzon, and Sauro Longhi. A feedback linearization approach to fault tolerance in quadrotor vehicles. In *IFAC World Congress, Milano, Italy*, pages 5413–5418, 2011.

[7] B. Zhao, B. Xian, Y. Zhang, and X. Zhang. Nonlinear robust adaptive tracking control of a quadrotor uav via immersion and invariance methodology. *IEEE Transactions on Industrial Electronics*, 62(5):2891–2902, May 2015.

[8] T. Lee. Robust adaptive attitude tracking on so(3) with an application to a quadrotor uav. *IEEE Transactions on Control Systems Technology*, 21(5):1924–1930, Sept 2013.

[9] Mark W. Mueller and Raffaello DAndrea. Relaxed hover solutions for multicopters: Application to algorithmic redundancy and novel vehicles. *The International Journal of Robotics Research*, 2015.

[10] A. Alaimo, V. Artale, C. Milazzo, A. Ricciardello, and L. Trefiletti. Mathematical modeling and control of a hexacopter. In *Unmanned Aircraft Systems (ICUAS), 2013 International Conference on*, pages 1043–1050, May 2013.

[11] Robert Leishman, John Macdonald, T. McLain, and R. Beard. Relative navigation and control of a hexacopter. In *Robotics and Automation (ICRA), 2012 IEEE International Conference on*, pages 4937–4942, May 2012.

[12] S. Rajappa, M. Ryll, H. H. Blthoff, and A. Franchi. Modeling, control and design optimization for a fully-actuated hexarotor aerial vehicle with tilted propellers. In *2015 IEEE International Conference on Robotics and Automation (ICRA)*, pages 4006–4013, May 2015.

[13] M. Ryll, D. Bicego, and A. Franchi. Modeling and control of fast-hex: A fully-actuated by synchronized-tilting hexarotor. In *2016 IEEE/RSJ International Conference on Intelligent Robots and Systems (IROS)*, pages 1689–1694, Oct 2016.

[14] Giulia Michieletto, Markus Ryll, and Antonio Franchi. Control of statically hoverable multi-rotor aerial vehicles and application to rotor-failure robustness for hexarotors. In *2017 IEEE International Conference on Robotics and Automation*, page 6p, 2017.

[15] Majd Saied, Hassan Shraim, Benjamin Lussier, Isabelle Fantoni, and Clovis Francis. Local controllability and attitude stabilization of multirotor uavs: Validation on a coaxial octorotor. *Robotics and Autonomous Systems*, 91:128 – 138, 2017.

[16] M. Saied, B. Lussier, I. Fantoni, C. Francis, H. Shraim, and G. Sanahuja. Fault diagnosis and fault-tolerant control strategy for rotor failure in an octorotor. In *Robotics and Automation (ICRA), 2015 IEEE International Conference on*, pages 5266–5271, May 2015.

[17] Majd Saied, Benjamin Lussier, Isabelle Fantoni, Clovis Francis, and Hassan Shraim. Fault tolerant control for multiple successive failures in an octorotor: Architecture and experiments. In *Intelligent Robots and Systems (IROS), 2015 IEEE/RSJ International Conference on*, pages 40–45, Sept 2015.

[18] A. L. Salih, M. Moghavvemi, H. A. F. Mohamed, and K. S. Gaeid. Modelling and pid controller design for a quadrotor unmanned air vehicle. In *Automation Quality and Testing Robotics (AQTR), 2010 IEEE International Conference on*, volume 1, pages 1–5, May 2010.

[19] J. Li and Y. Li. Dynamic analysis and pid control for a quadrotor. In *2011 IEEE International Conference on Mechatronics and Automation*, pages 573–578, Aug 2011.

[20] B. Erginer and E. Altug. Modeling and pd control of a quadrotor vtol vehicle. In *2007 IEEE Intelligent Vehicles Symposium*, pages 894–899, June 2007.

[21] Feng Pan, Lu Liu, and Dingyu Xue. Optimal pid controller design with kalman filter for qball-x4 quad-rotor unmanned aerial vehicle. *Transactions of the Institute of Measurement and Control*, page 0142331216656753, 2016.

[22] Farhad Goodarzi, Daewon Lee, and Taeyoung Lee. Geometric nonlinear pid control of a quadrotor uav on se (3). In *Control Conference (ECC), 2013 European*, pages 3845–3850. IEEE, 2013.

[23] Tyler Ryan and H Jin Kim. Pd-tunable h? control design for a quadrotor. In *AIAA Guidance, Navigation, and Control (GNC) Conference*, page 4530, 2013.

[24] M. D. Hua, T. Hamel, P. Morin, and C. Samson. Introduction to feedback control of underactuated vtolvehicles: A review of basic control design ideas and principles. *IEEE Control Systems*, 33(1):61–75, Feb 2013.

[25] Samir Bouabdallah. *Design and control of quadrotors with application to autonomous flying*. PhD thesis, Ecole Polytechnique Federale de Lausanne, 2007.

[26] Isabelle Fantoni and Rogelio Lozano. *Non-Linear Control for Underactuated Mechanical Systems*. Springer-Verlag New York, Inc., Secaucus, NJ, USA, 2001.

[27] Gang Tao. *Adaptive control design and analysis*. John Wiley & Sons, 2003.

[28] Gang Tao. Multivariable adaptive control: A survey. *Automatica*, 50(11):2737–2764, 2014.

[29] Gang Tao, Shuhao Chen, Xidong Tang, and Suresh M Joshi. *Adaptive control of systems with actuator failures*. Springer Science & Business Media, 2013.

[30] YM Zhang, Abbas Chamseddine, Camille Alain Rabbath, Brandon W Gordon, C-Y Su, Subhash Rakheja, Cameron Fulford, Jacob Apkarian, and Pierre Gosselin. Development of advanced fdd and ftc techniques with application to an unmanned quadrotor helicopter testbed. *Journal of the Franklin Institute*, 350(9):2396–2422, 2013.

[31] T-H Guo and J Nurre. Sensor failure detection and recovery by neural networks. In *IJCNN-91-Seattle international joint conference on neural networks*, volume 1, pages 221–226. IEEE, 1991.

[32] Kurt R Rohloff. Sensor failure tolerant supervisory control. In *Proceedings of the 44th IEEE Conference on Decision and Control*, pages 3493–3498. IEEE, 2005.

[33] M Hassan Tanveer, S Faiz Ahmed, Desa Hazry, Faizan A Warsi, and M Kamran Joyo. Stabilized controller design for attitude and altitude controlling of quad-rotor under disturbance and noisy conditions. *American Journal of Applied Sciences*, 10(8):819, 2013.

[34] Robert Leishman, John Macdonald, Tim McLain, and Randy Beard. Relative navigation and control of a hexacopter. In *2012 IEEE International Conference on Robotics and Automation*, pages 4937–4942. IEEE, 2012.

[35] Ali Reza Partovi, Ang Zong Yao Kevin, Hai Lin, Ben Chen, and Guowei Cai. Development of a cross style quadrotor. In *AIAA Guidance, Navigation, and Control Conference*, page 4780, 2012.

[36] Radoslaw Zawiski and Marian Blachuta. Dynamics and optimal control of quadrotor platform. In *AIAA Guidance, Navigation, and Control Conference*, page 4915, 2012.

[37] David W Kun and Inseok Hwang. Linear matrix inequality-based nonlinear adaptive robust control of quadrotor. *Journal of Guidance, Control, and Dynamics*, pages 996–1008, 2015.

[38] Z.T. Dydek, A.M. Annaswamy, and E. Lavretsky. Adaptive control of quadrotor uavs: A design trade study with flight evaluations. *Control Systems Technology, IEEE Transactions on*, 21(4):1400–1406, July 2013.

[39] S. Bouabdallah and R. Siegwart. Backstepping and sliding-mode techniques applied to an indoor micro quadrotor. In *Proceedings of the 2005 IEEE International Conference on Robotics and Automation*, pages 2247–2252, April 2005.

[40] Daewon Lee, H. Jin Kim, and Shankar Sastry. Feedback linearization vs. adaptive sliding mode control for a quadrotor helicopter. *International Journal of Control, Automation and Systems*, 7(3):419–428, 2009.

[41] Fuyang Chen, Rongqiang Jiang, Kangkang Zhang, Bin Jiang, and Gang Tao. Robust backstepping sliding-mode control and observer-based fault estimation for a quadrotor uav. *IEEE Transactions on Industrial Electronics*, 63(8):5044–5056, 2016.

[42] S. Bouabdallah, A. Noth, and R. Siegwart. Pid vs lq control techniques applied to an indoor micro quadrotor. In *Intelligent Robots and Systems, 2004. (IROS 2004). Proceedings. 2004 IEEE/RSJ International Conference on*, volume 3, pages 2451–2456 vol.3, Sept 2004.

[43] T. Dierks and S. Jagannathan. Output feedback control of a quadrotor uav using neural networks. *IEEE Transactions on Neural Networks*, 21(1):50–66, Jan 2010.

[44] Hana Boudjedir, Omar Bouhali, and Nassim Rizoug. Adaptive neural network control based on neural observer for quadrotor unmanned aerial vehicle. *Advanced Robotics*, 28(17):1151–1164, 2014.

[45] Dandan Zhao, Changyin Sun, Qingling Wang, and Wankou Yang. Neural network based pid control for quadrotor aircraft. In *International Conference on Intelligent Science and Big Data Engineering*, pages 287–297. Springer, 2015.

[46] Y. Kutsuna, M. Ando, and M. Yamada. Adaptive position control of quad-rotor helicopter in quaternion based on input-output linearization. In *Advanced Mechatronic Systems (ICAMechS), 2014 International Conference on*, pages 243–248, Aug 2014.

[47] Justin M Selfridge and Gang Tao. A multivariable adaptive controller for a quadrotor with guaranteed matching conditions. *Systems Science & Control Engineering: An Open Access Journal*, 2(1):24–33, 2014.

[48] Peng Lu and Erik-Jan van Kampen. Active fault-tolerant control for quadro-tors subjected to a complete rotor failure. In *Intelligent Robots and Systems (IROS), 2015 IEEE/RSJ International Conference on*, pages 4698–4703, Sept 2015.

[49] Hamidreza Jafarnejadsani, Donglei Sun, Hanmin Lee, and Naira Hovakimyan. Optimized l1 adaptive controller for trajectory tracking of an indoor quadro-tor. *Journal of Guidance, Control, and Dynamics*, 2017.

[50] Yu Sheng and Gang Tao. Multivariable mrac for a quadrotor uav with a non-diagonal interactor matrix. In *Asian Control Conference*, 2017.

[51] R. C. Avram, X. Zhang, and J. Muse. Nonlinear adaptive fault-tolerant quadrotor altitude and attitude tracking with multiple actuator faults. *IEEE Transactions on Control Systems Technology*, PP(99):1–7, 2017.

[52] Hao Liu, Dafizal Derawi, Jonghyuk Kim, and Yisheng Zhong. Robust optimal attitude control of hexarotor robotic vehicles. *Nonlinear Dynamics*, 74(4):1155–1168, 2013.

[53] R. Baranek and F. Solc. Modelling and control of a hexa-copter. In *Carpathian Control Conference (ICCC), 2012 13th International*, pages 19–23, May 2012.

[54] Andrea Alaimo, Valeria Artale, Cristina Lucia Rosa Milazzo, and Angela Ricciardello. Pid controller applied to hexacopter flight. *Journal of Intelligent & Robotic Systems*, 73(1):261–270, 2014.

[55] D. Brescianini and R. D'Andrea. Design, modeling and control of an omni-directional aerial vehicle. In *2016 IEEE International Conference on Robotics and Automation (ICRA)*, pages 3261–3266, May 2016.

[56] H. Mehmood, T. Nakamura, and E. N. Johnson. A maneuverability analysis of a novel hexarotor uav concept. In *2016 International Conference on Unmanned Aircraft Systems (ICUAS)*, pages 437–446, June 2016.

[57] A. Aliyu, M. Elshafei, A. W. A. Saif, and M. Dhaifullah. Performance evaluation of quadrotor with tilted rotors under wind gusts. In *2016 IEEE International Conference on Advanced Intelligent Mechatronics (AIM)*, pages 294–299, July 2016.

[58] J. M. Selfridge and G. Tao. Multivariable output feedback mrac for a quadrotor uav. In *2016 American Control Conference (ACC)*, pages 492–499, July 2016.

[59] H. Liu, D. Li, Z. Zuo, and Y. Zhong. Robust three-loop trajectory tracking control for quadrotors with multiple uncertainties. *IEEE Transactions on Industrial Electronics*, 63(4):2263–2274, April 2016.

[60] P. Pounds, R. Mahony, and P. Corke. Modelling and control of a large quadrotor robot. *Control Engineering Practice*, 18(7):691 – 699, 2010. Special Issue on Aerial Robotics.

[61] Masami Saeki and Yoshinobu Sakaue. Flight control design for a nonlinear non-minimum phase vtol aircraft via two-step linearization. In *Decision and*

Control, 2001. Proceedings of the 40th IEEE Conference on, volume 1, pages 217–222. IEEE, 2001.

[62] Deepak Gautam and Cheolkeun Ha. Control of a quadrotor using a smart self-tuning fuzzy pid controller. *International Journal of Advanced Robotic Systems*, 10, 2013.

[63] Paul E. I. Pounds, Daniel R. Bersak, and Aaron M. Dollar. Stability of small-scale uav helicopters and quadrotors with added payload mass under pid control. *Autonomous Robots*, 33(1):129–142, 2012.

[64] Prasenjit Mukherjee and Steven Waslander. Direct adaptive feedback linearization for quadrotor control. In *AIAA Guidance, Navigation, and Control Conference*, page 4917, 2012.

[65] Farhad A Goodarzi, Daewon Lee, and Taeyoung Lee. Geometric adaptive tracking control of a quadrotor unmanned aerial vehicle on se (3) for agile maneuvers. *Journal of Dynamic Systems, Measurement, and Control*, 137(9):091007, 2015.

[66] Yu Sheng and Gang Tao. Dynamics mutation and tracking control of quadrotors under multiple operating conditions. In *AIAA Guidance, Navigation, and Control Conference*, 2018.

[67] Yu Sheng and Gang Tao. An adaptive actuator failure compensation scheme for a hexarotor system. In *AIAA Guidance, Navigation, and Control Conference*, 2018.

[68] A. R. Merheb, H. Noura, and F. Bateman. Emergency control of ar drone quadrotor uav suffering a total loss of one rotor. *IEEE/ASME Transactions on Mechatronics*, 22(2):961–971, April 2017.

[69] Guang-Xun Du, Quan Quan, Binxian Yang, and Kai-Yuan Cai. Controllability analysis for multirotor helicopter rotor degradation and failure. *Journal of Guidance, Control, and Dynamics*, 38(5):978–985, 2015.

[70] Zhixiang Liu, Chi Yuan, Youmin Zhang, and Jun Luo. A learning-based fault tolerant tracking control of an unmanned quadrotor helicopter. *Journal of Intelligent & Robotic Systems*, pages 1–18, 2015.

[71] Ahmed Aboudonia, Ramy Rashad, and Ayman El-Badawy. Composite hierarchical anti-disturbance control of a quadrotor uav in the presence of matched and mismatched disturbances. *Journal of Intelligent & Robotic Systems*, Sep 2017.

[72] T. Madani and A. Benallegue. Control of a quadrotor mini-helicopter via full state backstepping technique. In *Proceedings of the 45th IEEE Conference on Decision and Control*, pages 1515–1520, Dec 2006.

[73] Brian Whitehead and Stefan Bieniawski. Model reference adaptive control of a quadrotor uav. In *AIAA Guidance, Navigation, and Control Conference*, page 8148, 2010.

[74] Guang-Xun Du, Quan Quan, and Kai-Yuan Cai. Controllability analysis and degraded control for a class of hexacopters subject to rotor failures. *Journal of Intelligent & Robotic Systems*, 78(1):143–157, 2015.

[75] Thomas Schneider, Guillaume Ducard, Rudin Konrad, and Strupler Pascal. Fault-tolerant control allocation for multirotor helicopters using parametric programming. In *International Micro Air Vehicle Conference and Flight Competition (IMAV)*, Braunschweig, Germany, July 2012.

[76] Bill Crowther, Alexander Lanzon, Martin Maya-Gonzalez, and David Langkamp. Kinematic analysis and control design for a nonplanar multi-

rotor vehicle. *Journal of Guidance, Control, and Dynamics*, 34(4):1157–1171, 2011.

[77] Yuichi Tadokoro, Tatsuya Ibuki, and Mitsuji Sampei. Maneuverability analysis of a fully-actuated hexrotor uav considering tilt angles and arrangement of rotors. *IFAC-PapersOnLine*, 50(1):8981 – 8986, 2017. 20th IFAC World Congress.

[78] D. Brescianini and R. DAndrea. Computationally efficient trajectory generation for fully actuated multirotor vehicles. *IEEE Transactions on Robotics*, pages 1–17, 2018.

[79] Bryan Convens, Kelly Merckaert, Marco M Nicotra, Roberto Naldi, and Emanuele Garone. Control of fully actuated unmanned aerial vehicles with actuator saturation. In *The 20th World Congress, The International Federation of Automatic Control*, 2017.

[80] Markus Ryll, Giuseppe Muscio, Francesco Pierri, Elisabetta Cataldi, Gianluca Antonelli, Fabrizio Caccavale, and Antonio Franchi. 6d physical interaction with a fully actuated aerial robot. In *2017 IEEE International Conference on Robotics and Automation*, 2017.

[81] Loz Blain. Tilt-rotor hexacopter puts a new twist on drone orientation. `https://newatlas.com/voliro-hexacopter-drone-orientation/49969/`.

[82] Petros A Ioannou and Jing Sun. *Robust adaptive control*. Courier Corporation, 2012.

[83] Kumpati S Narendra and Anuradha M Annaswamy. *Stable adaptive systems*. Courier Corporation, 2012.

[84] Y. Sheng and G. Tao. Dynamics mutation and tracking control of quadrotors under multiple operating conditions. Technical report, http://people.virginia.edu/~ys6wa/gnc18ys1-full.pdf, 2017.

[85] G. P. Falcon, J. Angelov, and F. Holzapfel. Hexacopter outdoor flight test results using adaptive control allocation subject to an unknown complete loss of one propeller. In *2016 3rd Conference on Control and Fault-Tolerant Systems (SysTol)*, pages 373–380, Sept 2016.

[86] J. I. Giribet, R. S. Sanchez-Pena, and A. S. Ghersin. Analysis and design of a tilted rotor hexacopter for fault tolerance. *IEEE Transactions on Aerospace and Electronic Systems*, 52(4):1555–1567, August 2016.

[87] C. D. Pose, J. I. Giribet, and A. S. Ghersin. Hexacopter fault tolerant actuator allocation analysis for optimal thrust. In *2017 International Conference on Unmanned Aircraft Systems (ICUAS)*, pages 663–671, June 2017.

[88] Joseph M Brown, Jesse A Coffey III, Dustin Harvey, and Jordan M Thayer. Characterization and prognosis of multirotor failures. In *Structural Health Monitoring and Damage Detection, Volume 7*, pages 157–173. Springer, 2015.

[89] Isaac J Olson and Ella M Atkins. Qualitative failure analysis for a small quadrotor unmanned aircraft system. In *Proceedings of the AIAA guidance, navigation, and control (GNC) conference. Boston*, pages 19–22, 2013.

[90] Neil Tardella. Flying with broken propellers. `https:// spectrum.ieee.org/automaton/robotics/industrial-robots/ earthbound-robots-today-need-to-take-flight`.

[91] A. Freddi, S. Longhi, A. Monteriu, and M. Prist. Actuator fault detection and isolation system for an hexacopter. In *Mechatronic and Embedded Systems and*

Applications (MESA), 2014 IEEE/ASME 10th International Conference on, pages 1–6, Sept 2014.

[92] R. C. Avram, X. Zhang, and J. Muse. Quadrotor actuator fault diagnosis and accommodation using nonlinear adaptive estimators. *IEEE Transactions on Control Systems Technology*, PP(99):1–8, 2017.

[93] G.P. Falconi, C.D. Heise, and F. Holzapfel. Fault-tolerant position tracking of a hexacopter using an extended state observer. In *Automation, Robotics and Applications (ICARA), 2015 6th International Conference on*, pages 550–556, Feb 2015.

[94] Jangho Lee, Hyoung Sik Choi, and Hyunchul Shim. Fault tolerant control of hexacopter for actuator faults using time delay control method. *International Journal of Aeronautical and Space Sciences*, 17(1):54–63, 2016.

[95] Christopher T Raabe. Adaptive, failure-tolerant control for hexacopters. In *AIAA Infotech@ Aerospace (I@ A) Conference*, page 4819, 2013.

[96] M. Miihlegg, P. Niermeyer, G.P. Falconi, and F. Holzapfel. L1 fault tolerant adaptive control of a hexacopter with control degradation. In *Control Applications (CCA), 2015 IEEE Conference on*, pages 750–755, Sept 2015.

[97] Guillermo P Falconı and Florian Holzapfel. Adaptive fault tolerant control allocation for a hexacopter system. In *Proceedings of the American Control Conference*, pages 6760–6766, 2016.

[98] D. T. Nguyen, D. Saussie, and L. Saydy. Quaternion-based robust fault-tolerant control of a quadrotor uav. In *2017 International Conference on Unmanned Aircraft Systems (ICUAS)*, pages 1333–1342, June 2017.

[99] A. Chamseddine, D. Theilliol, Y.M. Zhang, C. Join, and C.A. Rabbath. Active fault-tolerant control system design with trajectory re-planning against actuator faults and saturation: Application to a quadrotor unmanned aerial vehicle. *International Journal of Adaptive Control and Signal Processing*, 29(1):1–23, 2015.

[100] Tong Li, Youmin Zhang, and Brandon W Gordon. Passive and active nonlinear fault-tolerant control of a quadrotor unmanned aerial vehicle based on the sliding mode control technique. *Proceedings of the Institution of Mechanical Engineers, Part I: Journal of Systems and Control Engineering*, 227(1):12–23, 2013.

[101] Alexander Lanzon, Alessandro Freddi, and Sauro Longhi. Flight control of a quadrotor vehicle subsequent to a rotor failure. *Journal of Guidance, Control, and Dynamics*, 37(2):580–591, 2014.

[102] V. Lippiello, F. Ruggiero, and D. Serra. Emergency landing for a quadrotor in case of a propeller failure: A backstepping approach. In *2014 IEEE/RSJ International Conference on Intelligent Robots and Systems*, pages 4782–4788, Sept 2014.

[103] R. R. Warier, A. K. Sanyal, S. Sukumar, and S. P. Viswanathan. Feedback tracking control schemes for a class of underactuated vehicles in se(3). In *2017 American Control Conference (ACC)*, pages 899–904, May 2017.

[104] MGE Schneiders, MJG Van De Molengraft, and M Steinbuch. Benefits of over-actuation in motion systems. In *Proceedings of the 2004 American control conference*, volume 1, pages 505–510. IEEE, 2004.

[105] Alessandro Casavola and Emanuele Garone. Fault-tolerant adaptive control allocation schemes for overactuated systems. *International Journal of Robust and Nonlinear Control*, 20(17):1958–1980, 2010.

[106] Michael W Oppenheimer, David B Doman, and Michael A Bolender. Control allocation for over-actuated systems. In *2006 14th Mediterranean Conference on Control and Automation*, pages 1–6. IEEE, 2006.

[107] Yu Sheng, Gang Tao, and Peter Beling. An adaptive actuator failure compensation scheme for a hexarotor system with parameter uncertainties. In *The 2018 International Conference on Unmanned Aircraft Systems*, 2018.

[108] Yu. V. Morozov. Emergency control of a quadrocopter in case of failure of two symmetric propellers. *Automation and Remote Control*, 79(3):463–478, Mar 2018.

[109] S. Sun, L. M. C. Sijbers, X. Wang, and C. de Visser. High-speed flight of quadrotor despite loss of single rotor. *IEEE Robotics and Automation Letters*, pages 1–1, 2018.

[110] Johannes Stephan, Lorenz Schmitt, and Walter Fichter. Linear parameter-varying control for quadrotors in case of complete actuator loss. *Journal of Guidance, Control, and Dynamics*, pages 1–15, 2018.

[111] Yu Han, James D Biggs, and Naigang Cui. Adaptive fault-tolerant control of spacecraft attitude dynamics with actuator failures. *Journal of Guidance, Control, and Dynamics*, 38(10):2033–2042, 2015.

[112] Yajie Ma, Bin Jiang, Gang Tao, and Yuehua Cheng. Actuator failure compensation and attitude control for rigid satellite by adaptive control using quaternion feedback. *Journal of the Franklin Institute*, 351(1):296 – 314, 2014.

[113] Bing Xiao, Qinglei Hu, and William Singhose. Adaptive compensation control for spacecraft attitude stabilization with actuator misalignment and faults. In *AIAA Guidance, Navigation, and Control Conference*, page 4626, 2012.

[114] Xidong Tang, Gang Tao, and Suresh M. Joshi. Adaptive actuator failure compensation for nonlinear mimo systems with an aircraft control application. *Automatica*, 43(11):1869 – 1883, 2007.

[115] Y. Liu, X. Tang, G. Tao, and S. M. Joshi. Adaptive compensation of aircraft actuation failures using an engine differential model. *IEEE Transactions on Control Systems Technology*, 16(5):971–982, Sept 2008.

[116] Liyan Wen, Gang Tao, Hao Yang, and Yi Yang. Aircraft turbulence compensation using adaptive multivariable disturbance rejection techniques. *Journal of Guidance, Control, and Dynamics*, 38(5):954–963, 2014.

[117] Abhay A Pashilkar, N Sundararajan, and P Saratchandran. Adaptive nonlinear neural controller for aircraft under actuator failures. *Journal of guidance, control, and dynamics*, 30(3):835–847, 2007.

[118] Robert E Roberson and Richard Schwertassek. *Dynamics of multibody systems*, volume 18. Springer-Verlag Berlin, 1988.

[119] Emil Fresk and George Nikolakopoulos. Full quaternion based attitude control for a quadrotor. In *2013 European Control Conference (ECC)*, pages 3864–3869. IEEE, 2013.

[120] Jossué Carino, Hernan Abaunza, and P Castillo. Quadrotor quaternion control. In *2015 International Conference on Unmanned Aircraft Systems (ICUAS)*, pages 825–831. IEEE, 2015.

[121] A Alaimo, V Artale, C Milazzo, and A Ricciardello. Comparison between euler and quaternion parametrization in uav dynamics. In *AIP Conference Proceedings*, volume 1558, pages 1228–1231. AIP, 2013.

[122] Stefano Di Lucia, Gian Diego Tipaldi, and Wolfram Burgard. Attitude stabilization control of an aerial manipulator using a quaternion-based backstepping approach. In *2015 European Conference on Mobile Robots (ECMR)*, pages 1–6. IEEE, 2015.

[123] Ayman A El-Badawy and Mohamed A Bakr. Quadcopter aggressive maneuvers along singular configurations: an energy-quaternion based approach. *Journal of Control Science and Engineering*, 2016:4, 2016.

[124] Teppo Luukkonen. Modelling and control of quadcopter. *Independent research project in applied mathematics, Espoo*, 2011.

[125] Jiaxing Guo, Yu Liu, and Gang Tao. Multivariable mrac with state feedback for output tracking. In *American Control Conference, 2009. ACC '09.*, pages 592–597, June 2009.

[126] A. K. Imai, R. R. Costa, Liu Hsu, Gang Tao, and P. Kokotovic. Multivariable mrac using high frequency gain matrix factorization. In *Decision and Control, 2001. Proceedings of the 40th IEEE Conference on*, volume 2, pages 1193–1198 vol.2, 2001.

[127] Tor A. Johansen and Thor I. Fossen. Control allocation?a survey. *Automatica*, 49(5):1087 – 1103, 2013.

[128] R. Singh and K. Narendra. Prior information in the design of multivariable adaptive controllers. *IEEE Transactions on Automatic Control*, 29(12):1108–1111, Dec 1984.

[129] Jiaxing Guo, Gang Tao, and Yu Liu. Multivariable adaptive control of nasa generic transport aircraft model with damage. *Journal of Guidance, Control, and Dynamics*, 34(5):1495–1506, 2011.

[130] Wayne Durham, Kenneth A Bordignon, and Roger Beck. *Aircraft control allocation*. John Wiley & Sons, 2017.